# 16,000 YEARS OF PALEOENVIRONMENTAL CHANGE FROM THE LAKE PETERS-SCHRADER AREA, NORTHEASTERN BROOKS RANGE, ALASKA

By Christopher Warren Benson

A Thesis

Submitted in Partial Fulfillment

of the Requirements for the Degree of

Master of Science

in Geology

Northern Arizona University

May 2018

Approved:

Darrell Kaufman, Ph.D., Chair

Nick McKay, Ph.D.

Erik Schiefer, Ph.D.

# ABSTRACT

## 16,000 YEARS OF PALEOENVIRONMENTAL CHANGE FROM THE LAKE PETERS-SCHRADER AREA, NORTHEASTERN BROOKS RANGE, ALASKA

CHRISTOPHER WARREN BENSON

Paleoclimate reconstructions are essential to contextualize recent warming that is affecting the Arctic region faster than anywhere else on Earth. To better understand this rapidly changing landscape, I used sedimentological evidence from Lake Peters and Lake Schrader in the northeastern Brooks Range to infer changing environmental conditions over the past 16,000 years (16 ka). Across five core sites, distinct changes in the visual stratigraphy and physical sediment properties including sediment bulk density, organic-matter content, and grain-size distributions record changing environmental conditions. The oldest sediments accumulated rapidly and contain little organic matter, interpreted to represent a landscape dominated by glacial and paraglacial processes associated with the rapid upvalley retreat of glaciers. No robust evidence was found for a climate fluctuation concurrent with the Younger Dryas. A peak in organic-matter abundance between 12–10 ka is attributed to a maximum in Northern Hemisphere summer insolation and accords with other regional paleoclimate reconstructions. Following this, conditions appear to have become drier as indicated by sediments with high density and low organic content until 5 ka. Alternatively, these sediments could represent a glacial advance, but this is unlikely as regional evidence for cooler conditions is absent. From 5–2 ka, organic matter consistently increases in several cores and is attributed to increased river discharge, which

carried terrestrial organic matter into the lakes, or to increased summer temperatures, which led to higher productivity, or both. After 2 ka, sediments increase in density and decrease in organic content, which suggests the growth of glaciers within the catchment. Moraine mapping and lichenometry confirm previous studies and accord with changes in lake sediments. *Rhizocarpon geographicum* thallus diameters on boulders located on the outermost moraine crest suggest the maximum Holocene glacial extent is associated with increased moraine frequency from elsewhere in the Brooks Range dating to 2.5–1.9 ka. New measurements from a distinct moraine crest from an additional valley show consistency within the basin and are likely associated with a regional increase in moraine frequency from 1.1–1.0 ka. Increased sedimentation rates and organic productivity in both lakes may record glacier retreat during the last century. This study provides a framework for future research and fills an important gap in paleoenvironmental records for the northeastern Brooks Range.

Acknowledgements

This research has been made possible by the efforts of many individuals. I must first recognize my advisor, Darrell Kaufman, for his incredible talents as a scientist, as a writer, and for his ability to provide mentorship and support. Additionally, my research has benefitted immensely from the input and critical eye of my committee members, Nick McKay and Erik Schiefer. David Fortin was invaluable while leading the initial coring campaign. Katherine Whitacre was instrumental in providing me with lab training and support, as well as her amazing proficiency with preparing radiocarbon samples. R. Scott Anderson's identification of $^{14}C$ samples was incredibly helpful. Stacy Kish, Maryann Ramos, Ellie Broadman, and Rebecca Harris spent several weeks in the field adding to this effort. Furthermore, Rebecca Ellerbrook and Lorna Thurston added immensely to the research group by helping characterize the lake bathymetry and hydrology of the study area. Leo O'Neil and Dan Cameron aided in sample processing at NAU. Mike Retelle (Bates College) loaned his acoustical profiler and Ray Bradley (University of Massachusetts) loaned his vibracorer. John Southon (University of California, Irvine) analyzed the radiocarbon, Doug Hammond (University of Southern California) analyzed the Pb and Cs, Mike Ketterer (Metropolitan State University of Denver) analyzed the Pu, Lacustrine Core Facility (LacCore) at the University of Minnesota provided the initial core description datasets. US Fish and Wildlife Service, Arctic Refuge permitted the research activities, continuing the long tradition of research at the Holmes Research Station while respecting the wilderness values of the area. CH2MHill Polar Services provided logistical support. This project was funded by NSF-Office of Polar Programs, Arctic System Science award ARC-1418000.

# Table of Contents

**(Digital submission-all data)**

## List of Figures



## List of Figures (Appendix)

## List of Tables

## Preface

This thesis is organized into three chapters: Chapter 1 introduces this study in the context of the current body of literature. Chapter 2 is a manuscript for submission to *Quaternary Research.* Chapter 3 presents collated conclusions. A combined references-cited section follows and additional text containing detailed core descriptions and a moraine mapping summary are in the appendices.

# Chapter 1: Introduction

## Research motivation

To understand recent changes in the climate system, it is paramount to place instrumental observations within the larger framework of paleoclimate reconstructions as they can provide a record of climate variability that helps contextualize recent climate change. Over the last century, the Arctic has warmed about 1.3 °C, roughly twice as fast as the global average (Bekryaev et al., 2010). This warming trend contrasts markedly with 0.5 °C of cooling over the last 2000 years (Kaufman et al., 2009). Recent corresponding reductions in sea ice extent, glacier extent, and spring snow cover have been documented for the Arctic over the last several decades (Vaughn et al., 2013). These pronounced trends are due in part to Arctic amplification. This natural feature of the climate system is defined by the observation that temperature variability and trends in the Arctic region tend to be larger than elsewhere in the Northern Hemisphere or globe as a whole (e.g. Kelly et al., 1982). Because global climate trends tend to be amplified in the Arctic, this region is an important component of the climate system due to its seasonal fluctuations and feedback mechanisms like surface albedo, which tends to increase snow cover and sea ice extent (Serreze and Barry, 2011).

The Brooks Range in northern Alaska (N 68°, W 144-148°) hosts several types of paleoclimate archives including lake sediments and moraines. During the Last Glacial Maximum, this area was not covered by the Laurentide Ice Sheet but contained valley glaciers that extended up to 25 km from range fronts (Kaufman et al., 2011). As these glaciers receded

and occasionally re-advanced, evidence of past glacier extents was left in the form of moraines and glacilacustrine sediments. Dozens of studies have attempted to reconstruct Holocene climate for the Brooks Range, however, results are often conflicting and scant. This study focuses on the northeastern Brooks Range where relatively few paleoclimate studies have been undertaken to attempt to fill in a regional gap in paleoclimate archives. Furthermore, paleoclimate reconstructions may provide insight in understanding future changes for the Arctic region, which is projected to warm 5 °C (winter), 2.2 °C (summer) by 2100 under Representative Concentration Pathway 4.5 (Hartmann et al., 2013).

## Study site

### *Geography*

Lake Peters (N 69.32°, W 145.05°) and Lake Schrader (N 69.38°, W 145.0°) are a prominent pair of lakes located in the northeastern Brooks Range (Fig. 1). The east-west trending Brooks Range is the northernmost mountain chain in Alaska and is about 1000 km long and has an area of 190 000 $km^2$. The Brooks Range separates the Arctic Coastal Plain to the north from the Yukon Basin to the south. The Brooks Range increases in elevation from west to east, rising to a maximum of 2700 m a.s.l. near the study site. The elevation of Lake Peters and Lake Schrader is 853 m a.s.l. with a combined lake area of ~20 $km^2$, making them some of the largest lakes on the north side of the Brooks Range. The maximum lake depth is ~60 m and the combined drainage area of Lake Peters and Lake Schrader is ~300 $km^2$ with approximately 12% glacier ice cover in the Lake Peters basin.

*Geologic setting*

The bedrock geology of the Lake Peters area was mapped by Reed (1968). He mapped Devonian to Jurassic sedimentary and meta-sedimentary rocks, with the majority consisting of the Devonian, Neruokpuk Formation (Fig. A – 1). This formation consists of interbedded quartz wacke, quartz semischist, and phyllite, with subordinate amounts of metachert and quartzite. The local geologic structure is arranged in an east-west striking, northward dipping fold belt resulting from southward dipping thrust faults. The Lake Peters area has experienced three distinct deformation events, the first two occurring in the late Devonian and the third resulting from north-south directed compressional stress starting in Eocene time, and still active as evidenced by historic seismicity and deformed Quaternary sediments (Grantz et al., 1994).

*Modern ecotypes*

Lake Peters and Lake Schrader are located in the Arctic tundra biome, north of modern-day tree line in a region underlain by continuous permafrost with a thin active layer (Jorgenson and Heiner, 2003). Vegetation is dominantly shrub tundra with dwarf willow and birch, and willow shrubs near streams. Soils are rocky, excessively drained, strongly acidic, and have very thin surface organics.

*Modern climate*

At the Lake Peters study site, several temporary weather stations were installed by team members of the Arctic Glacial Lakes Project in 2015. Hourly averaged temperature from May 2015 to May 2016 was -9.8 °C, with monthly averages of December (-29.1°C) and July (8.5 °C). Strong temperature inversions developed during the winter with temperature differences between 850 and 1425 m a.s.l. as much as 15 °C. These temperatures are fairly consistent with multi decadal averages reported from Toolik Lake (roughly 170 km west of Lake Peters, 68.63°N, 149.61°W, 720 m a.s.l.) reported by Oswald et al. (2012). Liquid precipitation for the same time period from the study site was 166 mm. No snowfall data are available from the field site, but using Toolik field station as a proxy, mean annual precipitation is 300 mm suggesting that about half of the precipitation at Lake Peters falls as snow.

Higher-elevation weather stations in the Brooks Range include the McCall Glacier (2200 m a.s.l.) where precipitation is 500 mm $yr^{-1}$ with about half of this precipitation falling as snow, and average monthly air temperatures ranging from 0 to -30 °C (Wendler et al., 1972).

*Synoptic climatology and dominate modes of variability*

Two important semi-permanent synoptic features occur in the northern Pacific Ocean and Chukchi Sea: the Aleutian Low and the Beaufort High. Northern Hemisphere winters are characterized by a strengthening of the Aleutian Low, whereas summer patterns show Beaufort/Chukchi Lows with infrequent and weakened Aleutian Lows (Cassano et al., 2011). Variability in winter precipitation and temperatures in Alaska are mainly attributed to changes in

the position and strength of the Aleutian Low as it impacts storm tracks and synoptic scale circulation (Rodionov et al., 2007). In addition to semi-permanent synoptic features, the Arctic Oscillation (Thompson and Wallace, 1998, 2001) can help elucidate the dominate modes of climate variability for this region. In the negative phase, relatively weak low pressure in the Arctic correlates with an increased meridional jet stream and increased mixing between polar and mid-latitude air masses resulting in relatively warmer polar temperatures, and anomalously cold winters for lower latitudes.

On multidecadal time scales, Hartman and Wendler (2005) identified effects of the Pacific Decadal Oscillation (e.g. Mantua and Hare, 2002) on Alaska's climate and concluded that during the positive phase of the PDO, mean annual and seasonal temperatures were up to 3.1°C higher than for the negative phase. Additionally during the positive phase of the PDO, more moisture is advected into high latitudes. A similar climate index, the decadal North Pacific Index (NPI) has recently been linked to climate variables in the Brooks Range. Klein et al. (2016) linked variations in ice core oxygen isotopes and deuterium-excess from the McCall Glacier to the NPI. Variations in isotope values suggest that during positive NPI, moisture is primarily sourced from the ice-covered Arctic Ocean and from more humid open-water sources south of the McCall Glacier during negative NPI. These phases are linked to weaker and stronger Aleutian Lows respectively.

*Glaciers*

Glaciers grow and shrink in response to climate parameters including mean summer temperature and precipitation. Unarguably, glaciers and their associated landforms are important archives for paleoclimate information; however, Roe and Baker (2016) have shown that internal climate variability alone (e.g. variability that occurs in the absence of solar forcing, changes in atmospheric composition, or volcanic eruptions, etc.) may play a significant role in glacier size. Roe et al. (2016) analyzed glacier length trends on a global scale and demonstrated that, despite this internal variability, glaciers act as low-pass climate filters that respond to long-term climate trends. Therefore, reconstructing glacial extents is a valuable approach to understanding changes in regional climate (Owen et al., 2009).

Glaciers are classified based on their size, geometries, and terminus location (e.g. tidewater vs. valley glacier). Furthermore, glaciers have large variations in their internal temperature regimes from polar glaciers ( -40 °C) to temperate glaciers (near or close to 0 °C) with polythermal glaciers being composed of both warm and cold ice (Benn and Evans, 2010). Thermal regimes control the downslope movement of ice: basal sliding occurs in warm-based glaciers due to the availability of meltwater whereas cold-based glaciers are stuck to their beds and downslope flow mostly occurs through internal deformation. Polythermal glaciers are some combination of the two regimes. Temperate glaciers tend to have much higher erosion rates and sediment yields in comparison with polar glaciers. For example, Koppes et al. (2015) demonstrated that erosion rates can vary by three orders of magnitude across twenty degrees of latitude between Antarctic and southern Patagonian glaciers.

*Glacier reconstructions*

Estimates of past glacier extents can be made by identifying ice-marginal moraines. These deposits form by the deposition or deformation of sediment around the edge of active glacier termini through a variety of distinct, yet widely inclusive categories including proglacial glaciotectonic landforms, push and squeeze moraines, dump moraines/ice margin aprons, and latero-frontal fans and ramps (Benn and Evans, 2010). The outermost moraine ridge is often referred to as the terminal moraine, while moraines inboard of these ridges are commonly referred to as recessional moraines because they form during a period of overall recession albeit they actually form during a relatively small advance and/or standstill.

Early studies investigating linkages between glaciers and climate identified zones where permanent snow accumulated as "snowlines" or in more modern terms, the equilibrium line altitude (ELA) (e.g. Péwé and Reger, 1972; Péwé, 1975). The ELA is an elevational zone where ablation and accumulation are equal. For modern glaciers, ELAs tend to form such that about 70% of the total area of the glacier is occupied by the accumulation zone (Bradley, 2015). By using this relationship and comparing modern glacier positions with moraine deposits, it is possible to estimate changes in ELA (Δ ELA) through time. Because several climate factors including melt season temperatures and precipitation may affect ELAs, care must be taken when making paleoclimate inferences. It is important to note that moraine positions are controlled by the ELA and the underlying topography. Thus, studies that reconstruct ELAs are useful because variations in glacier hypsometry can produce large differences in moraine distributions across regions with varying glacier geometries and Δ ELA provides a consistent parameter of glacier extent.

Seminal studies using Holocene glacier front positions include the work of Denton and Karlén (1973) where they identified three major periods of worldwide advances 5800–4900, 3300–2400, and the LIA ~700–200 cal yr BP. Pioneering work by Porter (1975) reconstructed ELAs in the Southern Alps of New Zealand and set the stage for subsequent work by Dahl and Nesje (1992), who reconstructed precipitation for cirque glaciers in western Norway from the late Pleistocene through the Holocene. These types of glacier front studies have been undertaken for almost all mountainous parts of the world and several broad trends have been documented. Holocene glacier reconstructions from many alpine areas in the Northern Hemisphere show evidence of maximum recession during the early Holocene, and maximum extent during the Little Ice Age (LIA) (Davis et al., 2009).

Moraines provide important evidence of glacier fluctuations but are inherently biased to preserve glacial advances rather than recessions. Furthermore, in many mountainous areas, the most recent and most extensive advance (that of the LIA) has destroyed evidence of any possible previous advances. Lastly, dating moraines is problematic due to the often-low amounts of organic matter found in glaciated regions and the absence of soil development on moraines, precluding the application of standard geochronological methods. Time-lags associated with glacial advances and dateable surface development (e.g. lichen colonization) further complicate chronologies, providing only minimum age estimates of moraine stabilization following an advance. Lichenometry is often used to date moraines although this method lacks precision and has recently been heavily scrutinized (e.g. Osborn et al., 2015). Recent advances in cosmogenic isotope dating have been utilized and are preferable to lichenometry. These methods must still address problems such as inheritance, and in areas without the appropriate substrate, this method

is not applicable. While glacier front studies have limitations, they can be combined with glacilacustrine sediments which can provide a continuous signal of glacier fluctuations.

*Glacier reconstructions using glacilacustrine sediments*

Variations in glacilacustrine sediments reflect changes in upstream glacier activity (e.g. Karlén, 1976). The basal erosion from temperate and polythermal glaciers produces "rock flour" that consists of clay- and silt-sized particles, while non-glaciated streams lack this rock flour (Östrem, 1975; Dahl et al., 2003). Glaciated catchments contain turbid meltwater streams that carry these fine-grained particles in suspension, which form lacustrine deposits that are typically blueish-grey and contrast with characteristically brown-black, more organic-rich non-glacial sediment. This meltwater turbidity hampers autochthonous organic production and variations in the amount of sediment organic matter (OM) in lake sediments measured by weight loss-on-ignition (LOI) can be used to infer glacier extent. Used in conjunction with moraines, pioneering studies by Karlén (1976, 1981) used this relationship in glacilacustrine sediments to reconstruct Holocene glacier variations in northern Fennoscandia. Subsequent studies applied similar methodologies in other areas of Fennoscandia (e.g. Nesje et al., 1991; Nesje and Dahl, 1991; Mathews and Karlén, 1992; Karlén and Matthews, 1992; Dahl and Nesje, 1994; Matthews et al., 2000; Nesje et al., 2000, 2001).

The dry bulk density of glacilacustrine sediments tends to be negatively correlated with OM due to the obvious contrast between materials and the tendency for organic material to contain water, which also shows a similarly negative relationship to dry bulk density (Menounos, 1997). Furthermore, changes in bulk density are also controlled by particle size distributions with

poorly sorted (well sorted) sediments having higher (lower) density (Bakke et al., 2005a). Several studies have used particle size and density changes in addition to changes in OM to reconstruct glacier extents (e.g. Leeman and Niessen, 1994; Matthews et al., 2000; Nesje et al., 2001; Bakke et al., 2005a, 2005b).

Modern sediment fluxes in glacio-fluvial systems have been shown to correlate with glacier extent (Hallet et al., 1996). Leonard (1985, 1997) measured annually laminated sediments (varves) in the Canadian Rockies and demonstrated that sediment fluxes positively correlated with glacier extent over centennial to millennial time scales. On decadal time scales, sediment flux was shown to be complexly related with up-valley ice extent with high sedimentation rates associated with glacier maximum stands, or periods with glacier advances or recessions. Similarly, in an attempt to measure sediment influx related to glacial advances, Souch (1994) studied lake sediments in the Coast Mountains of British Columbia and used grain size distributions as a method for differentiating glacial from non-glacial lake sediment input sources.

Yet another parameter to infer the relative amounts of inorganic vs. organic material in lake sediments is their magnetic susceptibility (MS) (Thompson et al., 1975). Down-core variations in MS are related to the amount of magnetic minerals and many studies have used this relationship to identify periods of larger glacier extent as increased bedrock erosion results in more minerogenic material in meltwater streams and downstream lakes (e.g. Snowball and Sandgren, 1996). Furthermore, distinct peaks or fluctuations in MS may aid in correlations across cores, as well as identifying other beds useful for making correlations (e.g. tephra deposits). Geochemical element analysis using X-ray fluorescence (XRF) has more recently been used to detect glacial signals in lake sediments by measuring increases in silicon, aluminum, titanium, and iron (e.g. Bakke et al., 2010, 2013).

While many sediment parameters can be analyzed, Jansson et al. (2005) argued that paleoclimate inferences based on these measurements often overlooked the complexities associated with: sediment production beneath glaciers, sediment fluxes out from glaciers, sediment transport in proglacial environments, and lake-bottom sedimentation processes. Sediment production below glaciers is complicated by: variable response times of glaciers to climate forcings as well as variations in sediment development in cases where glaciers change their thermal structure (e.g. a glacier transitioning from cold-based to warm-based with increasing mean temperatures). Complications also arise in sediment fluxes from changing glaciers due to the availability of both water and sediment. For example, sediment yields may initially increase while a glacier is first receding. Sediment transport is complicated through varying residence times in paraglacial environments and by the possibility of episodic remobilization of sediments during periods of extreme precipitation events.

With these complexities in mind, it is important to choose a study site that will be sensitive to changes in glacier extent. Karlén (1976) reasoned that lakes most suitable for this technique would have relatively small glacier-covered areas when compared with the size of the lake. Furthermore, small glaciers that would alternatively melt away and re-form during changing climatic conditions would produce a strong signal in lake sediments. To record the entire Holocene, lakes should be located downstream of ice-proximal lakes, resulting in relatively low depositional rates (< 5–15 mm $yr^{-1}$). Jansson et al. (2005) further suggested that multiple, linked lakes can provide a more representative data set when reconstructing glacier extents and that single-core studies should be avoided as they lack reproducibility. Coring sites should be located away from steep slopes and stream inflows. Matthews and Karlén (1992) also

suggested that non-glacial lake sediments could be useful to compare with glacial-lake sediments when available.

Geochronology is crucial to place changes in glacilacustrine sediments into a meaningful temporal context. Wolfe et al. (2004) reviewed techniques for obtaining geochronologies from high-latitude lakes, which are often characterized by having extended periods of ice cover coupled with low terrestrial and aquatic production rates. These factors result in lakes with low amounts of organic matter, making radiocarbon dating difficult. Furthermore, many areas in the Arctic have a low likelihood of containing tephra due to their distal location from Holocene volcanism. Techniques to date younger sediments using $^{210}$Pb and $^{137}$Cs have been developed and are especially useful when used in conjunction with each other to date sediments younger than ~150 years.

## Previous work: Brooks Range paleoclimate studies

### *Regional trends in Holocene climate*

Recent efforts by Kaufman et al. (2016) synthesized evidence from a diverse set of paleoenvironmental records from eastern Beringia. Important findings relevant to the Brooks Range include variable and cold temperatures during the early Holocene, a thermal maximum (HTM) centered from 7 to 5 ka, and a widespread cooling trend that initiated between 4 and 3 ka. Temperature differences for individual records averaged over 500-year time spans typically ranged by 1-2 °C. This work updated a previous synthesis of Arctic Holocene paleoclimate (Kaufman et al., 2004). The general pattern of mid-Holocene warmth, followed by Neoglacial

cooling is seen across the Arctic, although considerable variation in the timing and extent of these trends is evident (Miller et al., 2010).

*Brooks Range moraine studies*

Glaciers in the Brooks Range have retreated as much as 25 km from their Last Glacial Maximum (~22 ka) positions (Kaufman et al., 2011). By ~14 ka, most glaciers retreated to within the range front and even within their modern limits (Badding et al., 2013; Pendleton et al., 2015). Early work by Detterman et al. (1958) and Porter and Denton (1967) provided the first timeline for Holocene glacier fluctuations using moraine evidence located in the north-central Brooks Range, near Anaktuvuk Pass. Other seminal studies of Brooks Range moraines include the work of Hamilton (1986, 2003) and Hamilton and Porter (1975). The Brooks Range is unique in that evidence for glacier advances early during the late Holocene (about 5-2 ka) is widespread (Porter, 2007). Because some modern glaciers in the Brooks Range are relatively small, Barclay et al. (2009) purposed that, during the Holocene thermal maximum, these glaciers may have disappeared completely.

Building off this early work, many studies have used lichenometric techniques and recognized several distinct Holocene advances in the Brooks Range (Calkin and Ellis, 1980; Ellis et al., 1981; Ellis and Calkin, 1984; Haworth et al., 1986; Calkin, 1988; Evison et al., 1996; Solomina et al., 2003; Sikorski et al., 2009). These findings suggest multiple pre-LIA advances, some as early as 4.5 ka, with most moraine ages dating to within the past 2 ka (Pendleton et al., 2017). Lichenometric ages have obvious limitations and complexities (unrepresentative over-sized lichens due to boulder inheritance, e.g. Jochimsen, 1973) and have recently been heavily

criticized (Osborn et al., 2015). To better constrain moraine ages, Badding et al. (2013) used $^{10}$Be surface exposure methods and confirmed the presence of pre-LIA moraines in the north-central Brooks Range in the Atigun and Kurupa River valleys with ages of 2.7 ± 0.2 and 4.6 ± 0.5 ka. Recent work by Pendleton et al. (2017) used $^{10}$Be methods and found pre-LIA moraines with ages of roughly 3.5 and 2.6 ka in the Arrigetch Peaks and Erratic Creek locations. These dates paired with rough lichenometric estimates suggest that glaciers in the Brooks Range reached their maximum Holocene extent as early as 4.6 ka and experienced numerous fluctuations prior to the LIA.

The glacier most proximal to Lake Peters is the Chamberlin Glacier (Fig. 1b). Early work by Holmes and Lewis (1965) identified several glaciations in the Lake Peters area, with the youngest named the Katak advance. Evison et al. (1996) further defined the deposits associated with this advance and found evidence of four distinct moraines in Chamberlin Glacier forefield with lichen-inferred dates of 2600, 1000, 450 and 60 lichen years BP. The Lake Peters area contains at least six other modern glaciers that might contain pre-LIA moraines but have not been studied in detail.

*Modern Brooks Range glaciers*

In the Lake Peters area, the McCall Glacier (located about 25 km east) is one of the most studied glaciers in the Alaskan Arctic. Rabus and Echelmeyer (1998) determined this glacier to be polythermal and also measured a temperature increase of about 1 °C at 10 m depth between 1972 and 1995, likely caused by warming trends (Rabus and Echelmeyer, 2002). Additionally, they documented the McCall Glacier as having an annual negative net mass balance of roughly

30 cm, which they interpreted to be representative of other glaciers in the northeastern Brooks Range. More recent studies have supported this thermal classification and negative mass balance trend for glaciers in the region (e.g. Klok et al., 2006; Delcourt et al., 2008; Pattyn et al., 2009; Geck et al., 2013).

*Brooks Range lake sediment studies*

Lake sediment studies in the Brooks Range have documented changes in vegetation as well climate parameters such as moisture balance and temperature. The longest records extend back to roughly 40 ka. Paleo lake-level studies reconstruct variations in precipitation and evaporation in the northern Alaska, at Burial Lake and Lake of the Pleistocene, and several hundred kilometers to the southeast at Birch Lake. These studies concluded that the LGM was more arid than the Holocene (Abbott et al., 2000; Mann et al., 2002; Abbott et al., 2010). Similarly, moraine evidence suggests that during the LIA, moisture decreased due to the minimal lowering of ELAs in comparison with the apparent temperature decrease during this time (Sikorski et al., 2009). Studies of Holocene paleoclimate in the Brooks Range using pollen evidence documented climate-related changes in vegetation at Kaiyak and Squirrel lakes (Anderson, 1985) and the nearby Noatak River drainage (Anderson, 1988). Other studies analyzed multiple sites across northern Alaska (e.g. Eisner and Colinvauxt, 1992; Anderson and Brubaker, 1994; Edwards and Barker, 1994). These reconstructions show that major vegetation changes occurred between the LGM and the early Holocene, with modern vegetation communities being established between 6 and 4 ka.

Lake sediment studies relevant to Holocene glacier extent in the Brooks Range have used physical sediment characteristics (e.g. grain size, sorting, amount of minerogenic material, varve thickness, etc.), biological characteristics (e.g. pollen and the amount of organic matter), and variations in stable isotopes in lake sediments to reconstruct paleoclimate. This section summarizes the pertinent conclusions from these studies, including evidence for a Holocene thermal maximum (HTM) and the onset of Neoglaciation. Study locations of selected studies are located in (Fig. 1a).

The longest lacustrine record in the Brooks Range comes from Burial Lake in the Noatak basin in the northwestern Brooks Range (Finkenbinder et al., 2015). As previously mentioned, sediments record dry conditions during the LGM. Following this, sediments display the highest levels of terrestrial and aquatic productivity from 16.5 to 8.8 ka, with a peak from 10.5 to 9.9 ka. Holocene sediments suggest landscape stabilization and relatively high and variable levels of aquatic productivity.

Much closer to the study area is Okpilak Lake (40 km east of Lake Peters), which is ~20 km downstream from several glaciers. This lake contains sedimentary and pollen evidence of warmer conditions in the mid-Holocene (Oswald et al., 2012). This evidence includes increasing organic material, a transition from Cyperaceae to *Betula*-dominated tundra, and a decrease in magnetic susceptibility after 8.5 ka. Other significant findings include the lack of a robust signal of Neoglacial cooling. Okpilak Lake contains one of the longest records (14.5 ka), and is located within a glaciated basin; however, changes in lake sediments may be influenced by channel shifts of the Okpilak River rather than climate parameters.

Wahoo Lake is 80 km west of Lake Peters. Vachula et al. (2017) suggested that, from 11.5 to 8.5 ka, summers were warm and dry based on high carbonate abundance and elevated

$\delta^{18}O$ values due to evaporative enrichment of lake water. These findings could reflect an early expression of the HTM. Evidence for Neoglaciation includes a decrease in $\delta^{18}O$ at 2.0-1.0 ka, possibly resulting from a temperature decrease or a winter precipitation increase.

Roughly 200 km to the southwest from Wahoo Lake, Anderson et al. (2001) analyzed isotopes in sediments from two lakes going back to 8.5 ka. Meli Lake $\delta^{18}O$ values suggest that conditions were more arid than present from 8.5 to 6.0 ka, and subsequently the region became increasingly wet. Temperatures inferred from Tangled Up Lake (about 100 km south of Meli Lake) using Charophyte calcite $\delta^{18}O$ suggest cool conditions for the last 6.7 ka, but with a warm period centered at 4.5 ka. Near the end of the mid-Holocene, conditions become slightly drier and warmer ($\delta^{18}O$ increased by 3 ‰), potentially indicating that the HTM in this region occurred around 4.2 ka. Neoglacial cooling could be represented by decreasing $\delta^{18}O$ values around 2.2 ka.

In the south-central Brooks Range, $\delta^{18}O$ values measured in *Chara*-stem encrustations from Takahula Lake provide a proxy for effective moisture over the last 8 ka (Clegg and Hu, 2010). Low $\delta^{18}O$ values indicate that effective moisture was relatively high from 8.0 to 5.0 ka, contrasting with the findings from elsewhere in the Brooks Range. At Takahula Lake, effective moisture subsequently decreased to a minimum around 4.0 ka, and then increased with fluctuations until 2.5 ka. A sharp increase around 0.4 ka was followed by a decrease to modern values. This record is likely affected by fluctuations in stream flow into the lake, and thus, I do not consider it further.

Apart from Okpilak Lake, none of these lakes are located within basins with modern glaciers; however, at Kurupa Lake, Boldt et al. (2015) reconstructed temperatures over the past 5.7 ka using reflectance spectroscopy to infer sedimentary chlorin which is considered to be a proxy for organic productivity. This approach estimated cooler summer temperatures (2 to 4 °C

below pre-industrial) from 5.7 to 3 ka, and warmer summer temperatures (1 to 2 °C above pre-industrial) from 3 to 2 ka. Following this warm period, reconstructed summer temperature reached a minimum around 250 AD and again around 650 AD. Subsequent cold phases occurred from around 1200–1300 and 1800–1900 AD. These cold periods were separated by relatively warm periods. Boldt (2013) also incorporated lichenometrically dated moraines, which yielded several distinct age populations, indicating moraine stabilization primarily centered around 150, 850, 1150, 1500, 1700, and 1850 AD. These dates of moraine stabilization are only moderately well correlated with inferred cold periods. Neoglacial cooling around 2 ka at Kurupa Lake correlates with other Brooks Range paleoclimate studies (Anderson et al., 2001; Vachula et al., 2017).

Two other important glacial lakes have been studied in the Brooks Range. Upper Kurupa Lake (Badding, 2012) and Shainin Lake located near Anaktuvuk Pass (Ceperley, 2014). Both of these integrated moraine and lake sediment analyses similar to Kurupa Lake but were not confident in reconstructing Holocene glacier extent. However, they were successful in adding important constraints to the ages of late glacial and Holocene moraines. Conclusions from these studies underscore the importance of lake site selection, and the inherent difficulties associated with asynchronous climate signals between paleoclimate proxies.

In addition to Upper and Lower Kurupa Lakes, Shainin Lake and Okpilak Lake, one other glacilacustrine study attempted to interpret changing environmental conditions and analyzed varve thickness at Blue Lake (Bird et al., 2009). Sediments recovered from Blue Lake were used to reconstruct temperature and precipitation over the last 2000 years. Although caution must be advised when correlating varve thickness with temperature, this study suggests warm

temperatures from 10 to 730 AD are represented by the thickest varves and an inferred increase in precipitation. Deceasing varve thickness around 730 AD suggests cooling.

Overall, the most consistent feature of lacustrine sediment studies is the onset of Neoglaciation by around 2 ka. Some evidence exists for warmer conditions during the mid-Holocene, but relatively few studies extend the full length of the Holocene to provide robust conclusions. Considerable variation in the timing, magnitude, and the direction of these proxies presents significant challenges in paleoclimate reconstructions. These discrepancies may be the result of heterogeneity in the way the specific locations and archives record changes in paleoclimate, or they may be a result of spatially and temporally variable paleoclimates.

*Other archives of regional paleoclimate*

Anchukaitis et al. (2013) reconstructed temperature spanning most of the last millennium near the Firth River in northeastern Alaska. This study found a warming trend in the last 30 year of the reconstruction that was 1.3 ± 0.4 °C warmer than the long-term preindustrial mean. Prior to this, multidecadal temperature fluctuations covary broadly with changes in natural radiative forcing with colder conditions in the thirteenth, seventeenth and nineteenth centuries.

Polyak et al. (2016) reconstructed Holocene sea-ice conditions in the Chukchi Sea margin using sediment cores that contained biomarkers inferred to be sensitive to changes in ice extent. They found evidence for sustained sea-ice cover during the Lateglacial period followed by trends that suggest an ice-marginal location during the early and middle Holocene. Other studies by de Vernal et al. (2013) suggest that the Chukchi Sea has been an area of marked variability in sea-ice cover.

# Chapter 2: 16,000 years of paleoenvironmental change from the Lake Peters-Schrader area, northeastern Brooks Range, Alaska

## Introduction

Long-term perspectives on natural climate variability help contextualize recent climate change. For example, over the last century the Arctic has warmed about 1.3 °C, roughly twice as fast as the global average (Bekryaev et al., 2010). This contrasts markedly with paleoclimate evidence that suggests a 0.5 °C cooling trend over the 2000 years that preceded the 20$^{th}$ century (Kaufman et al., 2009). Additional studies that characterize the natural climate variability of the Arctic are needed to further understand this abrupt contrast.

This study is a part of the Arctic Glacial Lakes project, a National Science Foundation Arctic System Science Program comparing three glaciated watersheds across environmental gradients. The overarching goal of this project is to develop the first quantitative system model to simulate the chain of processes that control how weather and climate are filtered through the glacier-hydrology-lake-sedimentation system and are recorded in glacilacustrine sediments. This study provides an initial description of the physical sediment properties and geochronology of several widely spaced core sites and provides a stratigraphic framework of sediments from Lake Peters and Lake Schrader in the northeastern Brooks Range, Alaska.

The Brooks Range in northern Alaska (N 68°, W 144-148°; Fig. 1a) is an area of considerable interest for paleoclimate research and concerted efforts have been made; however, this large region (~190 000 km$^2$) remains relatively understudied. More specifically, studies have

been conducted in the western and central Brooks Range, but comparatively little is known about the northeastern Brooks Range. Terrestrial paleoclimate archives including glacilacustrine sediments and moraine evidence from this region are likely affected by sea-ice extent due to the proximity to the Beaufort Sea (~100 km) because variations in sea-ice extent have a large effect on the temperature and precipitation for adjacent areas. For example, recent decreases in sea ice have been linked to increases in precipitation around the Arctic (Boisvert and Stroeve, 2015; Kopec et al., 2016).

Climatic variables influence glacilacustrine sediments. For example, in glaciated catchments, the basal erosion of glaciers produces silt- and clay-sized particles that remain in suspension in downstream lakes and obscure incoming short-wave radiation and hamper autochthonous primary production. This well-known glacial "rock flour" provides an important control on the amount of organic matter (OM) in lake sediments. Pioneering studies by Karlén (1976, 1981) combined moraine evidence with changes in visual stratigraphy, OM content, and sediment bulk density to reconstruct Holocene glacier variations in northern Fennoscandia.

Changes in regional hydroclimate affect lake levels and stream discharges, both of which have important influences on lake sediments. Variability in streamflow in terms of timing, magnitude, temperature, and sediment load interact with thermal stratification of lake waters to produce a range of depositional characteristics of lake sediments (Smith, 1978). Similar to glacier extent, variations in the frequency and magnitude of flood events influences the amount of OM in lake sediments as streams transport terrestrial vegetation during high-flow events.

Changes in primary production in seasonally ice-covered high-latitude lakes are affected by the length of the growing season (Smol, 1988). Similar to OM, another indicator of primary production in lakes is sedimentary chlorophyll content, which can be measured with non-

destructive visible reflectance spectroscopy (e.g. Das et al., 2005; Wolfe et al., 2006; Michelutti et al., 2010).

The primary objective of this study is to interpret environmental changes from glacilacustrine sediments from two lakes in northeastern Brooks Range, Alaska. I describe and correlate sedimentological units across multiple cores from both lakes by analyzing sediment properties (including dry and wet bulk density, OM content, grain-size distribution, and spectral reflectance data) and use Accelerator Mass Spectrometry (AMS) radiocarbon dating of aquatic and terrestrial macrofossils for age control. Comparison with other regional glacial, lacustrine, and sea-ice records provides an assessment and interpretation of regional climatic change in the northeastern Brooks Range dating back to around 16 ka.

## Study site

Lake Peters and Lake Schrader, also referred to as the Neruokpuk Lakes (N 69.3°, W 145.0°, 850 m a.s.l.) are a prominent pair (combined surface area 20 $km^2$) of lakes fed by a 320 $km^2$ catchment (Fig. 1b). Previous work has been undertaken at the study area in various disciplines: limnology (Hobbie, 1960, 1961), geology (Holmes and Lewis 1965; Reed, 1968), hydrology (Rainwater and Guy, 1958; Thurston, 2017), and environmental limnology (Gubala et al., 1995). This study provides the first description of the sedimentary sequence inferred from multiple cores across the lakes.

The study site is located within the 1000-km-long, east-west trending Brooks Range that separates the Arctic Coastal Plain to the north from the Yukon Basin to the south. The Brooks Range rises to its highest peaks (2735 m a.s.l.) in the northeastern portion of the range near the

study area. The lakes are connected by a 100-m-wide, 1-km-long, shallow interflow formed by the delta of a prominent drainage entering from the southwest (Whistler Creek, Fig. 1b). Lake Peters is upvalley and south of Lake Schrader, and receives the majority of streamflow from Carnivore Creek, and secondarily from Chamberlin Creek. The lakes are ice-covered from early October until mid-June through July, and both lakes tend to thermally stratify (Hobbie, 1961).

The Lake Peters catchment contains extant glaciers in seven valleys with a combined glacier-covered area of 12 $km^2$ (7.5%) out of the nearly 160 $km^2$ (Fig. 1b). In addition to inflow from Lake Peters, Lake Schrader receives water from Whistler Creek which is a 70 $km^2$ drainage with 1.3 $km^2$ (2%) of glacial cover, and Coke Creek, which drains an area of about 25 $km^2$ with 0.08 $km^2$ (0.3%) glacier cover (glacier areas are based on images from 2012). Nearby (~30 km east), the well-studied McCall Glacier is polythermal and is likely representative of other glaciers in the northeastern Brooks Range (Rabus and Echelmeyer, 1998). Additionally, a 1 °C temperature increase at 10 m depth between 1972 and 1995 in the McCall Glacier characterizes possible changes to the thermal structure of this and other glaciers due to warming trends (Rabus and Echelmeyer, 2002).

Lake Peters is surrounded by steep slopes with relief up to 1300 m adjacent to the lake (Fig. 1d). Immediately east (3 km), Mt. Chamberlin rises to 2712 m, making it the third highest peak in the North American Arctic (Nolan and DesLauriers, 2016). Lake Schrader is surrounded by comparatively lower relief (150 m) slopes of glacial till and colluvium and is bounded by a series of nested end moraines forming the bounding-topography of Lake Schrader (Fig. 1c). This Late Wisconsin-aged moraine was designated as the reference locality for the Schrader Glaciation by Holmes and Lewis (1965) and I correlate it with nearby Itkillik II moraines in the Jago and Okpilak River valleys dated to 23.2 ± 2.8 ka (Balascio et al., 2005).

The bedrock of the Lake Peters area is composed of Devonian to Jurassic sedimentary and meta-sedimentary rocks (Reed, 1968). This portion of the Brooks Range is thought to be tectonically active, on the basis of historic seismicity and deformed Quaternary sediments (Grantz et al., 1994). Lake Peters is located in the Arctic tundra biome, north of modern-day tree line in a region underlain by continuous permafrost with a thin active layer. Vegetation is dominantly shrub tundra (dwarf willow and birch), with tall willows along stream courses (Jorgenson and Heiner, 2003).

Long-term climate monitoring stations are sparse in northern Alaska. On the basis of meteorological data collected at the study site during this study, hourly averaged temperature along the shore of Lake Peters at 850 m a.s.l. from May 2015 to May 2016 was approximately -10 °C, with monthly averages ranging from -29°C (December) to 8 °C (July). Liquid precipitation for the same time period was 165 mm. Weather stations on the nearby McCall Glacier (2200 m a.s.l.) record 500 mm $yr^{-1}$ with about half of this precipitation falling as snow (Wendler et al., 1974). Both the Pacific and Arctic Oceans serve as moisture sources for this area of the Brooks Range (Rabus and Echelmeyer, 1998).

Two important semi-permanent synoptic features occur in the western Arctic, the Aleutian Low and the Beaufort High. Northern Hemisphere winters are characterized by a strengthening of the Aleutian Low, while summer patterns show Beaufort/Chukchi Lows with infrequent and weakened Aleutian Lows (Cassano et al., 2011). Regional variability in winter precipitation and temperatures are mainly attributed to changes in the position and strength of the Aleutian Low as it impacts storm tracks and synoptic-scale circulation (Rodionov et al., 2007).

## Methods

*Lake coring*

Sediment cores were extracted from six sites in Lake Peters and eight in Lake Schrader in April 2016 (Table 1). The coring followed a survey of sub-bottom stratigraphy (Lake Peters only) using a Knudsen 320BP acoustic profiler (200 kHz) and bathymetric mapping using a Lowrance sonar depth recorder in August 2015 (Fig. 2). Water depth at the core sites ranged from 13 to 56 m including approximately 1 m of ice at the time of coring. Seven, aluminum-cased vibracores ranging in length from 1.1 to 3.4 m (7.6 cm diameter) were collected using a Rossfelder P-3 underwater vibracorer from the two lakes in areas that displayed un-deformed acoustic stratigraphy. Furthermore, core locations were chosen to sample a range of sedimentation rates and avoid areas of deltaic and colluvial sedimentation. The weight and vibration of the vibracore disturbed the sediment-water interface, so at each site a corresponding surface core was taken using an Uwitec coring device. These surface cores ranged in length from 22 to 74 cm (9 cm diameter). Surface-core stratigraphy was correlated with the uppermost sections of adjacent vibracores based on prominent color bands and were spliced onto the vibracores to determine the offset between the vibracore and the lake floor (Table 1, column 7). Depths are referenced relative to (below) the lake floor (blf). Eight additional surface cores were taken to extend the spatial coverage across the large lakes including a small pond west of Lake Schrader.

*Geochronology*

In total, 29 samples of organic material for radiocarbon analysis were taken from two cores in Lake Peters and three cores in Lake Schrader (Table 2). Sediment samples (1-cm-thick, except one 3-cm-thick) were wet-sieved (150 μm) using distilled water mixed with sodium metahexaphosphate as a deflocculant to isolate macrofossils consisting of terrestrial and aquatic organic matter. Macrofossils were analyzed for $^{14}C$ at the Keck Carbon Cycle AMS Facility at the University of California, Irvine. $^{210}Pb$ and $^{137}Cs$ profiles from PTR48 and SCH8 were measured at the University of Southern California (Fig. 3a, Table 3). A $^{240/239}Pu$ profile was completed for core PTR2 at the Metropolitan State University of Denver (Table 3). Classical age-depth modeling using $^{14}C$ ages, radionuclides and the sediment-water interface (2016) was performed with a cubic spline (SCH8) or smooth spline (PTR49, PTR48, SCH6, SCH10) using the clam v2.1 code (Blaauw, 2010) except for the lower portion of SCH10, which used linear interpolation because of the step-wise increase in sedimentation rates in this section of the core (Fig. 3b). Individual $^{14}C$ ages are reported using output from CALIB 7.1 Radiocarbon Calibration (Stuiver et al., 2018).

*Sedimentological analyses*

Cores were split and initially analyzed using a multi-sensor core logger (MSCL) at 0.5 cm intervals at the Lacustrine Core Facility (LacCore), University of Minnesota (data for each core are in Appendices A, D-K). The MSCL utilized $^{137}Cs$-sourced gamma attenuation to measure wet bulk density (WBD), a surface sensor to measure magnetic susceptibility (MS), a

Konica Minolta spectrometer that measured reflectance at 10 nm increments between 400 and 700 nm, and a Geoscan V-5000-pixel linescan camera for high-definition core images. MS was not measured on vibracores due to the aluminum casing. One half of each split core was archived at LacCore, and the working halves were shipped to the Sedimentary Records of Environmental Change Laboratory at Northern Arizona University for sampling and analysis.

Using spectroscopy data, the relative absorption-band depth (RABD) between 660 and 670 nm was calculated as an estimate of sedimentary chlorophyll, which has absorption maxima between 660 and 690 nm (Wolfe et al., 2006). RABD was calculated using the following equation:

$$[(6 * R_{590} + 7 * R_{730})/13] / R_{min}\ (660;670)$$

where $R_{590}$ = reflectance at 590 nm, $R_{730}$ = reflectance at 730 nm, $R_{min}$ (660;670) = minimum reflectance at 660 or 670 nm (Rein and Sirocko, 2002).

The vibracores recovered the longest sedimentary sequence and were selected for further analysis, except for PTR46 and PTR51, which displayed considerable deformation. Dry bulk density (DBD) and organic matter (OM) content was measured on 1 $cm^3$ aliquots sampled at 5, 2, 2, 2.5, and 2 cm intervals for PTR48, PTR49, SCH6, SCH8 and SCH10, respectively. Sample intervals were based on inferred deposition rates to capture sub-centennial-scale variability. Volumetric samples were initially weighed to obtain wet bulk density (WBD), oven-dried overnight (12 hours) at 85 °C, and then re-weighed to obtain DBD. Samples were then heated to 550 °C for 5 hours and then reweighed to determine percent weight loss-on-ignition, which was used to estimate the OM content. Replicate analysis show that the reproducibility of the results is high (Appendix C).

Grain-size distributions were measured roughly every 10 cm and analyzed using a Coulter LS230 laser diffraction particle-size analyzer. Thirty samples from three cores (PTR48, SCH8, SCH10) were pretreated with 30% $H_2O_2$ and then heated overnight at 50 °C to remove organics. Additionally, 10% $Na_2CO_3$ was added for 5 hours and then removed to eliminate biogenic silica. The pretreated samples were deflocculated by adding sodium metahexaphosphate and shaking for 1 hour before performing particle-size analysis. No replicate analysis was performed for grain size.

## Results

*Geochronology and vertical accumulation rates*

Note: Data for each core are available in the Appendices.

Across the five vibracores, $^{14}C$ ages show only one age reversal, associated with a slump deposit at 41.5 cm blf in SCH6 (Fig. 3b, Table 2; individual depth vs. age plots are in appendices A – 2 through A –6). The northernmost core from Lake Peters (PTR48), located near the delta of Whistler Creek, has a basal age of 2.3 ka and displays variable accumulation rates (Fig. 3c). In terms of vertical accumulation, PTR48 varies between 1 to 5 mm $yr^{-1}$ in the lower portion of the core, decreasing to 0.53 mm $yr^{-1}$ in the upper 70 cm. PTR49 (1 km to the southwest, Fig. 2a) is located on a submerged ridge and has a basal age of 9.2 ka, with sedimentation rates of 0.4 mm $yr^{-1}$ in the lower 30 cm that decrease up core to 0.1 mm $yr^{-1}$. Lake Schrader cores from proximal to distal (SCH6, SCH8 and SCH10) have basal ages of 9.2, 13.1 and 15.9 ka and average Holocene sedimentation rates of 0.28, 0.23, and 0.07 mm $yr^{-1}$, respectively. Sedimentation rates in SCH10 vary by two orders of magnitude, from 2.8 mm $yr^{-1}$ over the lower 2.2 m of the core, to 0.07 mm $yr^{-1}$ over the upper 1.2 m. This sharp decrease in sedimentation rate occurs at around 15

ka. The lowest $^{14}C$ sample in SCH10 dates to 34 ka and was not included in the age model as this organic matter is likely older reworked material.

Short-lived isotope profiles constrain recent sedimentation rates at three core sites and show broad agreement with average Holocene rates (PTR48 and SCH8). Assuming the rate of supply of unsupported $^{210}Pb$ in PTR48 has remained constant, an exponential fit of unsupported $^{210}Pb$ activity indicates an average sedimentation rate of 1.06 ± 0.31 mm $yr^{-1}$ for sediments deposited during the last century (Fig. 3a, Table 3, Appendix E). This compares with $^{137}Cs$ peak activity at 35 mm depth in the core (assumed mid-depth of sample) indicating an average sedimentation rate of 0.66 ± 0.09 mm $yr^{-1}$ since the spike in atmospheric weapons testing in 1963.

In PTR2 (taken in 2013), $^{239+240}Pu$ shows a double peak at 9.75 and 8.25 cm blf, associated with nuclear weapons testing in 1959 and 1963 (Appleby, 2001), which suggests sedimentation rates of 1.80 and 1.67 mm $yr^{-1}$ (Fig. 3a, Table 3).

Near the top of SCH8, an exponential fit of unsupported $^{210}Pb$ activity indicates an average sedimentation rate of 0.28 ± 0.03 mm $yr^{-1}$ during the last century (Fig. 3a, Table 3, Appendix I). The peak in $^{137}Cs$ at 11.25 mm blf (assumed mid-depth of sample between 10 and 12.5 mm blf) suggests recent sedimentation rates of 0.21 ± 0.02 mm $yr^{-1}$.

Age-depth relations in surface cores that lack geochronology were inferred by visual correlations of marker beds and include PTR46A, PTR13A, PTR51A, SCH7, and SCH9. Sedimentation rates from PTR2 were used to infer the age-depth relation for nearby PTR46A (assuming 1.8 mm $yr^{-1}$). Sedimentation rates were estimated for PTR13A by comparing a dark, 4-mm-thick marker bed between core photos, which yielded a rate of 0.9 mm $yr^{-1}$. Similarly, sedimentation rates were estimated for PTR51 by comparing marker beds with PTR48 (using a

1.0 mm yr $^{-1}$ rate for PTR48), which yielded a rate of 1.35 mm yr$^{-1}$. Age-depth estimates for Lake Schrader surface cores were based on the ages from SCH8 and SCH10, and the age-depth model for the upper part of SCH6 was assumed to be a linear projection of average Holocene rates to overcome the artifacts from the cubic-spline age model as well as a slump deposit.

Average mass accumulation rates (MAR) over the last 400 yr BP of PTR48 (15 cm) and SCH8 (8.5 cm) are 0.047 g cm$^{-2}$ yr $^{-1}$ and 0.014 g cm$^{-2}$ yr $^{-1}$, respectively. PTR48 values are similar to previous estimates for the north end of Lake Peters (Thurston, 2017). The MAR for SCH8 is roughly half of that for PTR48, a trend that is similar to vertical accumulation rates (e.g. 0.53 vs. 0.23 mm yr $^{-1}$).

*Lithostratigraphy*

The lake sediments display considerable variation between lakes and core sites (Figs. 4-7). The proximity of individual core sites to tributary streams is a major influence on the sediment characteristics, with cores located near the modern- and paleo-channels of Whistler and Coke Creeks (PTR48, SCH4, SCH1, SCH5, SCH7) containing brown (5Y5/2), more organic-rich sandy beds, ranging in thickness from millimeters to several centimeters. Cores located away from inflow deltas generally lack these coarse-grained sediments and are dominantly composed of particles that have settled from suspension (PTR49, SCH6, SCH8, SCH10).

Sediments were classified into four distinct lithologic facies based on visible appearance and characteristic values for density, OM content, greyscale reflectance, and grain-size distribution (Fig. 4). The sequence of these facies is described in individual cores using the term

"units" (Appendix A). These units were correlated across the cores to form a temporal framework of six phases (*sensu* Bakke et al., 2005a) for the overall sedimentary sequence.

*Phase I* (approximately 16 to 15 ka) is represented only in the lower half of SCH10, and consists of brown-grey (GLEY 1 6/10Y) clayey silt (**Bgcs)** with light tan (5Y 8/1) laminations forming distinct couplets (Figs. 4, 5, and 6). These couplets range in thickness from centimeters at the bottom to millimeters in the upper part of Phase I. Although thin-section analysis was not performed, darker laminae are visibly coarse grained and gradationally fine upwards into lighter laminae, exhibiting a sharp overlying contact. Sediment deposited during Phase I are distinct from overlying sediments, with some of the highest values of WBD (ranging from 1.7 to 2.1 g $cm^{-3}$), highest clay content (35%), and lowest OM (< 3%) content (Fig. 5). Around 15 ka, density values increase abruptly and OM content decreases to around 2.5%, the lowest observed in this study.

*Phase II* (shortly after 15 ka to around 12.8 ka) is represented only in SCH10 (Fig. 5). The base is marked by an initial sharp decrease in WBD and further decreases from 1.6 to 1.4 g $cm^{-3}$. Sediment accumulation rates decrease by an order of magnitude between Phase I and Phase II (Fig. 3c), and sediments shift to light-colored silt (**Lsi**) (Fig. 5). OM is generally less than 5% and grain-size distributions consist of approximately 75% silt and 20% clay. Color alternates between tan (5Y 7/4) and dark olive green (5Y 6/6) laminations, with a relatively low frequency of distinct (1-10 mm thick) dark brown/black (5Y 3/2) organic-rich layers.

*Phase III* (around 12.8 to 10 ka) is represented in SCH8 and SCH10 by dark silt (**Dsi)** with >75% silt and 20% clay (Fig. 5). Color alternates between tan (5Y 7/4) and dark olive green (5Y 6/6) laminations, with relatively frequent dark brown/black (5Y 3/2) organic-rich layers. WBD decreases upwards in both cores and averages roughly 1.4 g $cm^{-3}$. Coarse-grained, 5- to

10-mm-thick beds between 280 and 270 cm blf in SCH8 correlate with high density values. OM content increases to ~7% in SCH10, while OM content in SCH8 shows no increase. Sedimentation rates increase in SCH8 between 11.6 and 11.1 (likely due to the presence of the course layers previously mentioned), while SCH10 sedimentation rates are fairly constant.

*Phase IV* (10 to 5 ka) is represented in PTR49 and all three Lake Schrader cores (Figs. 4, 5, and 6). The lithology returns to **Lsi**. Density increases towards a maximum around 8 ka (ranging from 1.5 to 1.7 g $cm^{-3}$, with OM showing correspondingly lower values (2-5%). In contrast, sediments in PTR49 contain the highest OM (6%) and lowest density (1.4 g $cm^{-3}$) values during this time, yet visually, sediments appear to have few organic-rich layers. The base of PTR49 contains two sub-angular, non-striated pebbles (~1.5 cm in diameter). The vibracore was not able to penetrate past these clasts suggesting the presence of an underlying rocky deposit, possibly glacial till.

*Phase V* (5 to 2 ka) sediments return to **Dsi**. Density values for Lake Schrader cores (1.3 to 1.5 g $cm^{-3}$) are among the lowest for the entire Holocene. OM increases to 6-8% and is consistently elevated across Lake Schrader cores from 5 to 2 ka. In contrast, OM content in PTR49 show a continuously decreasing trend with a step-wise drop around 3 ka (Fig. 4). Towards the end of Phase V (2.3 ka), the lower section of PTR48 contains **Bsa** (brown sand) consisting of brown (5Y 5/2) silty sand composed of distinct 5- to 50-mm-thick beds with sharp basal contacts.

*Phase VI* (2 ka to present) sediment is composed of **Lsi** in all cores. Sediment accumulation rates show a consistent increase for most cores (Fig. 3c). Density increases (0.2 to 0.3 g $cm^{-3}$) in all cores starting around 2 ka, while OM decreases (1-2%). In PTR49, OM content remains low. In PTR48, **Bsa** is absent after roughly 1.4 ka. Across the cores, the upper 1 to 20

cm is oxidized to reddish-brown (2.5Y 6/6), with cores located in shallower water tending to exhibit thicker red zones (e.g. PTR49 = 18 cm blf and SCH10 = 12 cm blf).

As noted earlier, surface cores from the proximal basin of Lake Schrader (Fig. 7a). (SCH4, SCH1, SCH5, SCH7) contain multiple 1- to 5-cm-thick layers of visibly coarse sediments that I interpret as trubidite deposits. Therefore, I focus primarily on SCH6, SCH8 and SCH10. WBD displays four distinct maxima, which seem to correspond with light-tan (5Y 7/4) sediments (Fig. 7a). These maxima date to CE ~900-1100, 1250-1400, 1500-1600, and 1700-1800. Similar to Lake Peters cores, RABD increases in the uppermost portions of nearly every core.

Lake Peters surface cores (with exception to PTR49 with relatively low sedimentation rates) show a consistent decrease in WBD starting around CE 1950 (Fig. 7b). RABD seems to consistently increase in the upper 3 cm blf in cores located in the northern portion of the lake in water depths less than 30 m.

## Discussion

*Glacial influence on sediment properties*

Glacilacustrine sediments can record changes in paleoenvironmental conditions but care must be taken to avoid over-interpretation by considering potentially complex interactions between climate, glacier behavior, and hydrology (e.g., Jannson et al., 2005; Hodder et al., 2007). One important physical parameter used to infer the abundance of rock flour in lacustrine sediment is the amount of organic matter. Many studies have shown that the amount of OM is inversely related to inorganic sediment flux (e.g. Karlén, 1976, 1981; Nesje et al., 1991; Dahl

and Nesje, 1994; Matthews et al., 2000; Nesje et al., 2000, 2001; Bakke et al., 2005a, 2005b). This characteristic of glacilacustrine sediment is caused by fine-grained particles resulting in high turbidity levels which hampers autochthonous primary production. In this model, the flux and subsequent deposition of minerogenic sediments in proglacial lakes is positively correlated with the relative size of glaciers within a catchment on multi-centennial to millennial time scales.

This model is supported by Hallet et al. (1996) who demonstrated that sediment yields are positively correlated with glacier size, among other important factors including climate regime and bedrock characteristics. Leonard (1997) demonstrated that sediment production varies with the time scale considered; long-term changes in sedimentation rates reflect changes in ice extent on the same scale, while on shorter time periods (decadal scale), increases in sedimentation rates are associated with glacier maximum stands, or with periods of glacier recession. This is due to the complexity associated with ice-driven sediment generation, lag times, and sediment availability associated with recently uncovered/destabilized sediment concurrent with glacier recession. Changes in glacier velocity, in part driven by thermal regime would also influence sediment production.

*Fluvial influence on sediment properties*

Fluvial processes have an important effect on sediment OM content in downstream lakes. In this study, OM is a combination of both autochthonous and allochthonous sources as material for $^{14}C$ analysis consisted of both terrestrial and aquatic plant macrofossils. Therefore, this proxy (OM), may reflect variations in both glacier size and stream flow. As noted earlier, cores located near inflows contain sediments deposited by dense underflows related to flood events. For example, the majority (about 40%) of the sediments in the lower portion of PTR48 consist of centimeter-scale sand beds with sharp basal contacts and varying amounts of terrestrial plant material. This suggests they were deposited by high-energy, underflows associated with large discharge events. Similar turbidites, are also found in several Lake Schrader surface cores located near the deltas of Whistler and Coke Creeks (Fig. 7a). In contrast, the thickness represented by turbidites in SCH8 (located 1 km from a major inflow) is less than 3% and turbidites are largely absent in PTR49, SCH6 and SCH10 (located > 2 km from inflows).

*Inter-relation among biophysical properties of lake sediment*

Several sedimentological variables were investigated using regression to quantify relations between parameters including density, OM content and grain size (Fig. 8). In Lake Schrader cores and PTR49, DBD and OM are negatively correlated (combined r values of -0.82, $p < 0.01$) suggesting that OM is an important control on sediment bulk density. In contrast, PTR48 displays a weaker relation between OM and DBD ($r = -0.22$ $p < 0.01$), suggesting a different sedimentological context. For all the vibracores (except PTR48), OM content is also closely related ($r = 0.83$, $p < 0.01$) to the water content (the difference in mass between WBD

and DBD). This relation between OM and water content in sediment has been documented in other lakes elsewhere (e.g. Menounos, 1997).

In addition to density and OM, several studies have related grain-size distributions of glacilacustrine sediment to glacier extent within the catchment (e.g. Bakke et al., 2005a, 2010). Sediment bulk density is affected by grain-size distributions; fine-grained and poorly sorted sediments correspond to higher bulk densities (Bakke et al., 2005a). More specifically, for glaciers in Norway, the medium silt fraction has been shown to significantly co-vary with DBD (Bakke et al., 2010). In this study, there was no apparent relation between density and grain-size distributions for Lake Schrader cores (Fig. 8). In contrast, in PTR48, dry bulk density and % clay content displays a negative correlation ($r = -0.70$, $p < 0.01$). Positive correlations between dry bulk density, mean grain size ($r = 0.44$, $p = 0.04$), and standard deviation (sorting) ($r = 0.48$, $p = 0.02$) are also present. This is likely a result of the abundance of turbidites in PTR48, where characteristically high-density values (e.g. 100 cm blf) tend to correspond to sandy layers that are poorly sorted and lack clay-sized particles. These relations help differentiate sediments that have been deposited via suspension settling from sediments deposited by dense underflows.

*Lateglacial (Phases I and II)*

Phase I sediments are interpreted to record glacial and paraglacial activity associated with the retreat of glaciers from near maximum extents. The age of the basal $^{14}C$ sample (~34,550 yr BP) in SCH10 is dubious. This sample is likely composed of older, reworked material and thus is not included in the age model. Additionally, the regional glacial geology suggests the presence of ice during the LGM at and downvalley of the core site (Kaufman et al., 2011). Below a more

reliable $^{14}C$ sample at 172.0 cm blf, the approximate number of rhythmic couplets roughly coincides with the projected basal age (16 ± 1.0 ka) using sedimentation rates calculated between this and the overlying $^{14}C$ age at 117.3 cm blf. I interpret these approximately 800 distinctly rhythmic laminations as clastic varves (e.g. Zolitschka et al., 2015). The absence of drop stones in these sediments suggests that ice had retreated upvalley of the lake by this time. The upward decrease in couplet thickness may represent declining sediment supply as glaciers in the Lake Peters area retreated (e.g. Ballantyne and Benn, 1994).

Phase I sediments provide insight into complex geomorphologic considerations related to moraines, lake terraces, and outwash deposits located on the northern and southwestern shores of Lake Peters and Lake Schrader, respectively (Fig. 2a). Outwash and lake-terrace deposits suggest that Lake Schrader was previously at least 13 m higher than present. Reed (1968) suggested that, sometime after the Peters Glaciation, the moraine enclosing Lake Schrader was downcut by the Kekiktuk River and resulted in a decrease in lake level. Early investigations (Holmes and Lewis, 1965; Reed, 1968) described deposits on the north end of Lake Peters, consisting of distinct knob-and-kettle topography and scattered boulders as the Peters Glaciation. They ascribed similar deposits in the valleys of Whistler and Coke Creeks, and Katak Creek (3 km east of Lake Schrader).. Adding to this complexity, my bathymetric survey, like Hobbie's (1960), shows a distinct, crescent-shaped ridge crossing the northern portion of Lake Peters that rises to ~6 m below the surface of the lake (Fig. 2a). Although Hobbie attributed this ridge to the presence of a highly resistant rock type (Kekiktuk Conglomerate), I argue that the size and convex-down-valley geometry suggest the presence of a submerged moraine.

Both the Peters Glaciation and the submerged moraines represent a pause or temporary readvance while glaciers were retreating behind the mountain front. They occupy

morphostratigraphic positions somewhat similar to the nearby (~35 km east of Lake Peters) Hubley moraine dated to 19.1 ± 2.8 ka (Balascio et al., 2005) as they are both the only moraine between the last glacial maximum and the Neoglacial moraines. Considering the chronological uncertainty, both of these moraines may be correlative to a widespread, late-Itkillik II advance dating to ~17 ka, which is known from several places in the northcentral Brooks Range (Pendleton et al., 2015) and is thought to be related to the decreasing size of Laurentide Ice Sheet (LIS) around ~19 ka. The reduced LIS could have reorganized atmospheric circulation bringing cold Arctic air masses and decreasing summer temperatures in northern Alaska (Dyke, 2004).

Towards the end of Phase I between 15.1 and 14.9 ka (unit $A_2$), sediment in SCH10 is marked by a distinct increase in density and decrease in OM values and a transition to thicker bedding (Fig. 5). I propose unit $A_2$ may be related to an increasing rate of glacial retreat, as sedimentation rates and density can initially increase during glacial retreat due to the presence of freshly uncovered glacial material (Leonard, 1997). Alternatively, unit $A_2$ is related to a glacial advance; however, this is unlikely as other sites in Alaska were experiencing glacial retreat driven by an increase in atmospheric $CO_2$ levels and summer insolation values (Briner et al., 2017).

Beginning in Phase II, a distinct decrease in both density and sedimentation rates occurs after 15 ka. This is perhaps one of the most robust paleoenvironmental signals in this study and indicates a substantial decrease in local glacier extents. Elsewhere in Alaska, Burial Lake (Finkenbinder et al., 2015) and Cascade Lake (Steen, 2016) show similar decreases in density around 15 ka, as does Lone Spruce Pond in the Ahklun Mountains (Kaufman et al., 2012). Elsewhere in the Brooks Range, it was initially suggested (Hamilton, 2003) that rapid alluviation documented in the Itkillik and Sagavanirktok River valleys between 15 and 13 ka represented a

glacial advance. However, this rapid alluviation is more likely the result of a continuation of a drastic reduction in glacier extents because multiple $^{10}$Be exposure ages on bedrock from the central Brooks Range suggest glaciers were close to, or even within their maximum Neoglacial extents by ~15 ka (Badding et al., 2013; Pendleton et al., 2015). This increase in the rate of glacier retreat is likely related to the Bølling transition, which began around 14.7 ka as dated in Greenland ice (Rasmussen et al., 2006). It also overlaps within age uncertainties with a 12 °C step-wise increase in July temperature inferred from chironomids from Hanging Lake, northern Yukon Territory (Kurek et al., 2009a) (Fig. 9).

In comparison to clear environmental changes around 15 ka, the Lateglacial-early Holocene transition is less pronounced. Beginning around 13 ka, two different cores contain variable WBD values with an overall average of ~1.5 g cm$^{-3}$, similar to Holocene values (1.45 g cm$^{-3}$) (Fig 9). The cores analyzed in this study lack evidence for a Younger Dryas (YD) climate fluctuation, and no candidate YD moraines have been identified. Moraine evidence for YD cooling is largely absent in Alaska, with the exception of moraines dating to 11.6 ± 0.3 ka in the northcentral Alaska Range (Young et al., 2009) and 12.4–11 ka in southwest Alaska (Briner et al., 2002). Few studies from northern Alaska have generated clear evidence for a climate fluctuation during the YD, a recent exception being isotopic evidence for YD cooling in fossil willows from the North Slope (Gaglioti et al., 2017). While further work is needed, the lack of signal in this study could be explained by the notion that Younger-Dryas cooling was mostly a wintertime phenomenon (Denton et al., 2005), and hence, may have had little effect on the size of glaciers in the Lake Peters area.

*Early and middle Holocene (Phases III and IV)*

Both SCH8 and SCH10 record early Holocene conditions and consist of **Dsi** (dark silt), which characterizes Phase III sediments (Figs. 5, 6, and 7). From 12–10 ka, SCH10 displays some of the highest values of OM content (6-9%) and relatively low WBD (1.3-1.4 g $cm^{-3}$) (Fig. 9). SCH8 shares a peak in OM at ~12 ka but then transitions to low OM. The high-density section just after 12 ka in SCH8 is likely related to the presence of several thin (~1 cm) coarse layers, interpreted as turbidites, which may explain the discordantly high-density values and low OM as compared with SCH10. Turbidites are otherwise rare in this core (except around 4 ka), suggesting they represent infrequent, high-discharge events.

In SCH10, the increase in OM from 12–10 ka is likely related to increased terrestrial and aquatic productivity associated with warmer-than-present summers, which were driven by orbitally controlled insolation that reached a maximum around ~10 ka for June at 70° N (Berger and Loutre, 1991). Similar increases in OM are found at Burial Lake in the northwestern Brooks Range (Finkenbinder et al., 2015). Summer temperatures reconstructed from Burial, Zagoskin, and Trout Lakes using fossil chironomidae assemblages provide additional evidence of increased summer temperatures (~1–2°C warmer than present) (Kurek et al., 2009b; Irvine et al., 2012) (Fig. 9). Other evidence suggesting regionally warm conditions during the early Holocene includes the highest rates of thaw-lake initiation and peat formation ages from 11–10 ka (Jones and Yu, 2010; Walter Anthony et al., 2014). Pollen evidence from Okpilak Lake (~40 km east of Lake Peters) suggests early Holocene warming represented by a shift from *Cyperaceae*- to *Betula*-dominated pollen assemblages around 12.0–11.6 ka (Oswald et al., 2012).

Phase IV sediments were deposited from 10–5 ka and consist of **Lsi** (light silt). Lake Schrader sediments show considerable variation but SCH8 increases in density from 10–8 ka, followed by a decrease from 8–5 ka. In SCH6, density reaches some of the highest values for the entire Holocene from 9–6 ka. OM shows a similar, but inverse pattern. This period of relatively high density could suggest that glaciers had expanded during this time; however, this contrasts with the majority of records from eastern Beringia. Instead, most temperature reconstructions show relatively warm conditions and there is little evidence of glacial advances around 8 ka in Alaska (Barclay et al., 2009).

Evidence of glacial advances around this time is present from elsewhere in the Arctic. Lake records suggest the presence of glaciers between 10 and 6 ka, in northeastern Baffin Island, followed by minimum extents from 6 to 2 ka (Thomas et al., 2012). In Scandinavia, marked early Holocene glacier fluctuations occurred throughout the early Holocene (Nesje, 2009). Considering this regional perspective, a glacier influence on Phase IV sediments cannot be entirely excluded.

Alternatively, decreased stream discharge under more arid conditions could explain the relatively high WBD and low OM content in Phase IV. In this scenario, less terrestrial OM would be transported via streams, resulting in higher sediment densities. Low lake levels across Alaska during the early Holocene provide evidence for aridity (Abbot et al., 2000; Barber and Finney, 2000; Finkenbinder et al., 2014; Kaufman et al., 2016). Additionally, isotopic evidence for early Holocene aridity is found at Wahoo Lake (80 km west of Lake Peters) where sediments are enriched in authogenic carbonate with elevated $\delta^{18}O$ values, possibly due to the evaporative enrichment of lake water from 11.5–8.9 ka (Vachula et al., 2017). Isotopic evidence from Meli Lake in the northcentral Brooks Range also suggests arid conditions from 8.5–6 ka (Anderson et

al., 2001). In contrast, low $\delta^{18}O$ values measured in *Chara*-stem encrustations from Takahula Lake in the southcentral Brooks Range (Clegg and Hu, 2010) indicate that effective moisture was relatively high from 8.0 to 5.0 ka; however, this record may have been affected by the avulsion of the inflow channel, and thus I do not include it in the comparison.

To distinguish between glacial advance and more arid conditions, sediment flux may provide a differing signal between glacial advances and periods of decreased stream discharge. During glacial advances, sediment flux is expected to increase whereas, during decreased stream discharges, flux should decrease. Sediment flux displays conflicting trends in Phase IV although it tends to be higher than in Phase V. Phase IV fluxes are similar to Phase VI; a time when glaciers are known to be re-forming in the catchment (Fig. 3c). Despite this somewhat equivocal change in sediment flux, I contend a reduction in discharge and delivery of organic matter to the lake is the most favorable explanation for high density sediments during Phase IV.

In contrast to Lake Schrader cores, PTR49 has relatively high OM content (7%) in Phase IV, which decreases with some variability until about 5 ka. This discordance is likely related to the depositional setting of PTR49, located at 13 m depth on the submerged moraine at the northern end of Lake Peters (Fig. 2). Four $^{14}C$ samples contain abundant aquatic insect remains including nearly intact caddisfly remnants, which suggest the presence of a nearby shore and rocky habitat as these macrofossils would not likely survive long transport distances. One mechanism to explain the presence of these macrofossils is lake-lowering due to decreased precipitation. Alternatively, the submerged moraine might have been roughly 5-10 m higher and subsided because, like many arctic moraines, it may have been ice-cored. Substantial amounts of ground ice exist in the region and have a pronounced effect on topography (Kanevskiy et al., 2012). Core PTR49 from the top of the ridge is the only core with pebbles at the base. If the core

captures the full post-glacial sediment sequence, the basal age of 9 ka might indicate that sedimentation in Lake Peters began around this time. However, this is unlikely considering the older age of sediments from Lake Schrader. Perhaps instead, the moraine was originally several meters higher and within wave base until melting subsurface ice caused the moraine to subside below wave base when it began accumulating sediment. It is also possible that the vibracore encountered a coarse layer and failed to retrieve the full post-glacial sequence.

In summary, phase IV sediments suggest arid and/or warm conditions and are somewhat difficult to reconcile with other available evidence.

*Late Holocene (Phase V)*

Around 5 ka, density decreases (with some variation) in Lake Schrader cores until ~3 ka (Fig. 9 and 10). OM increases during this time and reaches relatively high values, and together characterize Phase V sediments as **Dsi** (dark silt). This trend may record a decrease in glacier extent related to warmer summers and/or an increase in summer precipitation as both of these mechanisms could have resulted in the deposition of more autochthonous and/or allochthonous OM.

Mid-Holocene summer temperature reconstructions from Burial (Kurek et al., 2009b) and Trout Lakes (Irvine et al., 2012) show warmer-than-present values (Fig. 9). Qualitative temperatures inferred from Tangled Up Lake using *Chara* calcite $\delta^{18}O$ suggest cool conditions for the past 6.7 ka, but with a warm period around 4.5 ka (Anderson et al., 2001). In the north-central Brooks Range, a quantitative temperature reconstruction from Kurupa Lake using spectrally inferred sedimentary chlorophyll suggests summer temperatures were typically colder

than 20th century averages, but warmer from 3–2 ka (Boldt et al., 2015). Together, temperature reconstructions from northern Alaska bolster the interpretation that higher summer temperatures could have contributed to the protracted increase in OM during Phase V.

Increased precipitation may have also been a factor. Regional hydroclimate reconstructions from Meli Lake $\delta^{18}O$ values suggest increased moisture after 6 ka (Anderson et al., 2001) and rising lake levels at Wahoo Lake further support increasing effective moisture at this time (Vachula et al., 2017). Increases in precipitation may be related to decreases in sea-ice extent as modern examples of this have been observed around the Arctic (e.g. Boisvert and Stroeve, 2015; Kopec et al., 2016). Sea-ice reconstructions from the Chukchi Sea (~800 km to the northwest) indicate somewhat conflicting trends, but in general, suggest reduced extents at 6.5 and 3.5 ka (Farmer et al., 2011; Polyak et al., 2016; Stein et al., 2017). In contrast, the adjacent Beaufort Sea sea-ice reconstructions dating back to 4.5 ka suggest comparatively little variability (Bringué and Rochon, 2012).

Taken together, these records suggest an increase in Holocene summer temperatures coupled with increases in precipitation and reductions in sea-ice extent between 5 and 2 ka. Intriguingly, similar increases in OM are recorded in glacilacustrine sediments on Baffin Island (Thomas et al., 2010) and southern Greenland (Kaplan et al., 2002). However, this inferred warm and/or wet period appears to contrast with paleoclimate evidence throughout eastern Beringia where most records show a peak in summer warmth from 7–5 ka and subsequent cooling related to decreasing summer insolation (Kaufman et al., 2016). Perhaps Lake Peters and other Arctic sites that are heavily influenced by adjacent oceans record a consistent response to climate forcings that differs from more continental settings. More specifically, early Holocene warmth

seems to have a stronger signal in more northern sites across Arctic Canada and Greenland (Briner et al., 2016).

*Past 2000 years (Phase VI)*

Starting at 2 ka, sediments transition to **Lsi** (light silt), with density increasing (with fluctuations) and OM decreasing (with fluctuations) until the present. Sediment flux in nearly all cores increases during this time (Fig. 3c). I interpret this to represent the growth of glaciers in the catchment and/or decreases in precipitation, possibly related to greater sea-ice extent. Additional sedimentological evidence for the growth of glaciers in the catchment is present in PTR48. Turbidites dominate the lower portion of the core (Fig. 4). In the upper portion, a shift to finer-grained sediments suggests the catchment and paleo channel experienced aggradation and channel avulsion sometime after 1.4 ka, as the modern channel drains into Lake Schrader. Although several factors contribute to proglacial fluvial dynamics, glacial advances are associated with increases in sediment production and can result in aggradation and channel avulsion (Gurnell et al., 1999).

Moraine evidence from the nearby Chamberlin Glacier bolsters the interpretation that Phase VI sediments represent the expansion of mountain glaciers. The outermost moraine of the Chamberlin Glacier forefield was dated to ~2.6 ka using lichenometry and regional growth curves (Evison et al., 1996). Although cosmogenic $^{10}$Be exposure dating has generally superseded lichenometry as the preferred technique (Osborn et al., 2015), a recent comparison of Brooks Range lichen-inferred ages with $^{10}$Be surface exposure ages concluded that conflicts within and between these two methods made it unclear as to which is superior (Pendleton et al.,

2017). To confirm the findings of Evison et al. (1996) and to better understand the onset of Neoglaciation in the study area, I mapped moraines and lichen sizes in the forefields of the Chamberlin Glacier and the glacier in the tributary valley (GL3) to the south (Fig. B-1, Appendix L). Between these two valleys, I identified potentially correlative moraines that both exhibit subdued topography, visible soil development and hosted relatively large (40–56 mm) diameter lichens on boulder surfaces across 15, 30-m-long by 15-m-wide plots. At the Chamberlin Glacier forefield, Evison et al. (1996) inferred an age of ~1.0 ka for this moraine. Moraines upvalley of these ridges are flanked by steeper slopes and their boulder surfaces support smaller lichens, which Evison et al. (1996) assigned ages of 450 and 60 yr before 1950.

While I acknowledge the limitations of lichen-inferred ages, correlations between moraines in the Lake Peters area and moraines from around the Brooks Range show some similarities; foundational lichenometric studies suggest that most moraines in the Brooks Range formed after 2.5 ka (Pendleton et al., 2017). The oldest definitive moraine at Chamberlin Glacier may be associated with increased moraine frequency from elsewhere in the Brooks Range dating to 2.5–1.9 ka. A distinct increase in moraine frequency also occurs throughout the Brooks Range from 1.1–1.0 ka, which may be represented by the correlative moraine ridges in both Chamberlin and GL3 valleys. While uncertainty exists in the timing and relation to regional patterns in Neoglaciation, moraines and lake sediments both suggest the growth of glaciers in the Lake Peters area starting around 2 ka.

*Little Ice Age and modern glacier retreat*

The Little Ice Age (LIA) is widely recognized as the most recent period of Neoglacial cooling occurring from CE 1500–1850 (Matthews and Briffa, 2005). Inferred age-depth relationships based on $^{14}C$ chronologies from Lake Schrader surface cores suggest broadly synchronous increases in density during this time (Fig. 7a). These fluctuations roughly coincide with periods of known glacial advances throughout Alaska dating to: CE 1180s–1320s, 1540s–1710s and in the 1810s–1880s (Barclay et al., 2009).

In the northeastern Brooks Range, the youngest moraines are within 1 to 3 km of 2016 ice positions. These moraines have lichen-inferred ages 60 years before 1950, suggesting glaciers were at their most recent maximums around 1890 (Evison et al., 1996). A historical photograph of the Okpilak Glacier in 1907 (Leffingwell, 1919) shows that glacial retreat was underway by this time.

Modern glacier retreat could be represented in lake sediments by increases in sedimentation rates and OM content, as well as decreases in density over the last century. While considerable uncertainties exist concerning short-lived isotopes due to sampling resolution, average sedimentation rates based on $^{210}Pb$ suggest a 2- or 4-fold increase in PTR48 and a slight increase (8-34%) for SCH8. Estimates for SCH8 accord with Gubala et al. (1995) who found similar rates based on $^{210}Pb$ and $^{137}Cs$ (0.25–0.33 mm $yr^{-1}$) although it is unclear where in Lake Schrader the core site was located. $^{137}Cs$ inferred sedimentation rates are lower in both cores and suggest a decrease in sedimentation rates over the last ~50 years. These changes could represent glacier retreat similar to Leonard (1997) who documented increased sedimentation rates in the

decades following glacial retreat followed by subsequent decreases after sediment supply diminishes.

Several Lake Peters surface cores display density decreases starting around CE 1950 (Fig. 7b). While this would be expected in the uppermost portion of sediments due the lack of compaction, density decreases start as deep as 15 cm blf. This decrease may be related to decreases in rock flour production over the last several decades.

Another indicator of modern glacier retreat may be increases in OM content in the uppermost sediment of Lake Schrader vibracores (Fig. 5). In PTR48, however, OM does not increase, and it is unclear why this core shows an aberrant trend (Fig. 4). A more consistent trend is the increase in RABD in many of the surface cores (Fig. 7). This nearly ubiquitous increase in RABD in the top 4 cm suggests that, over the past century, autochthonous primary production has increased, similar to other Arctic lakes (e.g. Michelutti et al., 2005; Smol et al., 2005). In addition, increased OM and chlorophyll abundance could reflect increased delivery of organic material to the lake in response to higher river discharges.

As noted earlier, almost every core contains reddish-brown (2.5Y 6/6) zones near the sediment-water interface, which are thickest for cores located in shallow water. The distribution of these zones is independent of sediment type and age and may be related to the oxygen content of bottom water. Thermal stratification may reduce the mixing of deep bottom waters and oxygen consumption in isolated bottom waters leads to anoxic conditions (e.g. Davison, 1993). Cores located in relatively shallow water (<20 m) are probably exposed to oxygenated conditions more frequently. The presence of this redox boundary could suggest a shift in the lake's thermal and chemical structure as increased mixing due to longer ice-free seasons could have depressed and/or reduced a chemocline similar to warming-related observations of other high-latitude lakes

(e.g. Holm et al., 2012).

Alternatively, reddish-brown zones could simply represent a redox boundary within the sediment column. Reducing conditions at some critical depth would cause lake sediments to continuously transition to reduced conditions.

## Conclusion

I analyzed and described sedimentological characteristics across 12 surface cores and five widely spaced vibracores from a pair of glacier lakes in the northeastern Brooks Range. While the canonical glacier-meltwater-induced sedimentation model has been used extensively in Fennoscandia, I evoke an additional mechanism to explain changes in lake sediment parameters. Namely, I propose that sediment OM content is not solely controlled by glacier extent; rather, OM is also deposited during high-discharge events during which terrestrial vegetation is transported into lakes via river channels. Therefore, sediments in Lake Peters and Lake Schrader reflect environmental conditions including variations in precipitation and the size of glaciers within the catchment.

Basal sediments date to ~16 ka and represent an environment dominated by glacial and paraglacial processes. Initially high sedimentation rates suggest abundant sediment sources and rapid glacial retreat. Sedimentation rates then decreased as glaciers retreated farther up valley and sediment sources diminished. Low amounts of OM (~2%) suggest that vegetation was sparse until the early Holocene when sedimentation rates further decreased by an order of magnitude. Evidence for a climate fluctuation during the Younger Dryas is absent. A peak in OM from 12.4–10.2 ka suggests this area experienced similar increases in productivity as elsewhere in the region (e.g. Kurek et al., 2009b; Finkenbinder et al., 2015), and I attribute this to a maximum in

summer insolation around 10 ka. Subsequently, multiple cores show a trend towards high bulk density and low OM centered around 8 ka. While this could be interpreted as a glacial advance, regional evidence suggests this was a period of relative warmth and aridity (Anderson et al., 2001; Vachula et al., 2017). I suggest that a decrease in discharge could result in decreased transport of OM to the lake.

From 5–2 ka, a consistent increase in OM across Lake Schrader sediments suggest warmer and/or wetter conditions. Regional paleoclimate reconstructions bolster this interpretation, including decreased sea-ice extent over the Chukchi Sea centered around 3.5 ka (Farmer et al., 2011; Polyak et al., 2016; Stein et al., 2017) and relatively high summer temperatures in the north-central Brooks Range from 3–2 ka (Boldt et al., 2015). These findings differ from regional paleoclimate studies showing peak warmth from 7–5 ka (Kaufman et al., 2016), and more studies are needed to better understand this apparent discrepancy.

Glacilacustrine evidence of late Holocene glacial advances is present in lake sediments starting 2 ka and is accompanied by the formation of moraines within the catchment at that time (Evison et al., 1996), as well as elsewhere in the Brooks Range (Pendleton et al., 2017). Density increases in Lake Schrader sediments correspond to local and regional glacial advances around 1 ka and during the LIA. Glaciers in the Lake Peters catchment have likely been retreating since 1900. Recent increases in sedimentation rates, OM and chlorophyll content in the uppermost sediment likely record glacier recession.

# Chapter 3: Collated conclusions

- This study highlights the complexities in interpreting multiple sediment cores across relatively large lakes.
- Sedimentological characteristics across 12 surface cores and five widely spaced vibracores from Lake Peters and Lake Schrader in the northeastern Brooks Range reflect variations in river discharge and the size of glaciers within the catchment over the past 16 ka. To my knowledge, this is longest lacustrine record from a glacier-fed lake in the Brooks Range.
- During the early Holocene and from 5–2 ka, a consistent increase in organic-matter content across Lake Schrader sediments suggest warmer and/or wetter conditions. These findings differ from a large regional paleoclimate synthesis showing peak warmth from 7–5 ka and more studies are needed to better understand this apparent discrepancy.
- Moraine mapping confirmed the presence of Neoglacial moraines in the northeastern Brooks Range.
- Future work should focus on the intriguing paleoenvironmental and investigate the potential for a Lateglacial varve chronology. Furthermore, additional sedimentological analysis techniques may be able to discern sources of organic matter as well as reconstruct hydroclimate using variations in isotopes. Cosmogenic surface exposure dating of moraines could provide insight into Lateglacial standstills and Neoglacial advances.

# References-(Combined)


Abbott, M.B., Edwards, M.E., Finney, B.P., 2010. A 40,000-yr record of environmental change from Burial Lake in Northwest Alaska. Quaternary Research 74, 156–165.

Abbott, M.B., Finney, B.P., Edwards, M.E., Kelts, K.R., 2000. Lake-level reconstruction and paleohydrology of Birch Lake, central Alaska, based on seismic reflection profiles and core transects. Quaternary Research 53, 154–166.

Anchukaitis, K.J., D'Arrigo, R.D., Andreu-Hayles, L., Frank, D., Verstege, A., Curtis, A., Buckley, B.M., Jacoby, G.C., Cook, E.R., 2013. Tree-ring-reconstructed summer temperatures from Northwestern North America during the last nine centuries. Journal of Climate 26, 3001–3012. doi:10.1175/JCLI-D-11-00139.1.

Anderson, L., Abbott, M.B., Finney, B.P., 2001. Holocene climate inferred from oxygen isotope ratios in lake sediments, central Brooks Range, Alaska. Quaternary Research 55(3), 313–321. doi:10.1006/qres.2001.2219.

Anderson, P.M., 1985. Late Quaternary vegetational change in the Kotzebue sound area, northwestern Alaska. Quaternary Research 24, 307–321. doi:10.1016/0033-5894(85)90053-5.

Anderson, P.M., 1988. Late Quaternary pollen records from the Kobuk and Noatak River drainages, northwestern Alaska. Quaternary Research 29, 263–276.

Anderson, P.M., Brubaker, L.B., 1994. Vegetation history of north central Alaska: A mapped summary of late-Quaternary pollen data. Quaternary Science Reviews 41, 306–315.

Appleby, P.G., 2001. Chronostratigraphic techniques in recent sediments. In, Last, W.M., Smol, J.P., Eds., Tracking Environmental Change Using Lake Sediments, Volume 1: Basin Analysis, Coring and Chronological Techniques. Kluwer Academic Publisher, Dordrecht, The Netherlands, 171–204.

Badding, M.E., 2012. Reconstructing late Pleistocene deglaciation and Holocene glacial advance using lacustrine sediments and $^{10}$Be exposure dating, Brooks Range, Arctic Alaska. M.S. Thesis. University at Buffalo, State University of New York. 112 pp.

Badding, M.E., Briner, J.P., Kaufman, D.S., 2013. $^{10}$Be ages of late Pleistocene deglaciation and Neoglaciation in the north-central Brooks Range, Arctic Alaska. Journal of Quaternary Science 28, 95–102. doi:10.1002/jqs.2596.

Bakke, J., Lie, Ø., Nesje, A., Dahl, S.O., Paasche, Ø., 2005a. Utilizing physical sediment variability in glacier-fed lakes for continuous glacier reconstructions during the Holocene, northern Folgefonna, western Norway. The Holocene 15(2), 161–176.

Bakke, J.S., Dahl, S.O., Paasche, Ø., Løvlie, R., Nesje, A., 2005b. Glacier fluctuations, equilibrium-line altitudes and paleoclimate in Lyngen, northern Norway, during the Lateglacial and Holocene. The Holocene 15, 518–540.

Bakke, J.S., Dahl, S.O., Paasche, Ø., Simonsen, J.R., Kvisvik, B., Bakke, K., Nesje, A., 2010. A complete record of Holocene glacier variability at Austre Okstindbreen, northern Norway: an integrated approach. Quaternary Science Reviews 29, 1246–1262. doi:10.1016/j.quascirev.2010.02.012.

Bakke, J., Trachsel, M., Kvisvik, B.C., Nesje, A., Lyså, A., 2013. Numerical analyses of a multi-proxy data set from a distal glacier-fed lake, Sørsendalsvatn, western Norway. Quaternary Science Reviews 73, 182–195. doi:10.1016/j.quascirev.2013.05.003.

Balascio, N.L., Kaufman, D.S., Briner, J.P., Manley, W.F., 2005. Late Pleistocene glacial geology of the Okpilak-Kongakut Rivers region, northeastern Brooks Range. Alaska. Arctic, Antarctic and Alpine Research 37, 416–424.

Ballantyne, C.K., Benn, D.I., 1994. Paraglacial slope adjustment and resedimentation following recent glacier retreat, Fåbergstølsdalen, Norway. Arctic and Alpine Research 26, 255– 69.

Barber, V.A., Finney, B.P., 2000. Late Quaternary paleoclimatic reconstructions for interior Alaska based on paleolake-level data and hydrologic models. Journal of Paleolimnology 24, 29-41.

Barclay, D.J., Wiles, G.C., Calkin, P.E., 2009. Holocene glacier fluctuations in Alaska. Quaternary Science Reviews 28, 2034–2048. doi:10.1016/j.quascirev.2009.01.016.

Bekryaev, R.V., Polyakov, I.V., Alexeev, V.A., 2010. Role of polar amplification in long-term surface air temperature variations and modern arctic warming. Journal of Climate 23, 3888–3906. doi:10.1175/2010JCLI3297.1.

Benn, D.I., Evans, D.J., 2010. Glaciers and Glaciation, 2nd Edition. Routledge, New York.

Berger, A., Loutre, M.F., 1991. Insolation values for the climate of the last 10 million years. Quaternary Science Reviews 10, 297–317. doi:10.1016/0277-3791(91)90033-Q.

Bird, B.W., Abbott, M.B., Finney, B.P., Kutchko, B., 2009. A 2000 year varve-based climate record from the central Brooks Range, Alaska; Late Holocene climate and environmental change inferred from Arctic lake sediment. Journal of Paleolimnology 41, 25–41. doi:10.1007/s10933-008-9262-y.

Blaauw, M., 2010. Methods and code for "classical" age-modelling of radiocarbon sequences. Quaternary Geochronology 512–518. doi:10.1016/j.quageo.2010.01.002.

Boisvert, L.N., Stroeve, J.C., 2015. The Arctic is becoming warmer and wetter as revealed by the Atmospheric Infrared Sounder. Geophysical Research Letter 42, 4439-4446.

Boldt, B.R., 2013. A multi-proxy approach to reconstructing Holocene climate variability at Kurupa River Valley, Arctic Alaska. M.S. Thesis. Northern Arizona University. 114 pp.

Boldt, B.R., Kaufman, D.S., McKay, N.P., Briner, J.P., 2015. Holocene summer temperature reconstruction from sedimentary chlorophyll content, with treatment of age uncertainties, Kurupa Lake, Arctic Alaska. The Holocene 25, 641–650. doi:10.1177/0959683614565929.

Bradley, R.S., 2015. Paleoclimatology: Reconstructing Climates of the Quaternary, Third. ed. Academic Press. doi:10.1029/EO081i050p00613-01.

Briner, J.P., Kaufman, D.S., Werner, A., Caffee, M., Levy, L., Manley, W.F., Kaplan, M.R., Finkel, R.C., 2002. Glacier readvance during the late glacial (Younger Dryas?) in the Ahklun Mountains, southwestern Alaska. Geology 30, 679–682.

Briner, J.P. McKay N.P., Axford, Y., Bennike, O., Bradley R.S., de Vernal, A., Fisher, D., Francus, P., Fréchette, B., Gajewski, K, Jennings, A., Kaufman, D.S., Miller, G., Rouston, C. Wagner, B., 2016. Holocene climate change in Arctic Canada and Greenland. Quaternary Science Reviews 147, 340-364, https://doi.org/10.1016/j.quascirev.2016.02.010.

Briner, J.P., Tulenko, J.P., Kaufman, D.S., Young, N.E., Baichtal, J.F., Lesnek, A., 2017. The last deglaciation of Alaska. Cuadernos de Investigación Geográfica 43. doi:http://doi.org/10.18172/cig.3229.

Bringué, M., Rochon, A., 2012. Late Holocene paleoceanography and climate variability over the Mackenzie slope (Beaufort Sea, Canadian Arctic). Marine Geology 291-294, 83-96.

Calkin, P.E., 1988. Holocene glaciation of Alaska (and adjoining Yukon Territory, Canada). Quaternary Science Reviews 7, 159–184. doi:10.1016/0277-3791(88)90004-2.

Calkin, P.E., Ellis, J.M., 1980. A lichenometric dating curve and its application to Holocene glacier studies in the central Brooks Range, Alaska. Arctic and Alpine Research 12(3), 245–264.

Cassano, E.N., Cassano, J.J., Nolan, M., 2011. Synoptic weather pattern controls on temperature in Alaska. Journal of Geophysical Research Atmospheres 116, 1–19. doi:10.1029/2010JD015341.

Clegg, B.F., Hu, F.S., 2010. An oxygen-isotope record of Holocene climate change in the south-central Brooks Range, Alaska. Quaternary Science Reviews 29(7), 928–939. doi:10.1016/j.quascirev.2009.12.009.

Ceperley, E.G., 2014. Reconstructing late Pleistocene and Holocene glacier fluctuations using cosmogenic $^{10}$Be exposure dating and lacustrine sediment, Brooks Range, Arctic Alaska. M.S. Thesis. The University at Buffalo, State University of New York. 114 pp.

Dahl, S.O., Bakke, J., Lie, Ø., Nesje, A., 2003. Reconstruction of former glacier equilibrium-line altitudes based on proglacial sites: an evaluation of approaches and selection of sites. Quaternary Science Reviews 22(2), 275–287. doi:10.1016/S0277-3791(02)00135-X.

Dahl, S.O., Nesje, A., 1992. Paleoclimatic implications based on equilibrium-line altitude depressions of reconstructed Younger Dryas and Holocene cirque glaciers in inner Nordfjord, western Norway. Paleogeography, Paleoclimatology, Paleoecology 94, 87–97. doi:10.1016/0031-0182(92)90114-K.

Dahl, S.O., Nesje, A., 1994. Holocene glacier fluctuations at Hardangerjokulen, central-southern Norway: a high-resolution composite chronology from lacustrine and terrestrial deposits. The Holocene 4, 269–277.

Das, B., Vinebrooks, R., D., Sanchez-Azofeifa, A., Rivard, B., Wolfe, A.P., 2005. Inferring sedimentary concentrations with reflectance spectroscopy: A novel approach to reconstructing historical changes in the trophic status of mountain lakes. Canadian Journal of Fisheries and Aquatic Science 62, 1067–1078.

Davis, P.T., Menounos, B., Osborn, G., 2009. Holocene and latest Pleistocene alpine glacier fluctuations: a global perspective. Quaternary Science Reviews 28(21–22), 2021–2033. doi:10.1016/j.quascirev.2009.05.020.

Davison, W., 1993. Iron and manganese in lakes. Earth-Science Reviews 34, 119-163.

de Vernal, A., Hillaire-marcel, C., Rochon, A., Fréchette, B., Henry, M., Solignac, S., Bonnet, S., 2013. Dinocyst-based reconstructions of sea ice cover concentration during the Holocene in the Arctic Ocean, the northern North Atlantic Ocean and its adjacent seas. Quaternary Science Reviews 79, 111–121. doi:10.1016/j.quascirev.2013.07.006.

Delcourt, C., Pattyn, F., Nolan, M., 2008. Modelling historical and recent mass loss of McCall Glacier, Alaska, USA. Cryosphere 2, 23–31.

Denton, G.H., Alley, R.B., Comer, G.C., Broecker, W.S., 2005. The role of seasonality in abrupt climate change. Quaternary Science Reviews 24, 1159-1182. doi:10.1016/j.quascirev.2004.12.002.

Denton, G.H., Karlén, W., 1973. Holocene climatic variations-their pattern and possible cause. Quaternary Research 3, 155–174.

Detterman, R. L., Bowsher, A. L., and Dutro, J. T., Jr., 1958. Glaciation on the Arctic Slope of the Brooks Range, northern Alaska. Arctic 11(1), 43–61.

Dyke, A.S., 2004. An outline of North American deglaciation with emphasis on central and northern Canada, in Ehlers, J., and Gibbard, P.L., Eds., Quaternary Glaciations—Extent and Chronology: Part II: North America: Amsterdam, Elsevier, Developments in Quaternary Sciences, v. 2, 373–424. doi:10.1016/S1571-0866(04)80209-4.

Edwards, M.E., Barker, E.D., 1994. Climate and vegetation in northeastern Alaska 18,000 yr B.P.-present. Paleogeography, Paleoclimatology, Paleoecology 109, 127–135. doi:10.1016/0031-0182(94)90172-4.

Eisner, W.R., Colinvauxt, P.A., 1992. Late Quaternary pollen records from Oil Lake and Feniak Lake, Alaska, U.S.A. Arctic and Alpine Research 24, 56–63.

Ellis, J.M., Calkin, P.E., 1984. Chronology of Holocene glaciation, central Brooks Range, Alaska. Geological Society of America Bulletin 95, 897–912.

Ellis, J.M., Hamilton, T.D., Calkin, P.E., 1981. Holocene glaciation of the Arrigetch Peaks, Brooks Range, Alaska. Arctic 34(2), 158–168.

Evison, L., Calkin, P.E., Ellis, J.M., 1996. Late-Holocene glaciation and twentieth century retreat, northeastern Brooks Range, Alaska. The Holocene 6(1), 17–24.

Farmer, J.R., Cronin, T.M., de Vernal, A., Dwyer, G.S., Keigwin, L.D., Thunell, R.C., 2011. Western Arctic Ocean temperature variability during the last 8000 years. Geophysical Research Letter 38, L24602. http://dx.doi.org/10.1029/2011GL049714.

Finkenbinder, M.S., Abbott, M.B., Edwards, M.E., Langdon, C.T., Steinman, B.A., Finney, B.P., 2014. A 31,000 year record of paleoenvironmental and lake-level change from Harding Lake, Alaska, USA. Quaternary Science Reviews 87, 98–113. http://dx.doi.org/10.1016/j.quascirev.2014.01.005.

Finkenbinder, M.S., Abbott, M.B., Finney, B.P., Stoner, J.S., Dorfman, J.M., 2015. A multi-proxy reconstruction of environmental change spanning the last 37,000 years from Burial Lake, Arctic Alaska. Quaternary Science Reviews 126, 227–241. http://dx.doi.org/10.1016/j.quascirev.2015.08.031.

Gaglioti, B.V., Mann, D.H., Wooller, M.J., Jones, B.M., Wiles, G.C., Groves, P., Kunz, M.L., Baughman, C.A., Reanier, R.E., 2017. Younger-Dryas cooling and sea-ice feedbacks were prominent features of the Pleistocene-Holocene transition in Arctic Alaska. Quaternary Science Reviews 169, 330-343. http://dx.doi.org/10.1016/j.quascirev.2017.05.012.

Geck, J., Hock, R., Nolan, M., 2013. Geodetic Mass Balance of Glaciers in the Central Brooks Range, Alaska, U.S.A., from 1970 to 2001. Arctic, Antarctic and Alpine Research 45, 29–38. doi:10.1657/1938-4246-45.1.29.

Grantz, A., May, S.D., Hart, P.E., 1994. Geology of the Arctic continental margin of Alaska. In Plafker, G., Berg, H.C., Eds., The geology of Alaska: Geological Society of America, The Geology of North America G-1, 17–48.

Gubala, C.P., Landers, D.H., Monetti, M., Heit, M., Wade, T., Lasorsa, B., Allen-Gil, S., 1995. The rates of accumulation and chronologies of atmospherically derived pollutants in Arctic

Alaska, USA. The Science of the Total Environment 160/161, 347–361. doi:10.1016/0048-9697(95)04368-B.

Gurnell, A.M., Edwards, P.J., Petts, G.E., Ward, J.V., 1999. A conceptual model for alpine proglacial river channel evolution under changing climatic conditions. Catena 38, 223-242.

Hallet, B., Hunter, L., Bogen, J., 1996. Rates of erosion and sediment evacuation by glaciers: A review of field data and their implications. Global and Planetary Change 12, 213–235. doi:10.1016/0921-8181(95)00021-6.

Hamilton, T.D., 1986. Late Cenozoic glaciation of the central Brooks Range. In Hamilton, T.D., Reed, K.M., and Thorson, R.M., Eds., Glaciation in Alaska: the geologic record. Alaska Geological Society, Anchorage.

Hamilton, T.D., 2003. Surficial geology of the Dalton Highway (Itkillik-Sagavanirktok Rivers) area, southern Arctic Foothills. Professional Report, 121. Alaska Department of Natural Resources/Division Geological and Geophysical Surveys.

Hamilton, T.D., Porter, S.C., 1975. Itkillik glaciation in the Brooks Range, northern Alaska. Quaternary Research 5, 471-497.

Hartman, B., Wendler, G., 2005. The significance of the 1976 Pacific climate shift in the climatology of Alaska. Journal of Climate 18, 4824–4839.

Hartmann, D.L., A.M.G. Klein Tank, M. Rusticucci, L.V. Alexander, S. Brönnimann, Y. Charabi, F.J. Dentener, E.J. Dlugokencky, D.R. Easterling, A. Kaplan, B.J. Soden, P.W. Thorne, M. Wild and P.M. Zhai, 2013: Observations: Atmosphere and Surface. In: Climate Change 2013: The Physical Science Basis. Contribution of Working Group I to the Fifth Assessment Report of the Intergovernmental Panel on Climate Change [Stocker, T.F., D. Qin, G.-K. Plattner, M. Tignor, S.K. Allen, J. Boschung, A. Nauels, Y. Xia, V. Bex and P.M. Midgley (eds.)]. Cambridge University Press, Cambridge, United Kingdom and New York, NY, USA.

Haworth, L.A., Calkin, P.E., Ellis, J.M., 1986. Direct measurement of lichen growth in the central Brooks Range, Alaska, U.S.A., and its application to lichenometric dating. Arctic and Alpine Research 18, 289–296.

Hobbie, J.E., 1960. Limnological studies on Lakes Peters and Schrader, Alaska. Rep. 5 to Geophys. Res. Div., Air Force Cambridge Rcs. Center, Contr. AF 19(604)-2959.

Hobbie, J.E., 1961. Summer temperatures in Lake Schrader, Alaska. Limnology and Oceanography 6, 326-329.

Hodder K.R., Gilbert R., Desloges J.R. Glaciolacustrine varved sediment as an alpine hydroclimatic proxy. Journal of Paleolimnology. 2007 Oct 1;38(3):365-94

Holm, T. M., Koinig, K.A., Andersen, T., Donali, E., Hormes, A., Klaveness, D., Psenner, R., 2012. Rapid physicochemical changes in the High Arctic Lake Kongressvatn caused by recent climate change. Aquatic Science 74, 385-395.

Holmes, G.W., Lewis, C.R., 1965. Quaternary geology of the Mount Chamberlin area, Brooks Range, Alaska. U.S. Geological Survey Bulletin 1201-B, 1–38.

Irvine, F., Cwynar, L.C., Vermaire, J.C., Rees, A.B.H., 2012. Midge-inferred temperature reconstructions and vegetation change over the last ~15,000 years from Trout Lake, northern Yukon Territory, eastern Beringia. Journal of Paleolimnology 48, 133-146.

Jansson, P., Rosqvist, G., Schneider, T., 2005. Glacier fluctuations, suspended sediment flux and glacio-lacustrine sediments. Geografiska Annaler Series A Physical Geography 87, 37–50.

Jochimsen, M., 1973. Does the size of lichen thalli really constitute a valid measure for dating glacial deposits? Arctic and Alpine Research 5, 417–424.

Jones, M.C., Yu, Z., 2010. Rapid deglacial and early Holocene expansion of peatlands in Alaska. Proceedings of the National Academy of Sciences 107, 7347–7352. doi:10.1073/pnas.0911387107.

Jorgenson, M.T., Heiner, M., 2003. Ecosystems of Northern Alaska. 1:2.5 million-scale map by ABR, Inc., Fairbanks, AK and The Nature Conservancy, Anchorage, AK.

Kanevskiy, M., Shur, Y., Jorgenson, M.T., Ping, C.L., Michaelson, G.J., Fortier, D., Stephani, E., Dillon. M., Tumskoy, V., 2013. Ground ice in the upper permafrost of the Beaufort Sea coast of Alaska. Cold Regions Science and Technology 85, 56-70.

Kaplan, M.R., Wolfe, A.P., Miller, G.H., 2002. Holocene environmental variability in southern Greenland inferred from lake sediments. Quaternary Research 58, 149-159.

Karlén, W., 1976. Lacustrine sediments and tree-limit variations as indicators of Holocene climatic fluctuations in Lappland, Northern Sweden. Geografiska Annaler Series A Physical Geography 58, 1–34.

Karlén, W., 1981. Lacustrine sediment studies. Geografiska Annaler Series A Physical Geography 63, 273–281.

Karlén, W., Matthews, J.A., 1992. Reconstructing Holocene glacier variations from glacial lake sediments: Studies from Nordvestlandet and Jostedalsbreen-Jotunheimen, Southern Norway. Geografiska Annaler Series A Physical Geography 74, 327–348.

Kaufman, D.S., Ager, T.A., Anderson, N.J., Anderson, P.M., Andrews, J.T., Bartelein, P.J., Burbaker, L.B., Coats, L.L., Cwynar, L.C., Duval, M.L., Dyke, A.S., Edwards, M.E., Eiser, W.R., Gajewski, K., Geisodottir, A., Hu, F.S., Jennings, A.E., Kaplan, M.R., Kewin, M.W., Lozhkin, A.V., MacDonald, G.M., Miller, G.H., Mock, C.J., Oswald, W.W., Otto-Blisner, B.L.,

Porinchu, D.F., Rühland, K., Smol, J.P., Steig, E.J.,Wolfe, B.B., 2004. Holocene thermal maximum in the western Arctic (0-180 W). Quaternary Science Reviews 23, 529-560.

Kaufman, D.S., Axford, Y., Anderson, R.S. Lamoureux, S.F., Schindler, D.E., Walker, I.R., Werner, A., 2012. A multi-proxy record of the Last Glacial Maximum and last 14,500 years of paleoenvironmental change at Lone Spruce Pond, southwestern Alaska. Journal of Paleolimnology 48, 9-26.

Kaufman, D.S., Axford, Y.L., Henderson, A.C.G., Mckay, N.P., Oswald, W.W., Saenger, C., Anderson, R.S., Bailey, H.L., Clegg, B., Gajewski, K., Sheng, F., Jones, M.C., Massa, C., Routson, C.C., Werner, A., Wooller, M.J., Yu, Z., 2016. Holocene climate changes in eastern Beringia (NW North America)-A systematic review of multi-proxy evidence. Quaternary Science Reviews 147, 312–339. doi:10.1016/j.quascirev.2015.10.021.

Kaufman, D.S., Schneider, D.P., McKay, N.P., Ammann, C.M., Bradley, R.S., Briffa, K.R., Miller, G.H., Otto-Bliesner, B.L., Overpeck, J.T., Vinther, B.M., Arctic Lakes 2k Project Members, 2009. Recent warming reverses long-term Arctic cooling. Science 325, 1236–1239. doi:10.1126/science.1173983.

Kaufman, D.S., Young, N.E., Briner, J.P., Manley, W.F., 2011. Alaska Palaeo-Glacier Atlas (Version 2) In: Ehlers, J. & Gibbard, P.L. (eds), Quaternary Glaciations Extent and Chronology, Part IV: A Closer Look., Developments in Quaternary Science 15. Amsterdam. doi:10.1016/B978-0-444-53447-7.00033-7.

Kelly, P.M., Jones, P.D., Sear, C.B., Cherry, B.S.G., Tavakol, R.K., 1982. Variations in surface air temperatures: Part 2. Arctic regions, 1881–1980. Monthly Weather Review 110, 71–83.

Klein, E.S., Nolan, M., McConnell, J., Sigl, M., Cherry, J., Young, J., Welker, J.M., 2016. McCall Glacier record of Arctic climate change: Interpreting a northern Alaska ice core with regional water isotopes. Quaternary Science Reviews 131, 274–284. doi:10.1016/j.quascirev.2015.07.030

Klok, E.J., Nolan, M., Van Den Broeke, M.R., 2006. Analysis of meteorological data and the surface energy balance of McCall Glacier, Alaska, USA. Journal of Glaciology 51, 451–461. doi:10.3189/172756505781829241

Kopec, B.G., Feng, X., Michel, F.A., Posmentier, E.S., 2016. Influence of sea ice on Arctic precipitation. Proceedings of the National Academy of Sciences 113, 46-51.

Koppes, M., Hallet, B., Rignot, E., Wellner, J.S., Boldt, K., 2015. Observed latitudinal variations in erosion as a function of glacier dynamics. Nature 526, 100–102. doi:10.1038/nature15385.

Kurek, J., Cwynar, L.C., Vermaire, J.C., 2009a. A late Quaternary paleotemperature record from Hanging Lake, northern Yukon Territory, eastern Beringa. Quaternary Research 72, 246–257.

Kurek, J., Cwynar, L.C., Ager, T.A., Abbott, M.B., Edwards, M.E., 2009b. Late Quaternary paleoclimate of western Alaska inferred from fossil chironomids and its relation to vegetation histories. Quaternary Science Reviews 28, 799–811. doi:10.1016/j.quascirev.2008.12.001.

Leeman, A., Niessen, F., 1994. Holocene glacial activity and climatic variations in the Swiss Alps. The Holocene 4, 259–268.

Leffingwell, E. de K., 1919. The Canning River region, northeastern Alaska. US Geological Survey Professional Paper 109, 251 pp.

Leonard, E.M., 1985. Glaciological and climatic controls on lake sedimentation, Canadian Rocky Mountains. Zeitschrift für Gletscherkunde und Glazialgeologie f21, 35–42.

Leonard, E.M., 1997. The relationship between glacial activity and sediment production: evidence from a 4450-year varve record of Neoglacial sedimentation in Hector Lake, Alberta, Canada. Journal of Paleolimnology 17, 319–330.

Mann, D.H., Peteet, D.M., Reanier, R.E., Kunz, M.L., 2002. Responses of an arctic landscape to lateglacial and early Holocene climatic changes: The importance of moisture. Quaternary Science Reviews 21, 997–1021. doi:10.1016/S0277-3791(01)00116-0.

Mantua, N.J., Hare, S.R., 2002. The Pacific Decadal Oscillation. Journal of Oceanography 58, 35–44.

Marcott, S.A., Shakun, J.D., Clark, P.U., Mix, A.C., 2013. A reconstruction of regional and global temperature for the past 11,300 years. Science 339, 1198-1201.

Matthews, J.A., Briffa, K.R., 2005. The 'Little Ice Age'; Reevaluation of an evolving concept. Geografiska Annaler Series A Physical Geography 87A (1) 17-36.

Matthews, J.A., Dahl, S.O., Nesje, A., Berrisford, M.S., Andersson, C., 2000. Holocene glacier variations in central Jotunheimen, southern Norway based on distal glaciolacustrine sediment cores. Quaternary Science Reviews 19, 1625–1647. doi:10.1016/S0277-3791(00)00008-1.

Matthews, J.A., Karlén, W., 1992. Asynchronous Neoglaciation and Holocene climatic change reconstructed from Norwegian glaciolacustrine sedimentary sequences. Geology 20, 991–994.

Menounos, B., 1997. The water content of lake sediments and its relationship to other physical parameters: an alpine case study. The Holocene 7, 207–212.

Michelutti, N., Blais, J.M., Cumming, B.F., Paterson, A., M., Rühland, K., Wolfe, A.P., Smol, J.P., 2010. Do spectrally inferred determinations of chlorophyll a reflect trends in lake trophic status? Journal of Paleolimnology 43, 205–217. doi:10.1007/s10933-009-9325-8.

Michelutti, N., Wolfe, A.P., Vinebrooke, R.D., Rivard, B., Briner, J.P., 2005. Recent primary

production increases in arctic lakes. Geophysical Research Letter 32, 1–4. doi:10.1029/2005GL023693.

Miller, G.H., Brigham-Grette, J., Alley, R.B., Anderson, L., Bauch, H.A., Douglas, M.S.V., Edwards, M.E., Elias, S.A., Finney, B.P., Fitzpatrick, J.J., Funder, S. V., Herbert, T.D., Hinzman, L.D., Kaufman, D.S., MacDonald, G.M., Polyak, L., Robock, A., Serreze, M.C., Smol, J.P., Spielhagen, R., White, J.W.C., Wolfe, A.P., Wolff, E.W., 2010. Temperature and precipitation history of the Arctic. Quaternary Science Reviews 29, 1679–1715. doi:10.1016/j.quascirev.2010.03.001.

Nesje, A., 2009. Latest Pleistocene and Holocene alpine glacier fluctuations in Scandinavia. Quaternary Science Reviews 28, 21-22, 2119-2136.

Nesje, A., Dahl, S., 1991. Holocene glacier fluctuations in Bevringsdalen, Jostedalsbreen region, (western Norway ca 3200-1400 BP). The Holocene 1, 1–7.

Nesje, A., Dahl, S.O., Anderson, C., Matthews, J.A., 2000. The lacustrine sedimentary sequence in Sygneskardvatnet, western Norway: a continuous, high-resolution record of the Jostedalsbreen ice cap during the Holocene. Quaternary Science Reviews 19, 1047–1065.

Nesje, A., Matthews, J.A., Dahl, O., Berrisford, M.S., Andersson, C., 2001. Holocene glacier fluctuations of Flatebreen and winter-precipitation changes in the Jostedalsbreen region, western Norway, based on glaciolacustrine sediment records. The Holocene 11, 267–280. doi:10.1191/095968301669980885.

Nesje, A., Kvamme, M., Rye, N., Løvlie, R., 1991. Holocene glacial and climate history of the Jostedalsbreen region, Western Norway; evidence from lake sediments and terrestrial deposits. Quaternary Science Reviews 10, 87–114. doi:10.1016/0277-3791(91)90032-P.

Nolan, M. and DesLauriers, K., 2016. Which are the highest peaks in the US Arctic? Fodar settles the debate. Cryosphere 1245–1257. doi:10.5194/tc-10-1245-2016.

Osborn, G., McCarthy, D., LaBrie, A., Burke, R., 2015. Lichenometric dating: Science or pseudo-science? Quaternary Research 83, 1–12. doi:10.1016/j.yqres.2014.09.006.

Östrem, G., 1975. Sediment transport in glacial meltwater streams. In, Jopling, A., McDonald, B., Eds., Glacio-fluvial and glaciolacustrine sedimentation. Society of Economic Paleontologists and Mineralogists Special Publication 23, 101-122.

Oswald, W.W., Gavin, D.G., Anderson, P.M., Brubaker, L.B., Hu, F.S., 2012. A 14,500-year record of landscape change from Okpilak Lake, northeastern Brooks Range, northern Alaska. Journal of Paleolimnology. 48, 101–113. doi:10.1007/s10933-012-9605-6.

Owen, L.A., Thackray, G., Anderson, R.S., Briner, J., Kaufman, D., Roe, G., Pfeffer, W., Yi, C., 2009. Integrated research on mountain glaciers: Current status, priorities and future prospects. Geomorphology 103, 158–171. doi:10.1016/j.geomorph.2008.04.019

Pattyn, F., Delcourt, C., Samyn, D., Smedt, B.D.E., Nolan, M., 2009. Bed properties and hydrological conditions underneath McCall Glacier, Alaska, USA. Annals of Glaciology 50, 80–84.

Pendleton, S.L., Briner, J.P., Kaufman, D.S., Zimmerman, S.R., 2017. Using cosmogenic $^{10}$Be exposure dating and lichenometry to constrain Holocene glaciation in the central Brooks Range, Alaska. Arctic, Antarctic and Alpine Research 49, 115–132. doi:10.1657/AAAR0016-045.

Pendleton, S.L., Ceperley, E.G., Briner, J.P., Kaufman, D.S., Zimmerman, S.R., 2015. Rapid and early deglaciation in the central Brooks Range, Arctic Alaska. Geology 43, 419–422. doi:10.1130/G36430.1.

Péwé, T.L., 1975. Quaternary Geology of Alaska. Geological Survey Professional Paper 835, 152 pp.

Péwé, T.L., Reger, R.D., 1972. Modern and Wisconsinan snowlines in Alaska, in: International Geological Congress, Montreal: Proceedings No. 24, Section 12, Quaternary Geology, 187–197.

Polyak, L., Belt, S.T., Cabedo-Sanz, P., Yamamoto, M., Park, Y.H., 2016. Holocene sea-ice conditions and circulation at the Chukchi-Alaskan margin, Arctic Ocean, inferred from biomarker proxies. The Holocene 26, 1810–1821. doi:10.1177/0959683616645939.

Porter, S.C., 1975. Equilibrium-line altitudes of late Quaternary glaciers in the Southern Alps, New Zealand. Quaternary Research 5, 27–47. doi:10.1016/0033-5894(75)90047-2.

Porter, S.C., 2007. Neoglaciation in the American Cordilleras. In Elias, S.A., Mock, C.J., Eds., Encyclopedia of Quaternary Science (2nd Edition). Elsevier, Amsterdam, 269-276. doi:10.1016/B978-0-444-53643-3.00127-8.

Porter, S.C., Denton, G.H., 1967. Chronology of neoglaciation in the North American Cordillera. American Journal of Science 265(3), 177–210.

Rabus, B.T., Echelmeyer, K.A., 1998. The mass balance of McCall Glacier, Brooks Range Alaska, USA; its regional relevance and implication for climate change in the Arctic. Journal of Glaciology 44, 333–351.

Rabus, B.T., Echelmeyer, K.A., 2002. Increase of 10 m ice temperature: climate warming or glacier thinning? Journal of Glaciology 48, 279–286.

Rainwater, F.H., Guy, H.P. 1958. Some observations on the hydrochemistry and sedimentation of the Chamberlin Glacier Area Alaska. Shorter contributions to general Geology. Geological Survey Professional Paper 414-C, C1-C14.

Rasmussen, S.O. Andersen, K.K., Svensson, A.M., Steffensen, J.P., Vinther, B.M., Clausen, H.B., Siggaard-Andersen, M.-L., Johnsen, S.J., Larsen, L.B., Dahl-Jensen, D., Bigler, M.,

Röthlisberger, R., Fischer, H., Goto-Azuma, K., Hansson, M.E., Ruth, U., 2006. A new Greenland ice core chronology for the last glacial termination. Journal of Geophysical. Research 111, D06102, doi:10.1029/2005JD006079.

Reed, B., 1968. Geology of the Lake Peters area northeastern Brooks Range, Alaska. U.S. Geological Survey Bulletin 1236, 132 pp.

Rein, B., Sirocko, F., 2002. In-situ reflectance spectroscopy-analyzing techniques for high-resolution pigment logging in sediment cores. International Journal of Earth Sciences 91, 950-954.

Rodionov, S.N., Bond, N.A., Overland, J.E., 2007. The Aleutian Low, storm tracks, and winter climate variability in the Bering Sea. Deep Sea Research Part II Topical Studies in Oceanography 54, 2560–2577. doi:10.1016/j.dsr2.2007.08.002.

Roe, G.H., Baker, M.B., 2016. The response of glaciers to climatic persistence. Journal of Glaciology 62, 440–450. doi:10.1017/jog.2016.4.

Roe, G.H., Baker, M.B., Herla, F., 2016. Centennial glacier retreat as categorical evidence of regional climate change. Nature Geoscience 1, 95–99. doi:10.1038/ngeo2863.

Serreze, M.C., Barry, R.G., 2011. Processes and impacts of Arctic amplification: A research synthesis. Global and Planetary Change 77, 85–96. doi:10.1016/j.gloplacha.2011.03.004.

Sikorski, J.J., Kaufman, D.S., Manley, W.F., Nolan, M., 2009. Glacial-geologic evidence for decreased precipitation during the Little Ice Age. Arctic, Antarctic and Alpine Research 41, 138–150. doi:10.1657/1938-4246(07-078)

Smith, N.D., 1978, Sedimentary processes and patterns in a glacier-fed lake with low sediment input. Canadian Journal of Earth Science 15, 741–756.

Smol, J.P., 1988. Paleoclimatic proxy data from freshwater Arctic diatoms. Verhandlungen der Internationalen Verein für Limnologie 3, 37–44.

Smol, J.P., Wolfe, A.P., Birks, H.J.B., Douglas, M.S. V, Jones, V.J., Korhola, A., Pienitz, R., Rühland, K., Sorvari, S., Antoniades, D., Brooks, S.J., Fallu, M.-A., Hughes, M., Keatley, B.E., Laing, T.E., Michelutti, N., Nazarova, L., Nyman, M., Paterson, A.M., Perren, B., Quinlan, R., Rautio, M., Saulnier-Talbot, E., Siitonen, S., Solovieva, N., Weckström, J., 2005. Climate-driven regime shifts in the biological communities of arctic lakes. Proceedings of National Academy of Science 102, 4397–402. doi:10.1073/pnas.0500245102.

Snowball, I., Sandgren, P., 1996. Lake sediment studies of Holocene glacial activity in the Kårsa valley, northern Sweden: contrast in interpretation. The Holocene 6, 367– 372.

Solomina, O., Calkin, P., 2003. Lichenometry as applied to moraines in Alaska, U.S.A., and Kamchatka, Russia. Arctic, Antarctic, and Alpine Research 35, 129–143.

Souch, C., 1994. A methodology to interpret downvalley lake sediments as records of Neoglacial activity: Coast Mountains, British Columbia, Canada. Geografiska Annaler Series A Physical Geography 76, 169–185.

Steen, D.P., 2016. Late Quaternary paleomagnetism and environmental magnetism at Cascade and Shainin Lakes, north-central Brooks Range, Alaska. M.S. Thesis. Northern Arizona University. 129 pp.

Stein, R., Fahl, K, Schade, I., Manerung, A., Wassmuth, S., Niessen, F., Nam, S., 2017. Holocene variability in sea ice cover, primary production, and Pacific-Water inflow and climate change in the Chukchi and East Siberian Seas (Arctic Ocean). Quaternary Science 32, 362-379. doi:10.1002/jqs.2929.

Stuiver, M., Reimer, P.J., Reimer, R.W., 2018. CALIB 7.1 (WWW program and documentation). Available at: http://calib.qub.ac.uk/calib/.

Thomas, E.K., Szymanski, J., Briner, J.P., 2010. Holocene alpine glaciation inferred from lacustrine sediments on northeastern Baffin Island, Arctic Canada. Journal of Quaternary Science 25, 146–161. doi:10.1002/jqs.

Thompson, R., Battarbee, R.W., O'Sullivan, P.E., Oldfield, F., 1975. Magnetic susceptibility of lake sediments. Limnology and Oceanography 20(5) 687–698.

Thompson, D.W.J., Wallace, J.M., 1998. The Arctic Oscillation signature in the wintertime geopotential height and temperature fields. Geophysical Research Letters 25, 1297–1300.

Thompson, D.W.J., Wallace, J.M., 2001. Regional climate impacts of the Northern Hemisphere annular mode. Science 293, 85–89. doi:10.1126/science.1058958.

Thurston, L., 2017. Modeling fine-grained fluxes for estimating sediment yields and understanding hydroclimatic and geomorphic processes at Lake Peters, Brooks Range, Arctic Alaska, M.S. Thesis. Northern Arizona University. 89 pp.

Vachula, R.S., Chipman, M.L., Hu, F.S., 2017. Holocene climatic change in the Alaskan Arctic as inferred from oxygen-isotope and lake-sediment analyses at Wahoo Lake. The Holocene 27(11), 1631-1644. doi:10.1177/0959683617702230.

Vaughan, D.G., J.C. Comiso, I. Allison, J. Carrasco, G. Kaser, R. Kwok, P. Mote, T. Murray, F. Paul, J. Ren, E. Rignot, O. Solomina, K. Steffen and T. Zhang, 2013: Observations: Cryosphere. In: Climate Change 2013: The Physical Science Basis. Contribution of Working Group I to the Fifth Assessment Report of the Intergovernmental Panel on Climate Change [Stocker, T.F., D. Qin, G.-K. Plattner, M. Tignor, S.K. Allen, J. Boschung, A. Nauels, Y. Xia, V. Bex and P.M. Midgley (eds.)]. Cambridge University Press, Cambridge, United Kingdom and New York, NY, USA.

Walter Anthony, K.M., Zimov, S.A., Grosse, G., Jones, M.C., Anthony, P.M., Chapin III, F.S., Finlay, J.C., Mack, M.C., Davydov, S., Frenzel, P., Froking, S., 2014. A shift of thermokarst lakes from carbon sources to sinks during the Holocene epoch. Nature 511, 452-456.

Wendler, G., Fahl, C., Corbin, S., 1972. Mass balance studies on McCall Glacier Brooks Range, Alaska. Arctic and Alpine Research 4(3), 211–222. doi:10.1657/1523-0430(07-069).

Wendler, G, Ishikawa, N., Streten, N., 1974. The climate of the McCall Glacier, Brooks Range, Alaska, in relation to its geographical setting. Arctic and Alpine Research 6(3), 307-318. doi: 10.2307/1550067.

Wolfe, A.P., Miller, G.H., Olsen, C.A., Forman, S.L., Doran, P.T., Holmgren, S.U., 2004. Geochronology of high latitude lake sediments. In Pienitz, R., Douglas, M.S.V., Smol, J.P., Eds., Long-term Environmental Change in Arctic and Antarctic Lakes. Springer, Dordrecht, 19–52.

Wolfe, A.P., Vinebrooke, R.D., Michelutti, N., Rivard, B., Das, B., 2006. Experimental calibration of lake-sediment spectral reflectance to chlorophyll-a concentrations: methodology and paleolimnological validation. Journal of Paleolimnology 36(1), 91-100.

Young, S.E., Briner, J.P., Kaufman, D.S., 2009. Late Pleistocene and Holocene glaciation of the Fish Lake valley, northeastern Alaska Range, Alaska. Journal of Quaternary Science 24, 677–689. doi:10.1002/jqs.

Zolitschka, B., Francus, P., Ojala, A. E., Schimmelmann, A., 2015. Varves in lake sediments – a review. Quaternary Science Reviews 117, 1-41. doi:10.1016/j.quascirev.2015.03.019.

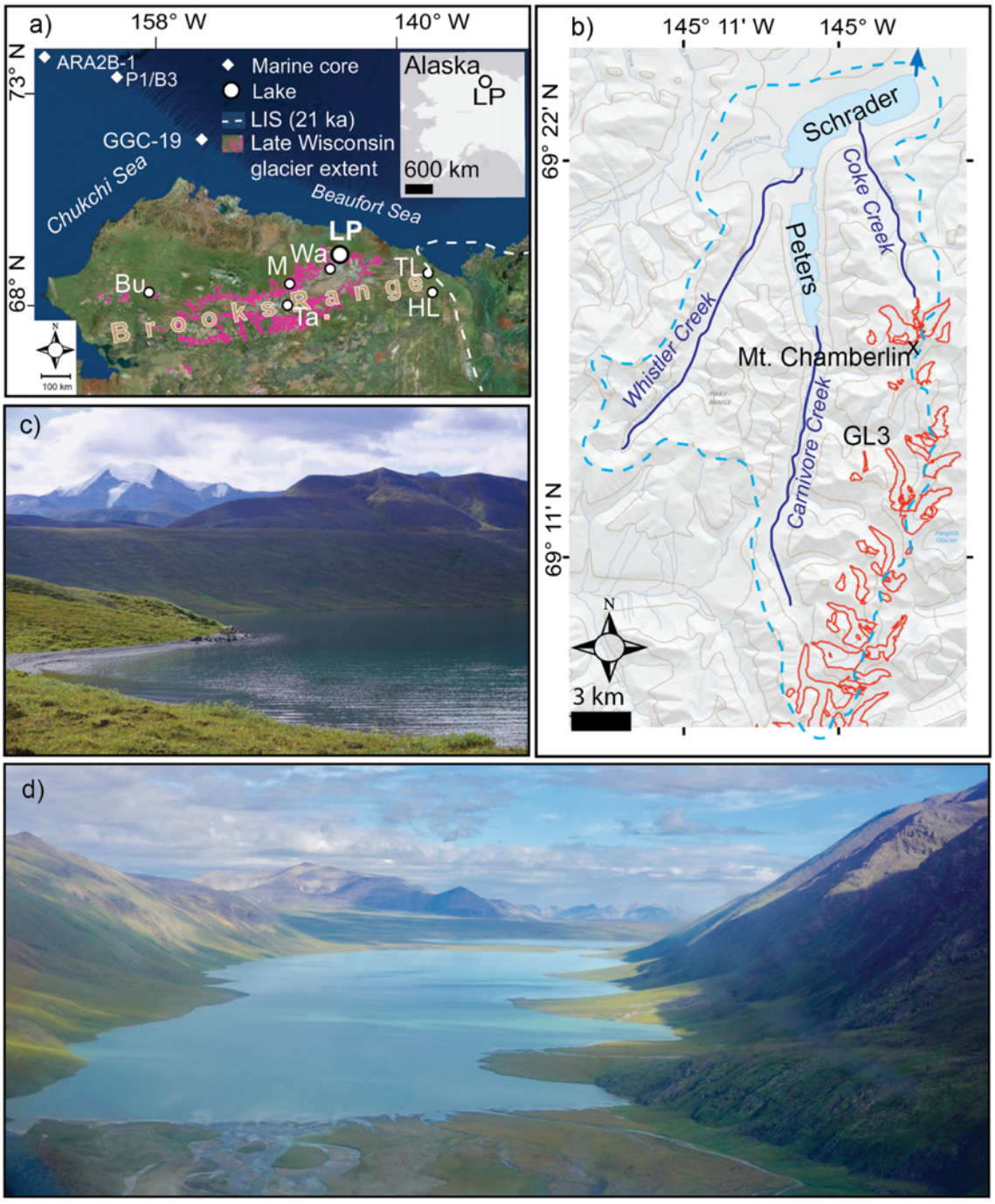


**Figure 1.** Study area locations and photographs. (a) Northern Alaska showing LGM glacier extent and the Laurentide Ice Sheet (LIS). **Chukchi Sea** cores ARA2B-1 (Stein et al., 2017), P1/B3 & GGC-19 (Farmer et al., 2011); **Bu** = Burial Lake (Abbot et al., 2010; Finkenbinder et al., 2015); **M** = Meli Lake and **Ta** = Tangled Up Lake (Anderson et al., 2001); **Wa** = Wahoo Lake (Vachula et al., 2017); **LP** = Lake Peters; **TL** = Trout Lake (Irvine et al., 2012); **HL** = Hanging Lake (Kurek et al., 2009a). (b) Lake Peters-Schrader watershed (blue dashed line) showing major tributaries, and 2016 glaciers outlines. (c) View to the south towards Mt. Chamberlin from distal Schrader Lake. (d) View to the north towards across Lake Peters.

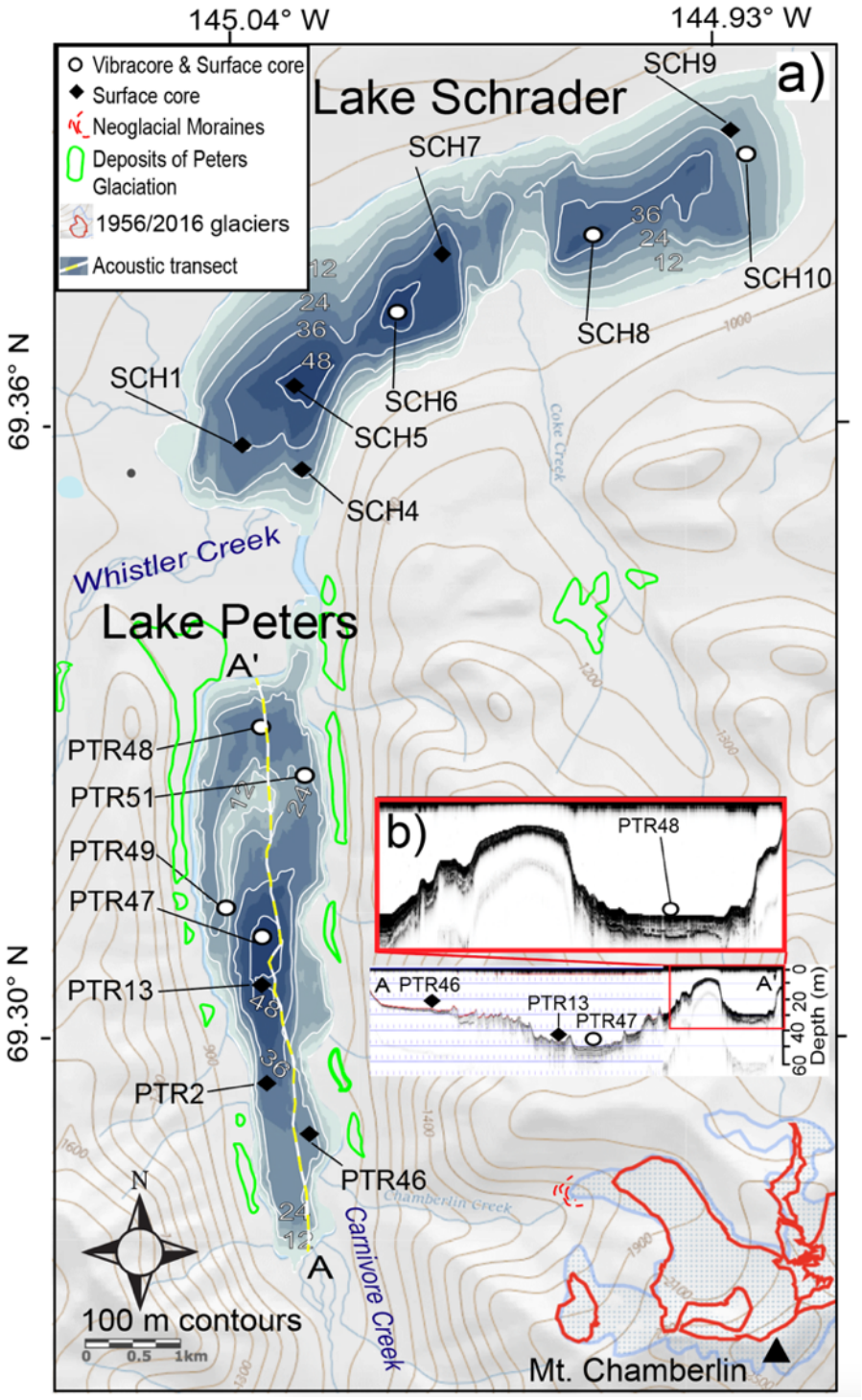


**Figure 2.** Lake Peters and Lake Schrader area. (a) Topography, bathymetry, and core locations (table 1). 1956 glacier outlines approximated based on USGS Mt. Michelson (B-2) map. 2016 glacier outlines based on FODAR data. (b) Acoustic profile from A to A' of Lake Peters showing core locations.

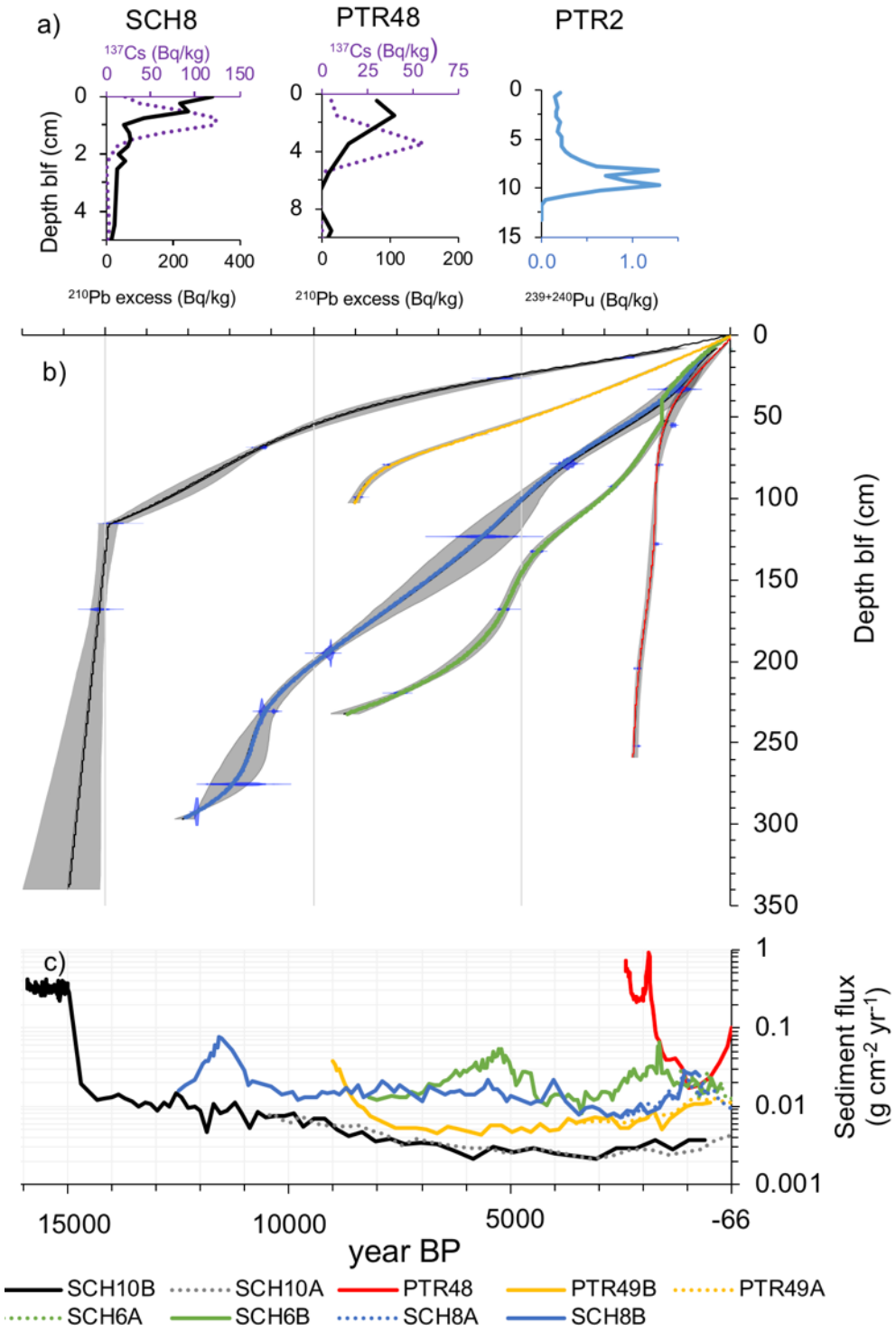


**Figure 3.** Age-depth models for cores from Lake Peters (PTR) and Lake Schrader (SCH). (a) $^{137}$Cs and $^{210}$Pb excess profiles for SCH8A, PTR48A and $^{239+240}$Pu profile for PTR13-2A (Table 3). (b) Radiocarbon-based age models based on classical age-depth modeling. Thin lines and shading indicate 95% confidence range (Table 2). (c) Sediment flux on semi-log plot. Individual age models are in appendices E, F, H, I, and J.

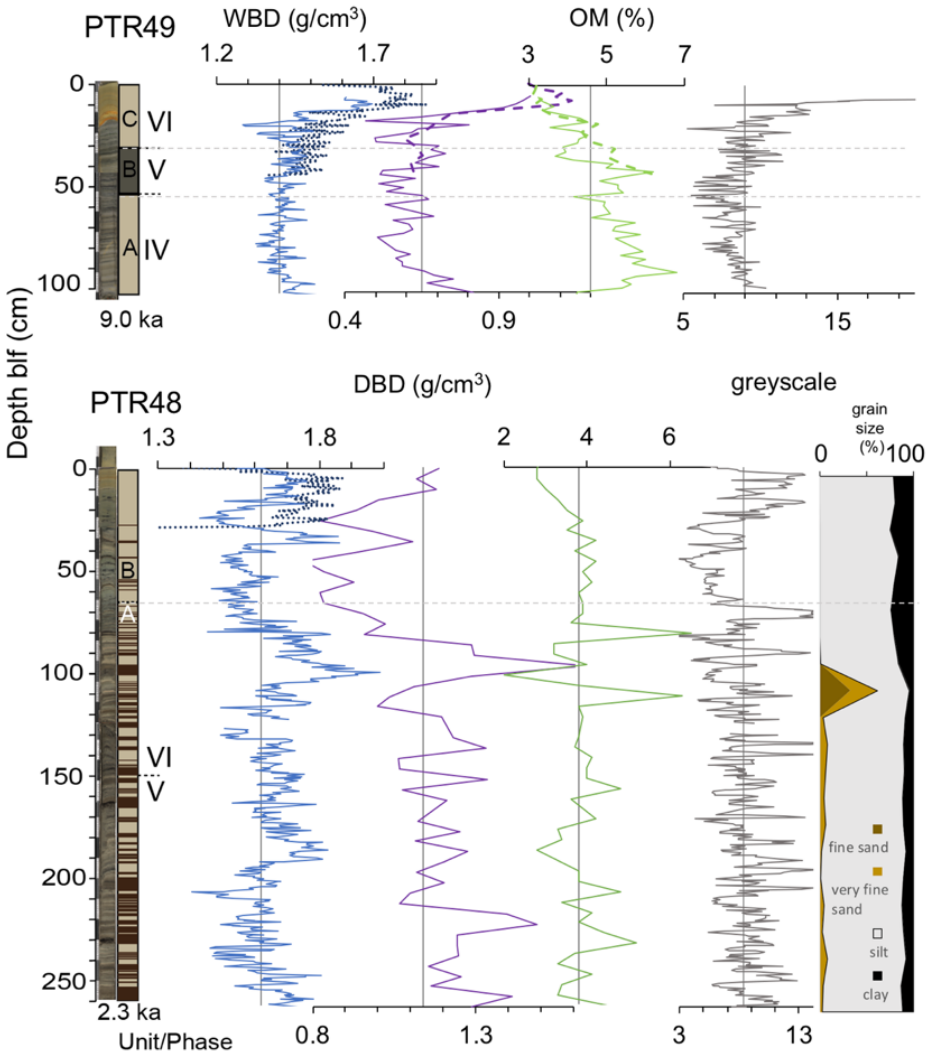


| | Bsa | Dsi | Lsi | Bgcs |
|---|---|---|---|---|
| Facies | brown sand | dark silt | light silt | brown-grey clayey silt |
| Wet bulk density (g cm$^{-3}$) | ~1.6 | < 1.4 | > 1.4 | > 1.7 |
| Organic matter content (%) | 4–6 | > 5 | < 5 | < 4 |
| Greyscale reflectance | ~5 | < 9 | ~9 | 5–17 |
| Bed thickness (cm) | 0.5–5 | < 0.5 | < 1 | 0.1–1 |
| Sedimentary structures | graded bedding | laminated | laminated | laminated |
| Bedding plane contacts | sharp | variable | variable | sharp |

**Figure 4.** (top) Lake Peters sediment profiles. From left to right: core face image, unit and phases, wet bulk density (WBD), dry bulk density (DBD), organic matter (OM), greyscale, and grain-size distribution. Dashed lines are surface cores. Data are in appendices A, E, F. (bottom) Facies classification.

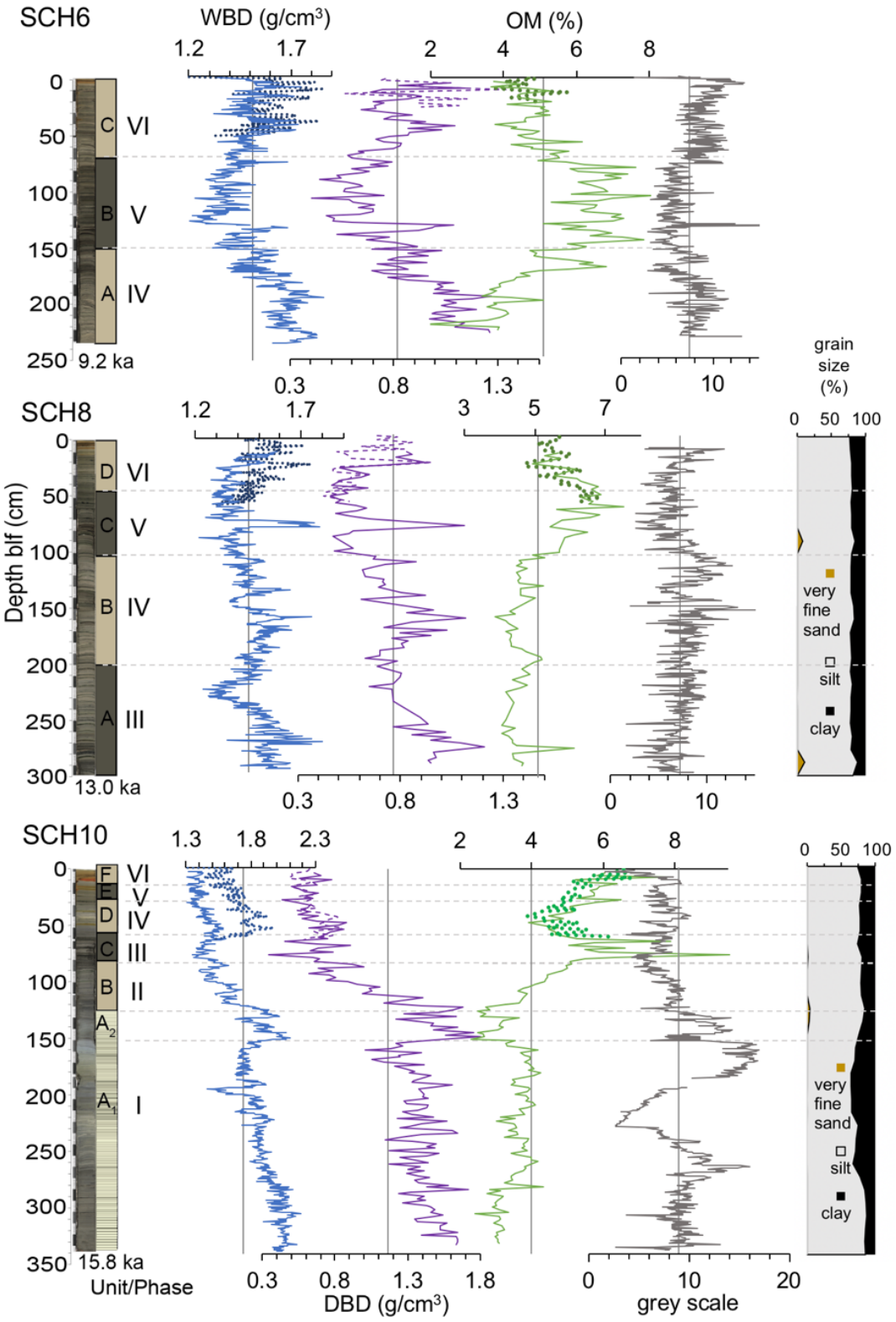


**Figure 5.** (top) Lake Peters sediment profiles. From left to right: core face image, unit and phases, wet bulk density (WBD), dry bulk density (DBD), organic matter (OM), greyscale, and grain-size distribution. Dashed lines are surface cores. Data are in appendices A, H, I, J.

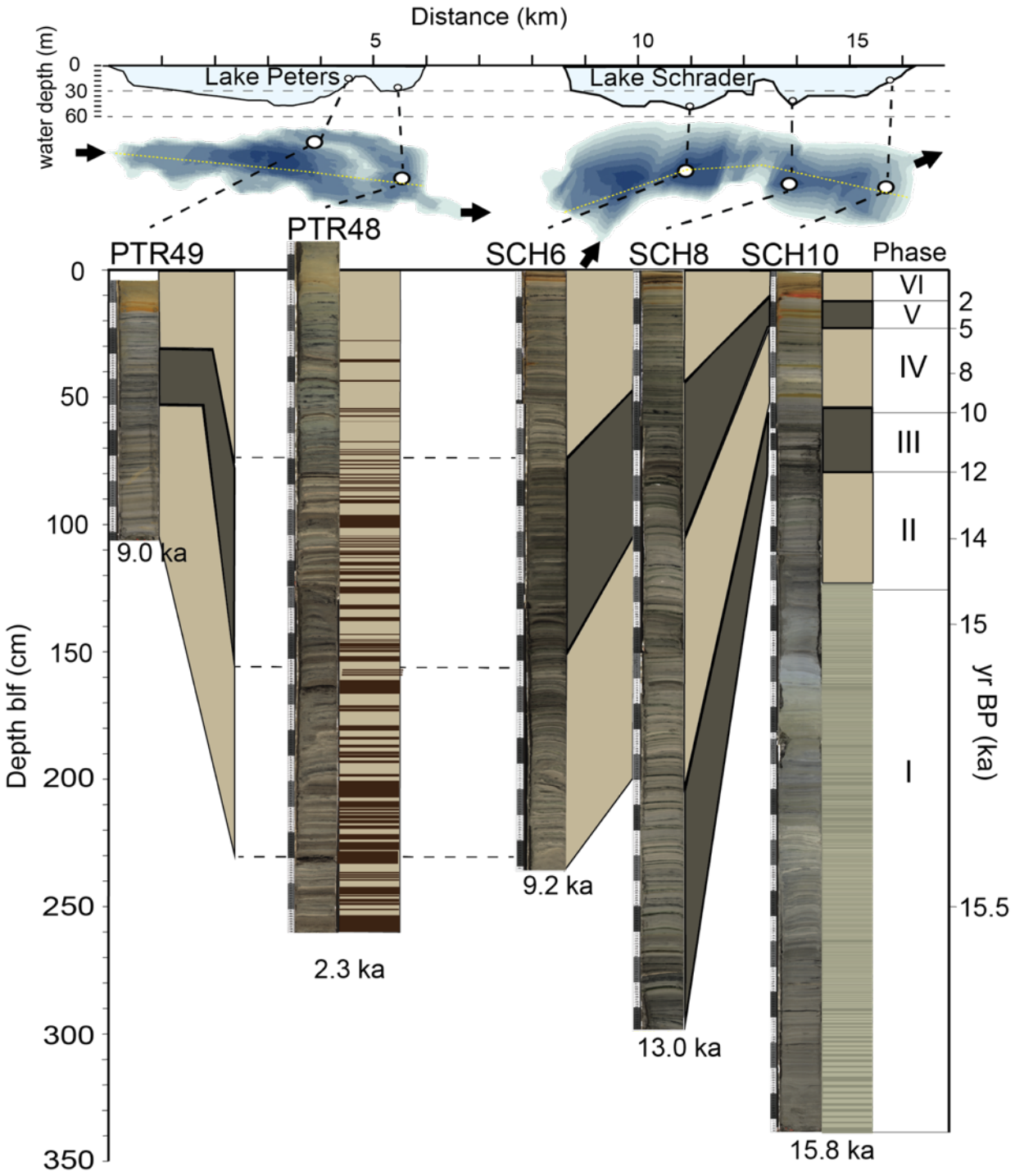


**Figure 6.** Lake Peters and Lake Schrader vibracores from proximal to distal with core locations along transect and bathymetry (top). Colors indicate facies, core stratigraphy, and correlative phases. Dashed lines indicate uncertainty in correlating PTR48. Basal ages are shown for each core and ages for SCH10 are plotted on the right.

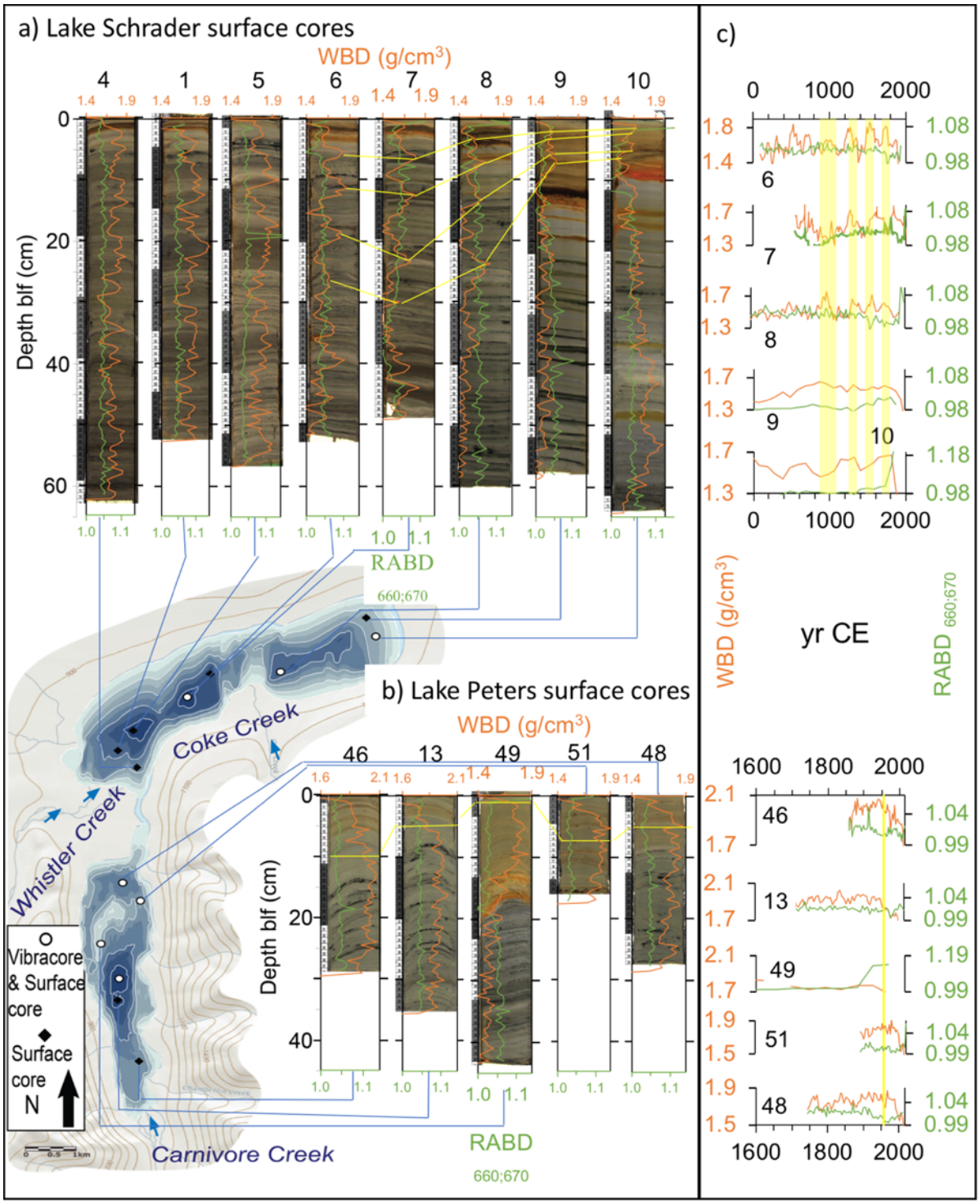


**Figure 7.** (a) Lake Schrader and (b) Lake Peters surface cores from proximal (left) to distal (right) with wet bulk density (WBD, orange) and relative adsorption band depth (RABD, green). Yellow lines show tie lines. (c) WBD and RABD plotted through time, with yellow vertical bars corresponding to yellow tie lines.

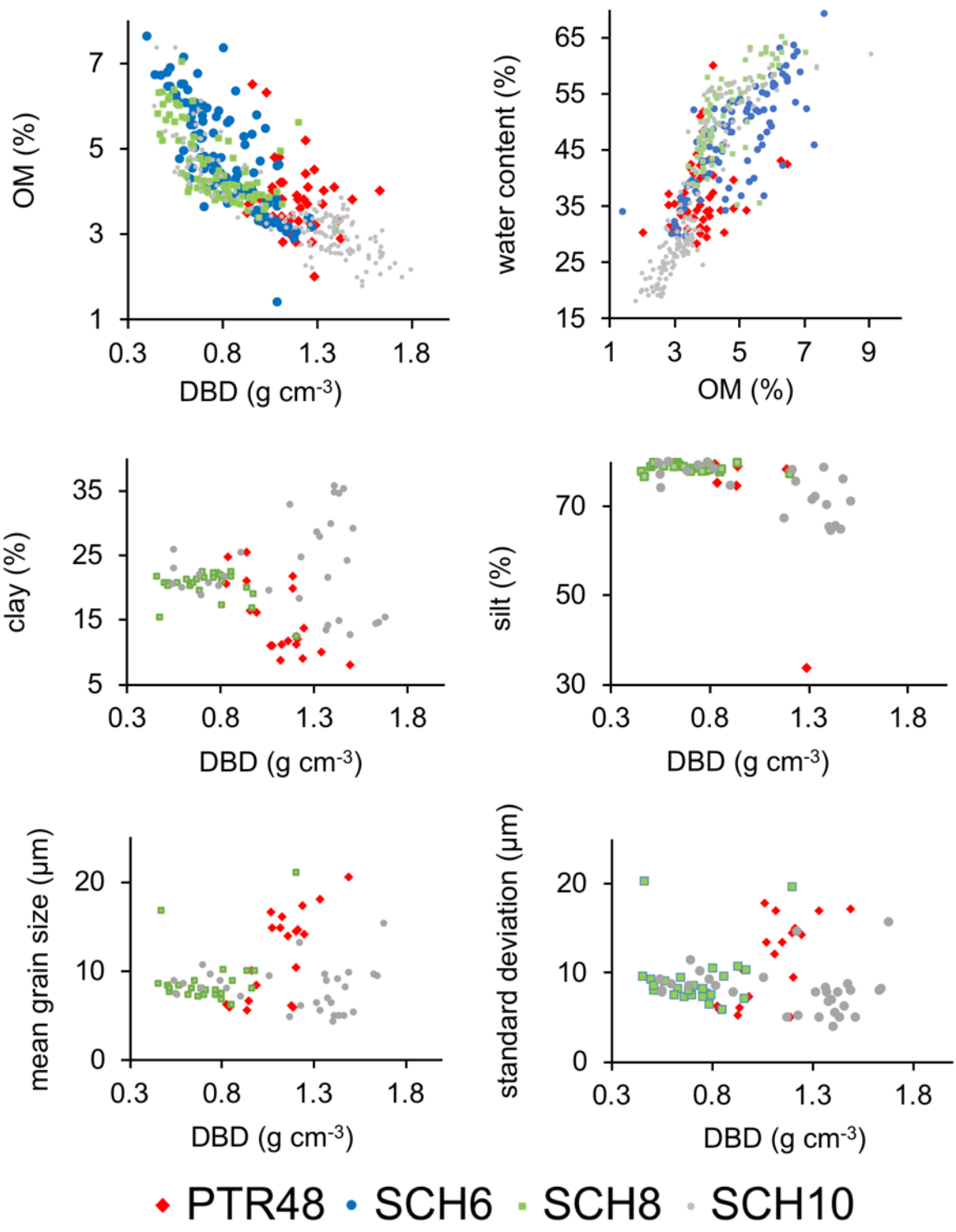


**Figure 8.** Scatterplots of sediment parameters. Dry Bulk Density (DBD), Organic Matter (OM). PTR48 DBD vs. Silt outlier associated with coarse turbidite layer.

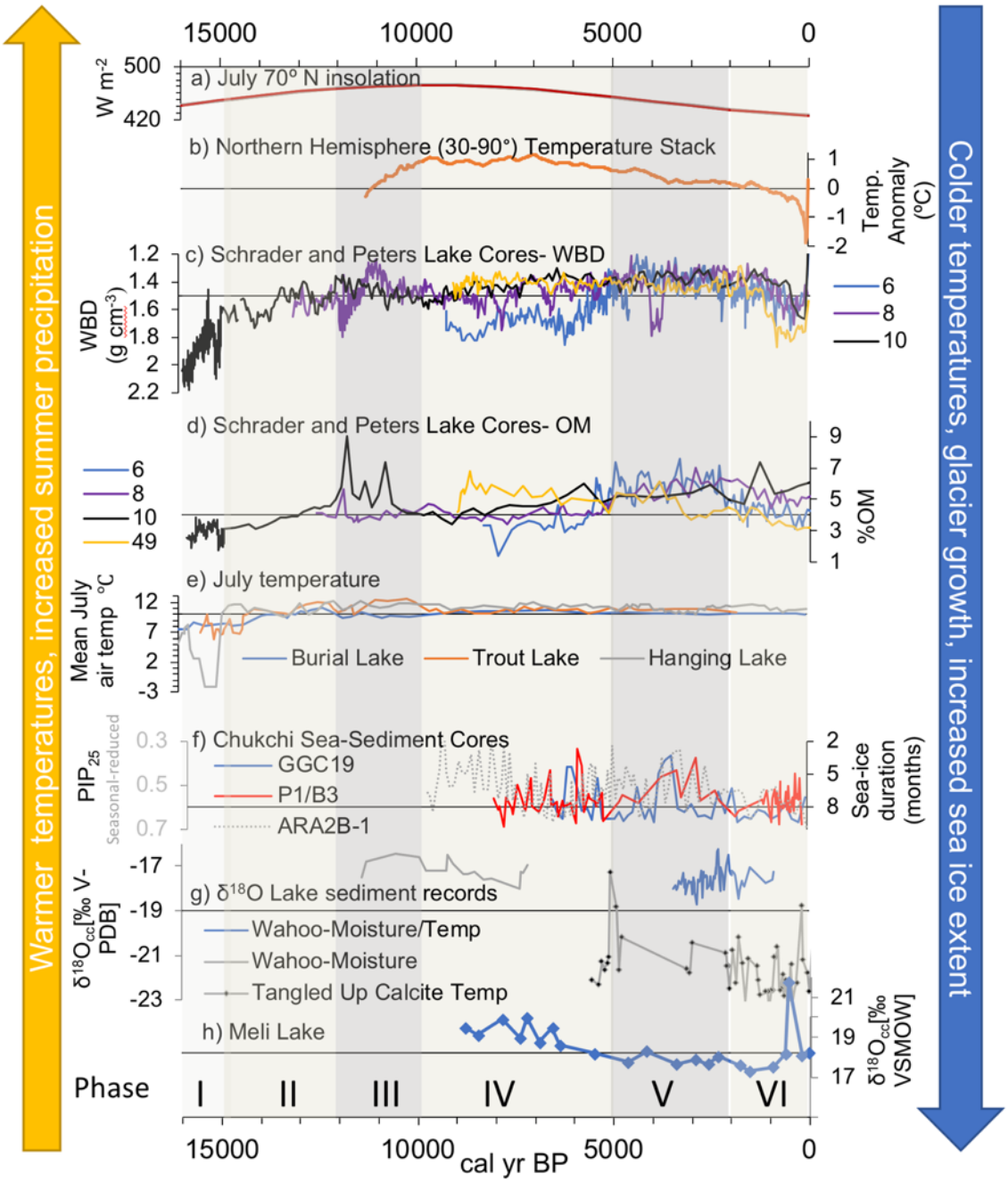


**Figure 9.** Comparision of organic-matter (OM) content and wet bulk density (WBD), the two most consistent bio-physcial properties of the dated cores from Lake Peters and Lake Schrader with other regional paleoenvironmental records. a) Berger and Loutre, 1991; b) Marcott et al., 2013; c) Wet Bulk Density and d) Organic Matter from Lake Peters and Lake Schrader cores; e) Burial Lake-Kurek et al., 2009b; Trout Lake-Irvine et al., 2012; Hanging Lake-Kurek et al., 2009a; f) Chukchi Sea cores-Farmer et al., 2011; Stein at al., 2017; g) Tangled Up Lakes-Anderson et al., 2001; Wahoo Lake-Vachula et al., 2017; h) Meli Lake Anderson et al., 2001.

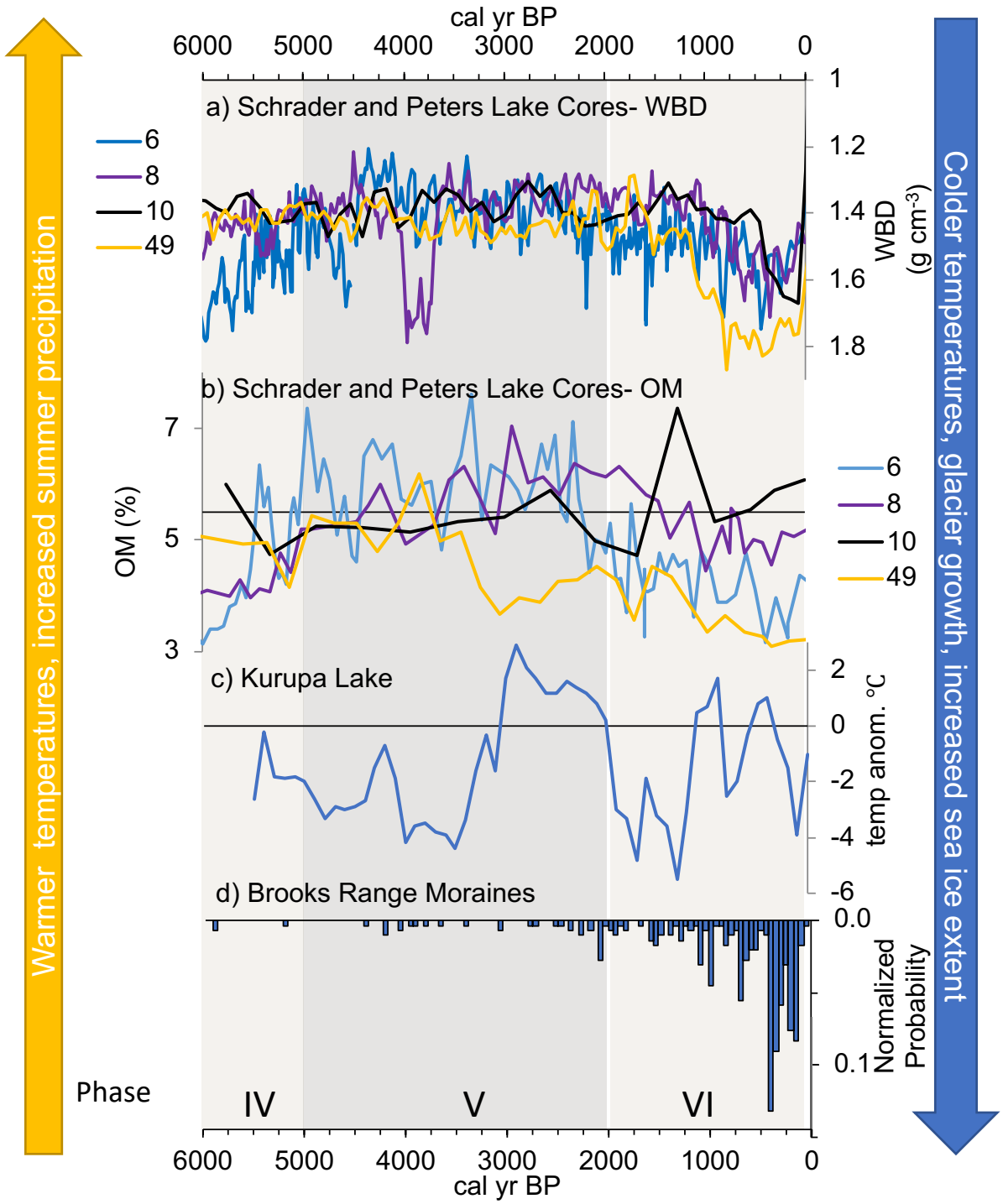


**Figure 10.** Comparision of organic-matter (OM) content and wet bulk density (WBD), over the last 6 ka with other regional paleoclimate records. a) WBD and b) OM from Lake Peters and Lake Schrader cores; c) Kurupa Lake (Boldt et al., 2015); d) Brooks Range Moraines (Pendleton et al., 2017).

**Table 1.** Core inventory. [a]individual core codes have been simplified in the text.
[b] PTR16-47B has no surface core and no blf conversion is only an approximation.

| Core ID[a] | Date | Water depth (m) | Latitude (°N) | Longitude (°W) | Core length (cm) | Tube depth (x) to blf (y) conversion: | Coring device |
|---|---|---|---|---|---|---|---|
| PTR13-2A | 5/6/13 | 37.0 | 69.304 | -145.039 | 49.0 | y = x - 8.2 | Universal |
| PTR16-13 | 4/23/16 | 49.0 | 69.310 | -145.047 | 47.8 | y = x - 10.0 | Uwitec |
| PTR16-46A | 4/29/16 | 27.9 | 69.297 | -145.033 | 40.6 | y = x - 8.7 | Uwitec |
| PTR16-47B-1[b] | 4/20/16 | 50.3 | 69.316 | -145.045 | 150.0 | y = x - 15.0 | Vibracore |
| PTR16-47B-2 | " | " | " | " | 121.0 | y = x + 92.9 | " |
| PTR16-48A | 4/25/16 | 31.2 | 69.336 | -145.046 | 37.5 | y = x - 7.3 | Uwitec |
| PTR16-48B-1 | 4/18/16 | 31.2 | 69.336 | -145.045 | 150.5 | y = x - 26.0 | Vibracore |
| PTR16-48B-2 | " | " | " | " | 146.5 | y = x + 124.0 | " |
| PTR16-49A | 4/26/16 | 13.0 | 69.319 | -145.055 | 53.0 | y = x - 6.5 | Uwitec |
| PTR16-49B | 4/26/16 | 13.0 | 69.319 | -145.055 | 109.8 | y = x + 2.9 | Vibracore |
| PTR16-51A | 4/28/16 | 25.9 | 69.331 | -145.034 | 26.0 | y = x - 5.9 | Uwitec |
| PTR16-51B-1 | 4/28/16 | 25.9 | 69.331 | -145.034 | 98.0 | y = x - 5.0 | Vibracore |
| PTR16-51B-2 | " | " | " | " | 155.5 | y = x + 92.9 | " |
| SCH16-1A | 4/25/16 | 35.5 | 69.363 | -145.046 | 70.5 | y = x - 15.4 | Uwitec |
| SCH16-4A | 4/25/16 | 27.6 | 69.359 | -145.036 | 76.5 | y = x - 10.9 | Uwitec |
| SCH16-5A | 4/25/16 | 56.2 | 69.368 | -145.041 | 69.3 | y = x - 8.6 | Uwitec |
| SCH16-6A | 4/22/16 | 54.1 | 69.376 | -145.023 | 69.3 | y = x - 10.3 | Uwitec |
| SCH16-6B-1 | 4/20/16 | 54.1 | 69.376 | -145.023 | 150.0 | y = x - 18.7 | Vibracore |
| SCH16-6B-2 | " | " | " | " | 120.0 | y = x + 122.4 | " |
| SCH16-7A | 4/21/16 | 47.3 | 69.382 | -144.999 | 61.5 | y = x - 10.4 | Uwitec |
| SCH16-8A | 4/22/16 | 46.5 | 69.382 | -144.957 | 72.8 | y = x - 9.9 | Uwitec |
| SCH16-8B-1 | 4/19/16 | 46.5 | 69.382 | -144.957 | 150.5 | y = x - 1.0 | Vibracore |
| SCH16-8B-2 | " | " | " | " | 155.5 | y = x +149.5 | " |
| SCH16-9A | 4/22/16 | 25.4 | 69.392 | -144.922 | 69.3 | y = x - 8.0 | Uwitec |
| SCH16-10A | 4/22/16 | 20.5 | 69.389 | -144.921 | 74.0 | y = x - 8.5 | Uwitec |
| SCH16-10B-1 | 4/23/16 | 20.5 | 69.389 | -144.921 | 111.5 | y = x + 0.5 | Vibracore |
| SCH16-10B-2 | " | " | " | " | 75.5 | y = x + 111.8 | " |
| SCH16-10B-3 | " | " | " | " | 155.0 | y = x + 184.2 | " |
| PTR17-32 | 5-19-17 | 44 | 69.31001 | 145.04175 | 37 | | Uwitec |
| PTR17-06 | 5-19-17 | 30 | 69.32435 | 145.04709 | 37.5 | | Uwitec |
| PTR17-11 | 5-20-17 | 50 | 69.31442 | 145.04474 | 32.4 | | Uwitec |
| PTR17-18 | 5-20-17 | 36 | 69.30258 | 145.04438 | 42.1 | | Uwitec |
| PTR17-16 | 5-23-17 | 24 | 69.29654 | 145.04183 | 29.3 | | Uwitec |
| PTR17-12 | 5-23-17 | 42 | 69.31936 | 145.04481 | 38.3 | | Uwitec |
| PTR17-20 | 5-23-17 | 42 | 69.29186 | 145.03942 | 42.4 | | Uwitec |

**Table 2.** Radiocarbon and calibrated ages for this study.

| Lab ID[a] | Core ID | Tube depth (cm)[b] | Depth blf (cm)[b] | $^{14}$C age (yr BP) | ± | Cal age[c] | ± | Material |
|---|---|---|---|---|---|---|---|---|
| 16528 | PTR16-49B | 36.5 | 39.4 | 3380 | 25 | 3620 | 60 | aquatic insect remains; caddisfly cases and parts; bryophyte piece |
| 16529 | PTR16-49B | 58.0 | 60.9 | 5220 | 35 | 5970 | 130 | aquatic insect remains; caddisfly cases and parts; midges |
| 16530 | PTR16-49B | 76.5 | 79.4 | 7360 | 30 | 8180 | 130 | aquatic insect remains; midges; oospores; no terrestrial material |
| 16531 | PTR16-49B | 96.5 | 99.4 | 8005 | 30 | 8880 | 120 | aquatic insect remains; midges; leaf stalk; caddisfly case, oospore |
| 15616 | PTR16-48B-1 | 60.5 | 34.5 | 1575 | 20 | 1470 | 60 | bryophyte and moss fragments, moss leaves, moss twigs, aquatic insect chitin, chironomids head capsules |
| 15615 | PTR16-48B-1 | 104.5 | 78.5 | 1795 | 15 | 1720 | 90 | moss leaves, woody branches, twigs, non-specific plant debris, insect chitin |
| 15614 | PTR16-48B-2 | 5.5 | 127.5 | 1840 | 15 | 1780 | 50 | mosses, small plant fragments, some roots, |
| 15613 | PTR16-48B-2 | 84.5 | 204.5 | 2235 | 15 | 2220 | 80 | terrestrial leaf fragments, bryophyte and bryophyte twigs, woody stem material, kalmia leaf |
| 15612 | PTR16-48B-2 | 132.5 | 252.5 | 2275 | 20 | 2320 | 80 | terrestrial leaf fragments, bryophyte twigs, round spheres, carbonaceous sphere, fungal spores |
| 196903 | SCH16-6B-1 | 52.5 | 33.8 | 1540 | 20 | 1460 | 70 | cladocera, resting eggs, plant fibers, pronotum of an insect |
| 191211 | SCH16-6B-1 | 60.5 | 41.8 | 2680 | 30 | 2780 | 50 | finely dissected plant debris, resting eggs, bryophyte leaves, some cladocera, 1 chironomids head capsule |
| 196904 | SCH16-6B-1 | 77.5 | 58.8 | 1560 | 20 | 1470 | 60 | cladocera, resting eggs, slightly more plant fibers, pronotum of an insect |
| 191210 | SCH16-6B-1 | 114.5 | 95.8 | 2765 | 25 | 2860 | 70 | cladocera chitin, finely dissected organic remains, bryophyte leaves |
| 191209 | SCH16-6B-2 | 12.5 | 134.9 | 4115 | 30 | 4640 | 140 | plant fragments, bryophyte leaves, egg cases, cladocera chitin, other insect chitin, |
| 191208 | SCH16-6B-2 | 47.5 | 169.9 | 4710 | 60 | 5450 | 130 | very finely dissected organic fragments, moss leaves, egg cases, cladocera, other insect head capsules, bryophyte twigs and leaves |
| 191207 | SCH16-6B-2 | 98.0 | 220.4 | 7080 | 80 | 7900 | 160 | daphnia and ephippia, egg cases, other insect chitin, few plant fragments |
| 188321 | SCH16-8B-1 | 32.5 | 31.5 | 1310 | 170 | 1220 | 380 | fruiting graminoid head |
| 188322 | SCH16-8B-1 | 78.5 | 77.5 | 3570 | 70 | 3880 | 470 | bryophyte twigs |
| 190158 | SCH16-8B-1 | 123.5 | 122.5 | 5100 | 310 | 5850 | 740 | small organic debris, round resting egg, 1 chironomid head capsule |
| 188323 | SCH16-8B-2 | 45.5 | 195.0 | 8590 | 70 | 9570 | 140 | egg cases, finely dissected organic debris, chironomid head capsules |
| 188324 | SCH16-8B-2 | 81.5 | 231.0 | 9740 | 60 | 11170 | 220 | resting eggs, insect chitin, leaf vein fragments, cladocera, chironomid head capsule |
| 188328 | SCH16-8B-2 | 126.5 | 276.0 | 10050 | 220 | 11660 | 820 | bryophyte twigs, chironomid head capsules, resting eggs, insect remains, leaf fragments |
| 180845 | SCH16-8B-2 | 143.5 | 293.0 | 10895 | 25 | 12750 | 50 | resting spore, cladocera remains, graminoid fragments, bryophyte twigs |
| 191202 | SCH16-10B-1 | 13.5 | 14.0 | 2445 | 50 | 2520 | 170 | egg casings, cladocera chitin, chironomids head capsules, non-specific plant debris, fecal pellets |
| 196902 | SCH16-10B-1 | 26.5 | 27.0 | 4820 | 140 | 5540 | 410 | resting eggs, leaf/plant fragments, chironomids, non-specific chitin |
| 191203 | SCH16-10B-1 | 69.5 | 70.0 | 9910 | 40 | 11300 | 190 | chironomid head capsules, cladocera chitin, daphnia ephippia, bryophyte twigs, leaf fragments, caddis fly cases, betula seed, *Chara*, oo spore, woody twigs, elytra beetle |
| 191204 | SCH16-10B-2 | 5.5 | 117.3 | 12590 | 50 | 14950 | 250 | leaf fragments, bryophytes and bryophyte twigs, chironomid head capsules, other insect head capsules, ledum leaf, cladocera remains |
| 191205 | SCH16-10B-2 | 60.5 | 172.3 | 12710 | 60 | 15140 | 230 | very finely dissected organic remains (leafy), insect chitin |
| 191206 | SCH16-10B-3 | 121.5 | 305.7 | 30500 | 1700 | 34550 | 3560 | finely dissected plant debris, bryophyte leaves and twigs |

[a] Keck Carbon Cycle AMS Facility, University of California Irvine (UCIAMS).
[b] Centered sample depth; samples 1.0 cm thick, except for 188324, which was 3 cm thick.
[c] Median probability ± one half of the 2-sigma range; calibrated using CALIB 7.1 (Stuiver et al., 2018)

**Table 3.** $^{210}$Pb, $^{226}$Ra, $^{137}$Cs profiles from core PTR16-48A, SCH16-8A and $^{240/239}$Pu profile from core PTR13-2A.

| Depth blf (cm)[a] | total $^{210}$Pb (Bq/kg) | ± | Ave $^{226}$Ra (Bq/kg) | ± | $^{210}$Pb excess (Bq/kg) | ± | $^{137}$Cs (Bq/kg) | ± |
|---|---|---|---|---|---|---|---|---|
| *PTR48* | | | | | | | | |
| 0.50 | 133.24 | 23.96 | 55.08 | 8.08 | 79.57 | 25.74 | 4.67 | 4.12 |
| 1.50 | 163.61 | 19.72 | 59.88 | 7.82 | 105.62 | 21.60 | 7.76 | 3.73 |
| 3.50 | 84.50 | 19.96 | 45.68 | 6.98 | 39.53 | 21.53 | 56.20 | 4.82 |
| 5.50 | 70.77 | 17.04 | 61.94 | 7.93 | 8.99 | 19.14 | -1.94 | 3.57 |
| 7.50 | 52.51 | 16.01 | 62.14 | 7.72 | -9.81 | 18.11 | -1.57 | 2.88 |
| 9.50 | 71.39 | 17.28 | 58.79 | 7.67 | 12.84 | 19.26 | -0.55 | 2.96 |
| 11.50 | 65.64 | 17.93 | 72.64 | 9.23 | -7.13 | 20.56 | 0.76 | 3.29 |
| 12.50 | 80.30 | 18.50 | 67.00 | 8.66 | 13.56 | 20.82 | 4.35 | 3.43 |
| 13.50 | 90.95 | 19.77 | 64.35 | 8.65 | 27.12 | 22.00 | -3.18 | 3.61 |
| 14.50 | 74.27 | 12.27 | 67.21 | 7.55 | 7.20 | 14.69 | -1.32 | 2.25 |
| 17.00 | 75.44 | 10.36 | 65.18 | 7.13 | 10.48 | 12.84 | -0.49 | 1.56 |
| 18.50 | 61.49 | 12.09 | 61.70 | 7.38 | -0.22 | 14.46 | -0.84 | 2.02 |
| 20.50 | 84.76 | 12.67 | 64.73 | 7.41 | 20.45 | 14.99 | -3.18 | 2.05 |
| 21.50 | 62.16 | 12.47 | 71.98 | 8.07 | -10.03 | 15.17 | -2.67 | 2.05 |
| 23.50 | 39.17 | 11.52 | 47.89 | 5.88 | -8.90 | 13.21 | -3.06 | 1.86 |
| 28.00 | 69.21 | 11.44 | 62.01 | 6.95 | 7.36 | 13.68 | -2.58 | 1.81 |
| 33.00 | 87.49 | 15.22 | 73.65 | 8.32 | 14.14 | 17.73 | -2.81 | 1.99 |
| 38.00 | 70.96 | 8.86 | 67.18 | 7.10 | 3.86 | 11.60 | -2.73 | 1.38 |
| 43.00 | 51.23 | 9.29 | 60.20 | 6.71 | -9.18 | 11.72 | 0.10 | 1.57 |
| 48.00 | 34.73 | 10.06 | 62.47 | 7.32 | -28.37 | 12.73 | -1.71 | 2.20 |
| *SCH8* | | | | | | | | |
| 0.00 | 363.60 | 25.20 | 56.45 | 7.14 | 315.56 | 26.91 | 20.04 | 4.31 |
| 0.25 | 274.21 | 22.41 | 59.19 | 7.34 | 220.93 | 24.24 | 36.82 | 4.65 |
| 0.50 | 304.37 | 29.50 | 67.17 | 8.02 | 243.77 | 31.42 | 89.99 | 6.10 |
| 0.75 | 178.19 | 20.65 | 70.81 | 7.74 | 110.42 | 22.68 | 122.80 | 5.57 |
| 1.00 | 128.91 | 22.33 | 81.12 | 8.61 | 49.16 | 24.61 | 121.76 | 5.91 |
| 1.25 | 127.20 | 15.36 | 61.42 | 5.97 | 67.68 | 16.95 | 63.33 | 3.44 |
| 1.50 | 143.05 | 17.82 | 72.72 | 6.84 | 72.39 | 19.65 | 27.58 | 3.68 |
| 1.75 | 140.81 | 16.30 | 78.47 | 7.04 | 64.22 | 18.29 | 12.22 | 3.16 |
| 2.00 | 108.30 | 18.97 | 75.26 | 7.23 | 34.06 | 20.93 | 5.05 | 2.84 |
| 2.25 | 137.21 | 19.78 | 82.18 | 7.97 | 56.74 | 21.98 | 1.08 | 2.98 |
| 2.50 | 110.00 | 11.58 | 79.24 | 6.46 | 31.48 | 13.51 | -0.32 | 1.71 |
| 4.50 | 97.00 | 14.39 | 73.64 | 6.32 | 24.10 | 16.01 | 2.63 | 1.90 |
| 6.50 | 67.00 | 8.97 | 81.40 | 6.40 | -14.48 | 11.23 | -0.14 | 1.51 |

| PTR2 depth blf (cm) | $^{240/239}$Pu | $^{240/239}$ sd | Bq/kg | Bq/kg sd |
|---|---|---|---|---|
| 0.25 | 0.19 | 0.00 | 0.20 | 0.01 |
| 0.75 | 0.20 | 0.06 | 0.15 | 0.03 |
| 1.25 | 0.17 | 0.06 | 0.16 | 0.02 |
| 1.75 | 0.19 | 0.08 | 0.17 | 0.00 |
| 2.25 | 0.15 | 0.15 | 0.16 | 0.05 |
| 2.75 | 0.19 | 0.06 | 0.16 | 0.02 |
| 3.25 | 0.18 | 0.02 | 0.21 | 0.05 |
| 3.75 | 0.16 | 0.01 | 0.18 | 0.01 |
| 4.25 | 0.06 | 0.01 | 0.16 | 0.00 |
| 4.75 | 0.16 | 0.01 | 0.22 | 0.01 |
| 5.25 | 0.17 | 0.10 | 0.22 | 0.07 |
| 5.75 | 0.20 | 0.04 | 0.22 | 0.02 |
| 6.25 | 0.14 | 0.11 | 0.27 | 0.04 |
| 6.75 | 0.20 | 0.03 | 0.31 | 0.02 |
| 7.25 | 0.16 | 0.03 | 0.44 | 0.06 |
| 7.75 | 0.15 | 0.01 | 0.60 | 0.02 |
| 8.25 | 0.21 | 0.02 | 1.27 | 0.08 |
| 8.75 | 0.16 | 0.04 | 0.69 | 0.07 |
| 9.25 | 0.20 | 0.02 | 0.94 | 0.02 |
| 9.75 | 0.20 | 0.01 | 1.29 | 0.05 |
| 10.25 | 0.20 | 0.04 | 0.64 | 0.05 |

[a] Depth is measured to mid-depth of sample of for cores PTR48 and PTR2 and to top of samples for SCH8.

# Appendix A – Core descriptions

*PTR16-49*

Note: Appendices A, B, and C, provide detailed core descriptions, a summary of moraine mapping and lichenometry, and a summary of analytical uncertainty associated with sedimentological analysis respectively. Appendices D through L contain all data for digital submission.

PTR49 (110 cm) was recovered in 13 m of water in the proximal basin in Lake Peters on a submerged ridge. Using a smooth spline to model age-depth relationships, four macrofossil samples suggest fairly consistent sedimentation rates of 0.1 mm $yr^{-1}$ above 80 cm blf with higher sedimentation rates of up to (0.4 mm $yr^{-1}$). The base of this core projects to 9.0ka. There were no age reversals. This suggests DBD/OM samples collected every 2 cm over the length of the core represent ~100-year time periods, with ~200 years between samples. Grain size analysis was not performed on this core however, based on the lithology that is similar SCH6, it is likely that this core is dominated by the silt fraction (> 75 %). Several sandy layers were evident while sieving for macrofossils. These sandy layers were located near 15 cm blf.

Unit A (103–53 cm blf) is composed of **Lsi** (light silt) and characteristically tan (5Y 7/4) with variable but distinctive dark brown/black (5Y 3/2) 1-3 mm-thick layers that are more abundant in the upper portion of the unit. Two pebble-sized, sub-angular clasts (1-2 cm in diameter) were present in the basal sediment. These clasts appear to be composed of the local Neruokpuk Formation. No distinguished striation marks were present. Above these clasts, sediment density is above average and decreases up core. OM is also above average and decreases up core (~5.5%). Greyscale values are average.

Unit B (53–33 cm blf) is composed of **Dsi** (dark silt) and alternates between dark olive green (5Y 6/6) with frequent dark brown/black (5Y 3/2) bands. Density is average. OM is above average and decreases sharply in the upper portion of the unit. Greyscale values are slightly below average.

Unit C (23–0 cm blf) is composed of **Lsi** (light silt) and characteristically tan (5Y 7/4) with variable but distinctive dark brown/black (5Y 3/2) 1-3 mm-thick layers. Density increases in a step-wise fashion and then continues to increase with above 15 cm blf. OM content increases after a minimum around 30 cm, reaches a relative maximum around 20 cm blf and then decreases up core. Greyscale increases to above average values. Towards the top of the core (15 cm blf) several (light red (5YR 6/6) layers are present.

*PTR16-48*

PTR16-48 (260 cm) was recovered in 31.2 m of water in the distal basin of Lake Peters. The core site is located roughly 0.5 km south of the Whistler Creek delta, and 0.3 km from a smaller delta to the east. Note: when taking this core, the casing inadvertently hit lake bottom before the drill was turned on. Subsequently, the tube casing was brought to the surface, cleaned, and the tripod was repositioned (~ 0.5 m). The casing and drill were then redeployed. This may explain the "extra sediment" in the upper portion of PTR48B-1 (i.e. due to poor cleaning and or disturbed sediment around the core site). Five macrofossil samples with no age reversals show extremely variable sedimentation rates with the base of the core projecting to 2.3 ka. These rates vary from 1 to 5 mm $yr^{-1}$ and a dramatic decrease in sedimentation rates occurs above the uppermost $^{14}C$ sample where they drop to ~0.23 mm $yr^{-1}$. $^{137}Cs$ activity peak and drop in Pb

levels 35 mm below lake floor (blf) suggests recent sedimentation rates of 0.66 mm $yr^{-1}$. Using this range of sedimentation rates for the lower core, DBD/OM measured every 5 cm, suggests samples collected represent ~10 to 2-year time periods, with ~50 to 10 years between samples. In the upper core, samples likely represent multidecadal time periods with centennial-scale sample spacing.

Lithology is composed of **Lsi** (Light silt) with the lower core containing abundant, 5–50 mm-thick **Bsa** (brown sand) beds. *Unit A* (260–65 cm blf) alternates between dark olive green (5Y 6/6) and tan (5Y 7/4) with discrete and ubiquitous beds of brown (5Y 5/2) silty-sand that range in thickness between 5–50 mm. These beds tend to have sharp basal contacts, while the upper portions tend to grade into finer material. Density is generally higher in the lower portion of the core and fluctuates with increase near 95 cm blf associated with an 8 cm-thick layer of coarse sediment (grains are apparent in the line-scan image). OM averages ~3.8 % with maxima around 110 and 80 cm blf. Sediment grain size is dominated by the silt fraction, with an exception at 100 cm blf, which consists of very fine sand and fine sand both approximately 25% (silty sand). This sample was extracted from a 3-cm-thick layer that contains visibly coarse grains. Although only one sample displayed this coarse grainsize distribution, similar beds of coarse sediment occur frequently in the lower core and likely contain similar grain size distributions. Occasionally, these sandy beds are associated with 3-10 mm-thick laminae that are dark brown/black (5Y 3/2) and contain visible plant fragments.

*Unit B* (65–0 cm blf) is similar to *Unit A* and composed of **Lsi** (light silt) though it mostly lacks the sand beds. In the upper unit, color changes to thinly laminated, blue-grey (GLEY 1 7/5GY) and tan (5Y 7/4) with occasional dark brown/black (5Y 3/2) organic-rich layers. Density decreases to minima around 50 and 30 cm blf, and then increases with variation towards the

present, with exception of the top ~2 cm. A brownish red (2.5Y 6/4) zone occurs in the top of the core near 10 cm blf.

*SCH16-6*

SCH16-6 (230 cm) was recovered in 54.1 m of water in the proximal basin in Lake Schrader, about 2 km from the Whistler Creek delta. Seven macrofossil samples suggest fairly consistent sedimentation rates of (0.28 mm $yr^{-1)}$ with a basal age of 9.2 ka. One age reversal occurred due to a $^{14}C$ sample from 41.8 cm blf. Visible evidence of deformed beds from 40 to 53 cm blf suggest a slump deposit. This suggests DBD/OM sample collected every 2 cm over the length of the core represent ~30-year time periods, with ~60 years between samples. Grain size analysis was not performed on this core however, based on the lithology that is similar SCH16-8, it is likely that this core is dominated by the silt fraction (>75 %). Measurements of DBD and OM between the surface core and vibracore show similar trends.

*Unit A* (230–150 cm blf) is composed of **Lsi** (light silt) and characteristically tan (5Y 7/4) with variable but distinctive dark brown/black (5Y 3/2) 1-3 mm-thick layers that increase in frequency up core. Density is above average, and OM is below average. Greyscale values are above average.

*Unit B* (150–75cm blf) is composed of **Dsi** (dark silt) and alternates between dark olive green (5Y 6/6) with frequent dark brown/black (5Y 3/2) bands. Density displays a discrete step-wise shift to below average values, with the exception of a peak near 135 cm blf. OM increases and fluctuates between ~%5-6. Greyscale values are correspondingly below average.

*Unit C* (75–0 cm blf) is composed of **Lsi** (light silt) and characteristically tan (5Y 7/4) with variable but distinctive dark brown/black (5Y 3/2) 1-3 mm-thick layers. Density increases with variation with maxima at 45 and 10 cm blf. OM displays below average values and greyscale is above average. Towards the top of the core (~4 cm blf) several (light red (5YR 6/6) layers are present.

*SCH16-8*

SCH16-8 (297 cm) was recovered in 46.5 m of water in the distal sub-basin in Lake Schrader, about 0.6 km from the Coke Creek delta. Seven macrofossil samples suggest fairly consistent sedimentation rates (0.23 mm $yr^{-1)}$ with a basal age of 13,000 cal yr BP. There were no age reversals. Near the top of the core, an initial peak in $^{137}$Cs associated with nuclear weapons testing in 1963 at 12.5 mm blf suggests recent sedimentation rates of 0.23 mm $yr^{-1}$. This suggests DBD/OM sample collected every 2.5 cm over the length of the entire core represent ~45-year time periods, with 113 years between samples. The silt fraction dominates throughout the core, with every value >75 % with the exception of two samples that contained <10% very fine sand that are associated with discrete, thin layers similar to those found in PTR16-48. Measurements of DBD and OM between the surface core and vibracore accord.

*Unit A* (297–204 cm blf) is composed of **Dsi** (dark silt) and consists of dark olive green (5Y 6/6) bedding with frequent dark brown/black (5Y 3/2) bands. Density is above average and decreases up core. OM is below average with exception of a peak associated with several thinly-bedded coarse grained layers at ~268 cm blf. DBD and WBD show accordance with exception to ~220 blf where DBD shows a relative increase while WBD does not. Grain size analysis of these

thin coarse beds showed they contained ~10% very fine sand, which is a significant departure from the overall silt-dominated grain size for the rest of the core. Greyscale values are below average.

*Unit B* (204–104 cm blf) is composed of **Lsi** (light silt) and characteristically tan (5Y 7/4) with variable but distinctive dark brown/black (5Y 3/2) 1-10 mm thick layers that are spaced from 1 to 4 cm apart. Density is above average, and OM is below average. A distinct thin bed of coarse sand is present at 162 cm blf and is associated with an increase in density. Greyscale values are variable, but often above average.

*Unit C* (104–45 cm blf) is composed of **Dsi** (dark silt) and alternates between dark olive green (5Y 6/6) with frequent 1-3 mm thick, dark brown/black (5Y 3/2) bands. Density decreases with some variation to below average values, with the exception of a peak near 75 cm blf associated with several small thin sandy layers. These thin sandy layers are visually similar to the ones identified in *unit A*. OM displays a clear, step-wise increases and rises to a peak (7-8%) near 60 cm blf. Throughout *unit C*, OM displays consistently high values as compared to the rest of the core. Accordingly, this unit has low greyscale values.

*Unit D* (45–0 cm blf) returns to **Lsi** (light silt) and consists of tan (5Y7/4) with variable but distinctive dark brown/black (5Y 3/2), 1-5 mm thick layers. Density initially increases, then decreases, and then increases to average values while OM shows an opposite pattern with overall decreases towards average values. Greyscale increases. Towards the top of the core from 1 to 7 cm blf, several light red (5YR 6/6) layers are present.

*SCH16-10*

SCH16-10 (339 cm) was recovered in 20 m of water in the distal sub-basin in Lake Schrader, about 0.8 km from shore. Five macrofossil samples provide an age model with sedimentation rates that vary by two orders of magnitude from basal rates of 2.8 mm $yr^{-1}$ that decrease up core to 0.07 mm $yr^{-1}$. There were no age reversals, however, the lowest $^{14}C$ sample dates to 34550 ±1840 cal yr BP and we did not include it in the age model as this organic material is likely composed of erroneously old, reworked material. Two macrofossil samples in the middle section of the core suggest sedimentation rates of (~2.8 mm $yr^{-1}$) from 15140 to 14950 ±100-130 cal yr BP and projecting these vertical accumulation rates estimates a basal age of ~ 16 ka. Above this, sedimentation rates decrease (0.07 mm $yr^{-1}$) and continue to do so as the uppermost macrofossil sample suggests a rate of 0.05 mm $yr^{-1}$ over the last 2.5 ka. These sedimentation rates imply that in the upper core, each DBD/OM sample collected every 2 cm represents ~143 years, with 286 years between samples. Measurements of DBD and OM between the surface core and vibracore show similar trends.

*Unit A* (339–122 cm blf) is unequivocally different than overlying sediments and can be subdivided into two sub units; $A_1$ and $A_2$. $A_1$ (339–150 cm blf) alternates between brown-blue grey (GLEY 6/10Y) and light tan (5Y 8/1) laminations of clayey silt that appear to systematically alternate and form couplets. This distinct lithological unit, **Bgcs** (brown-grey clayey silt) is only found in lower section of this core. Couplets are cm-scale in the lower portion of the unit, and thin upward to mm-scale around 250 cm blf. $^{14}C$ dates suggest sedimentation rates that roughly correlate to the thickness of these couplets such that, the inferred age-depth relationship suggests that they may represent a process with an annual periodicity. These

couplets tend to disappear, then reappear in the top of $A_1$. Basal density values are the highest for any of the cores (WBD = ~2 g/cm$^3$) and decreases towards the top of *$A_1$*. OM for this unit is corresponding low and averages ~ 3%. Particle size distributions are dominated by silt in the lower portion, while % clay increases to almost 35% towards the top of *$A_1$*. The increase in clay content corresponds with the increased frequency of the light tan (5Y 8/1) laminations of clayey silt. Greyscale values show considerable variation, however, begin with average values, then decrease and subsequently increase towards the top of the unit. Near the top of *Unit $A_1$*, a striking blue-grey (GLEY 1 7/5G) color change is visible, which forms the somewhat gradational transition between the units.

In *Unit $A_2$* (150–122 cm blf), density values show an abrupt increase that is accompanied by the consistently lowest amounts of OM (~2.5%) for any of the sediments in this study. The aforementioned couplets reappear for about 10 cm in the lower portion of *$A_2$* before transitioning to a darker and thicker-bedded character. Clay content decreases with a small amount (4%) of very fine sand, which, constitutes the coarsest grain size present in this core. Visual inspection reveals several thinly bedded (~1 cm) coarse layers towards the top of this sub unit near 135- 125 cm blf. Greyscale values show a sharp decrease from the underlying unit followed by variable values.

*Unit B* (122–80 cm blf) is composed or **Lsi** (light silt) and alternates between tan (5Y 7/4) and dark olive green (5Y 6/6) laminations, with a high frequency of distinct (1-3 mm thick) dark brown/black (5Y3/2) towards the bottom of the unit. Both WBD and DBD show a sharp decrease from the underlying unit of roughly ~0.7 and ~1.0 g/cm$^3$ respectively. Grain size is predominantly silt with ~20% clay. OM steadily increases from 2 to 5 %. Greyscale values are average and decrease upwards.

*Unit C* (80–55 cm blf) is composed of **Dsi** (dark silt) and similar *unit B*, but is characterized by an increase in dark brown/black (5Y 3/2) laminae containing low density values and some of the highest OM values for the entire core (6-8.5 %). Greyscale values are below average.

*Unit D* (55–22 cm blf) is composed of **Lsi** (light silt) and characterized by a relative decrease in dark brown/black (5Y 3/2) laminae. Density values increase slightly. OM values decrease to relatively-lowest values for the upper portion of the core. Greyscale shows low values associated with dark laminae.

*Unit E* (22–12 cm blf) is composed of **Dsi** (Dark silt) and similar to *unit C*, with a higher frequency of dark brown/black (5Y 3/2) as compared with the underlying *unit D*. Density values decrease with variation until they increase at the base of the overlying unit. OM increases with variation. Towards the top of *unit E*, a series of light red (5YR 6/6) layers are present at ~10 cm blf.

*Unit F* (12–0 cm blf) is likely composed of **Lsi** (light silt), however, no grain size data was analyzed for this unit. It has a distinct reddish-brown (2.5Y 6/6) appearance. Density shows an increase with some variation in the upper most centimeters of the core. OM initially decreases compared to unit E, but then increases with variation in the upper most portion of the core. Greyscale values decrease.

## **Appendix B** – Moraine mapping and lichenometry

*Methods*

We measured *Rhizocarpon geographicum* maximum thallus diameters on distinct moraine ridges in two different valleys the Lake Peters basin (Fig. 1b, B-1). In the Chamberlin Glacier forefield, we replicated the previous work of Evison et al. (1996). We also obtained new measurements from a tributary valley ~5 km to the south of Lake Peters (GL3). Plots were 30-m-long by 15-m-wide and avoided areas with apparent slope instability. The mean of the five largest maximum diameters was calculated with corrections for inheritance when the largest lichen (about 2% of the measurements) was 20% larger than the second largest (e.g. Jochimsen, 1973).

*Results*

In total, roughly 500 individual lichen thalli were measured across 32 plots with an average of 16 measurements per plot. At the Chamberlin Glacier forefield, three distinct moraine ridges were apparent both in field mapping, and in the distribution of lichen sizes (10–20, 40–50, and 100–110 mm) with two plots having diameters ranging from 20–30 mm on a less-distinct ridge immediately adjacent to the ridge associated with 10–20 mm lichens (Fig. B-1). In general, steep-sided moraine ridges with infrequent and smaller lichens were inset and uphill of more subdued ridges with larger lichens and more soil development (Fig. B-2). These results accord with Evison et al. (1996), but with two notable exceptions. We measured 105 diameter lichens on

the outermost moraine, contrasting with previous measurements of 80 mm. Furthermore, we had difficultly delineating between two inner ridges with average lichen diameters of 20 and 10 mm mapped by the previous study. Rather, we measured lichens on the innermost moraine to be between 12 and 17 mm. Only two plots yielded lichen diameters from 22–25 mm and it is unclear if they were located on a distinct moraine ridge as Evison et al. (1996) suggested.

At GL3, a greater spread in lichen sizes was apparent with the absence of the largest lichen sizes found at Chamberlin Glacier (Fig. B-1). The outermost moraine consisted of a broad ridge with visible soil development, with larger lichens (55 vs. 47 mm) when compared to the second oldest moraine found at Chamberlin Glacier. Up valley of this moraine, we mapped a distinct ridge with lichen sizes of 20–30 mm, although this ridge only appeared to be preserved on the north side of the valley (Fig. B-3). Two plots up valley from this distinct ridge had smaller lichen sizes (11 and 6 mm) and were part of several clear linear features, however, this area appeared to be affected by ice melt, mass wasting, and lake de-watering events.

## **Appendix C –** Analytical error in sediment analysis

Thirty duplicate samples from a range of depths were compared for three cores (PTR49 n = 22, SCH8 n= 3, and SCH10 n = 5) in order to assess the reproducibility in measuring wet bulk density (WBD), dry bulk density DBD and organic-matter content (OM). The corresponding average of the absolute value of differences in WBD were 0.06, 0.04, and 0.19 g $cm^{-3}$. For DBD, corresponding values of 0.04, 0.02, and 0.13 g $cm^{-3}$. Duplicate OM measurements differed by 0.33%, 0.09%, and 0.17%. The uncertainty associated with these measurements is relatively low compared to the down-core variability of about 0.8 g $cm^{-3}$ for both WBD and DBD, and 3-8 % for OM.

To determine the reproducibility between samples taken from two cores typically several meters apart using two coring devices, these parameters were also compared at sites PTR49, SCH6, SCH8 and SCH10 by performing duplicate measurements on correlative depths. In contrast to the duplicate samples, differences between surface cores and vibracores were larger, likely due to uncertainty associated with correlation across the cores, samples not being taken at precisely the same depths, and the possible effects of the vibracoring process for example compaction. For WBD, corresponding average of the absolute value of differences in WBD were 0.08, 0.19, 0.17, and 0.15g $cm^{-3}$. For DBD, corresponding values of 0.10, 0.22, and 0.10 g $cm^{-3}$. For OM content, measurements differed by 0.35%, 0.53%, 0.73%, and 0.65%. Systematic off-set is evident in gamma-ray attenuation WBD measurements between surface cores and vibracores. This is likely due to the method by which short core (split core in vertical configuration) and long cores (whole core in horizontal configuration) are analyzed. No duplicate analyzes were performed for grain size.

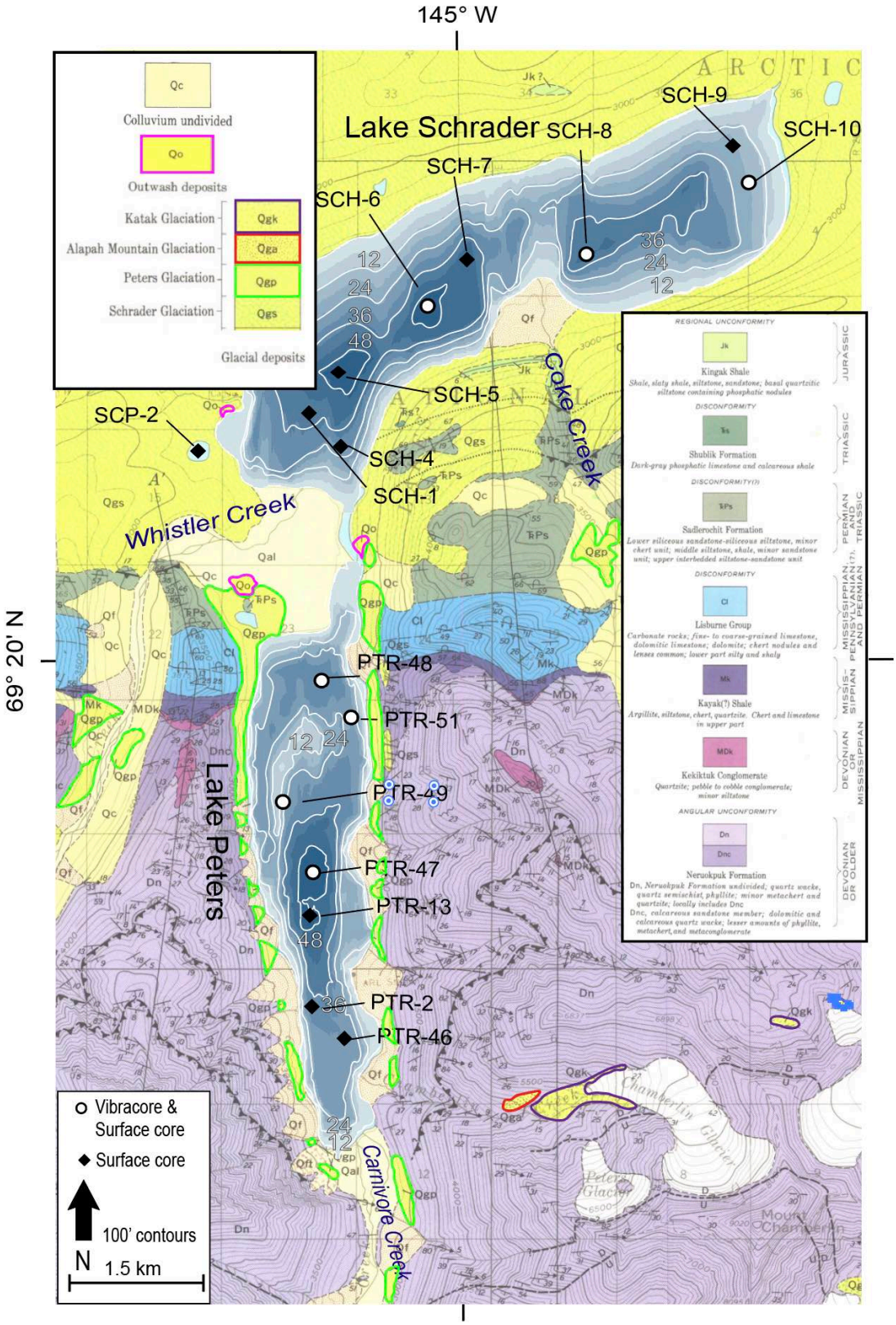


**Figure A-1.** Geologic map of Lake Peters area (Reed, 1968).

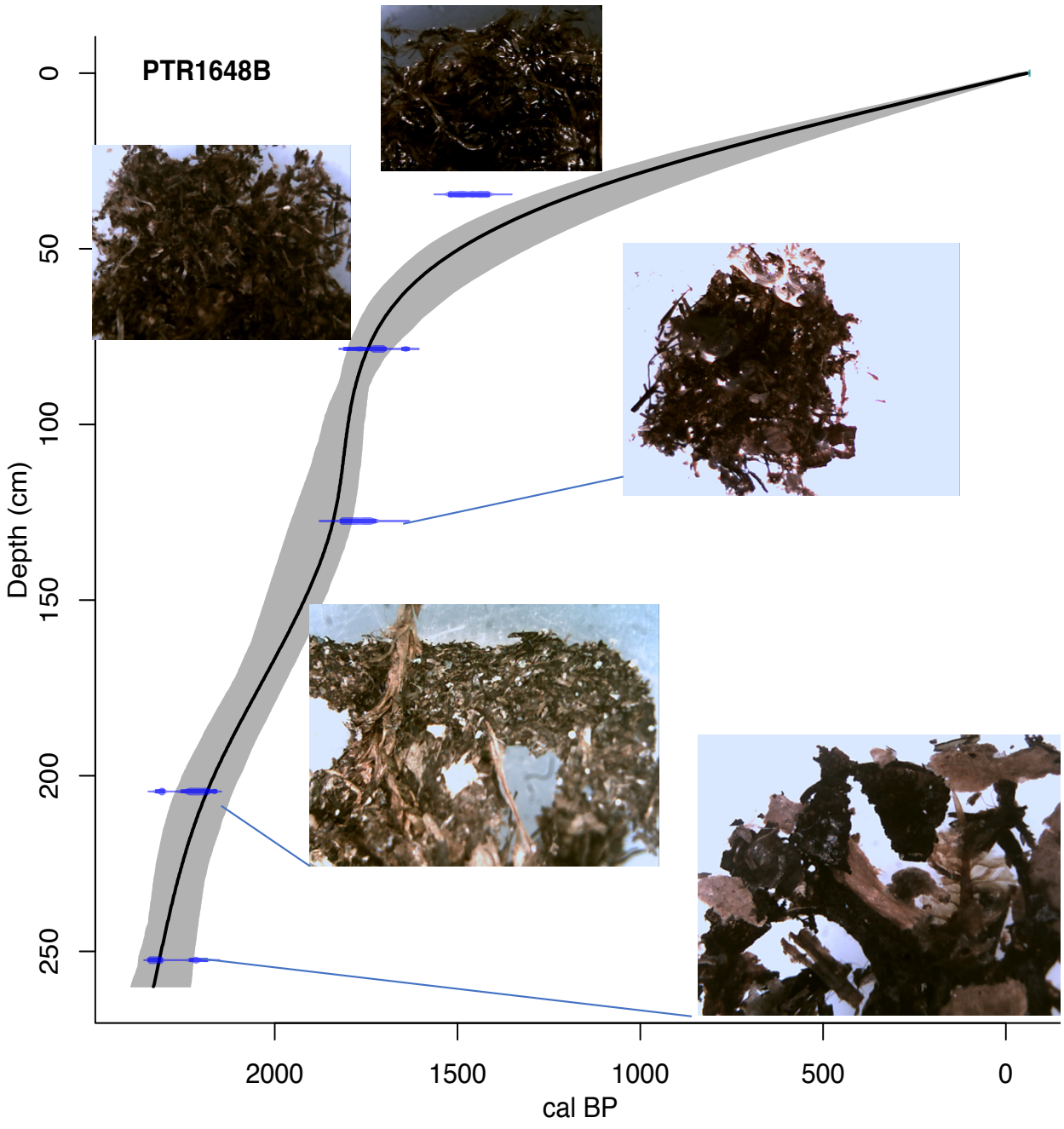


**Figure A-2.** Age model for PTR48B and photos of $^{14}C$ samples.

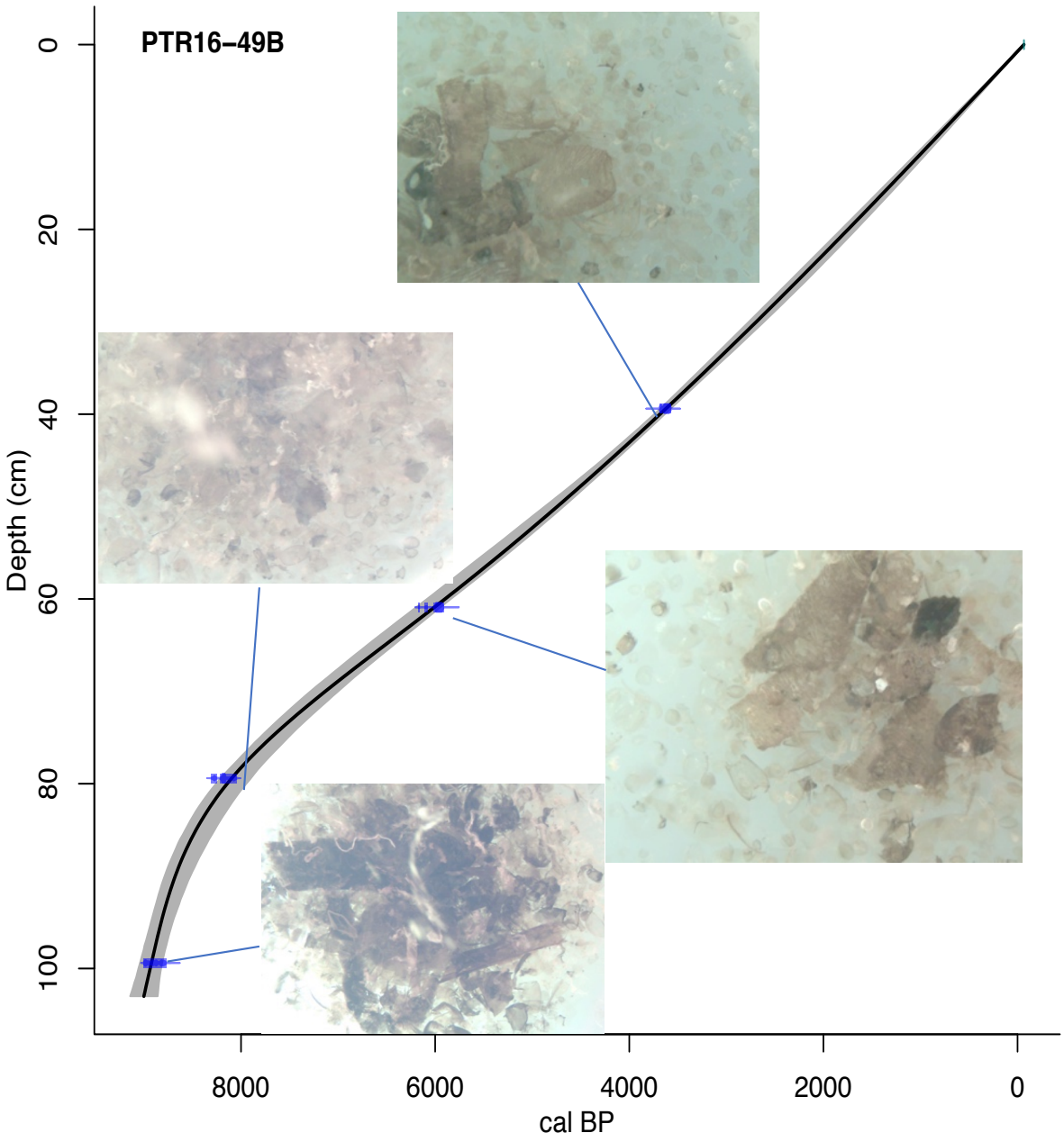


**Figure A-3.** Age model for PTR49B and photos of $^{14}C$ samples.

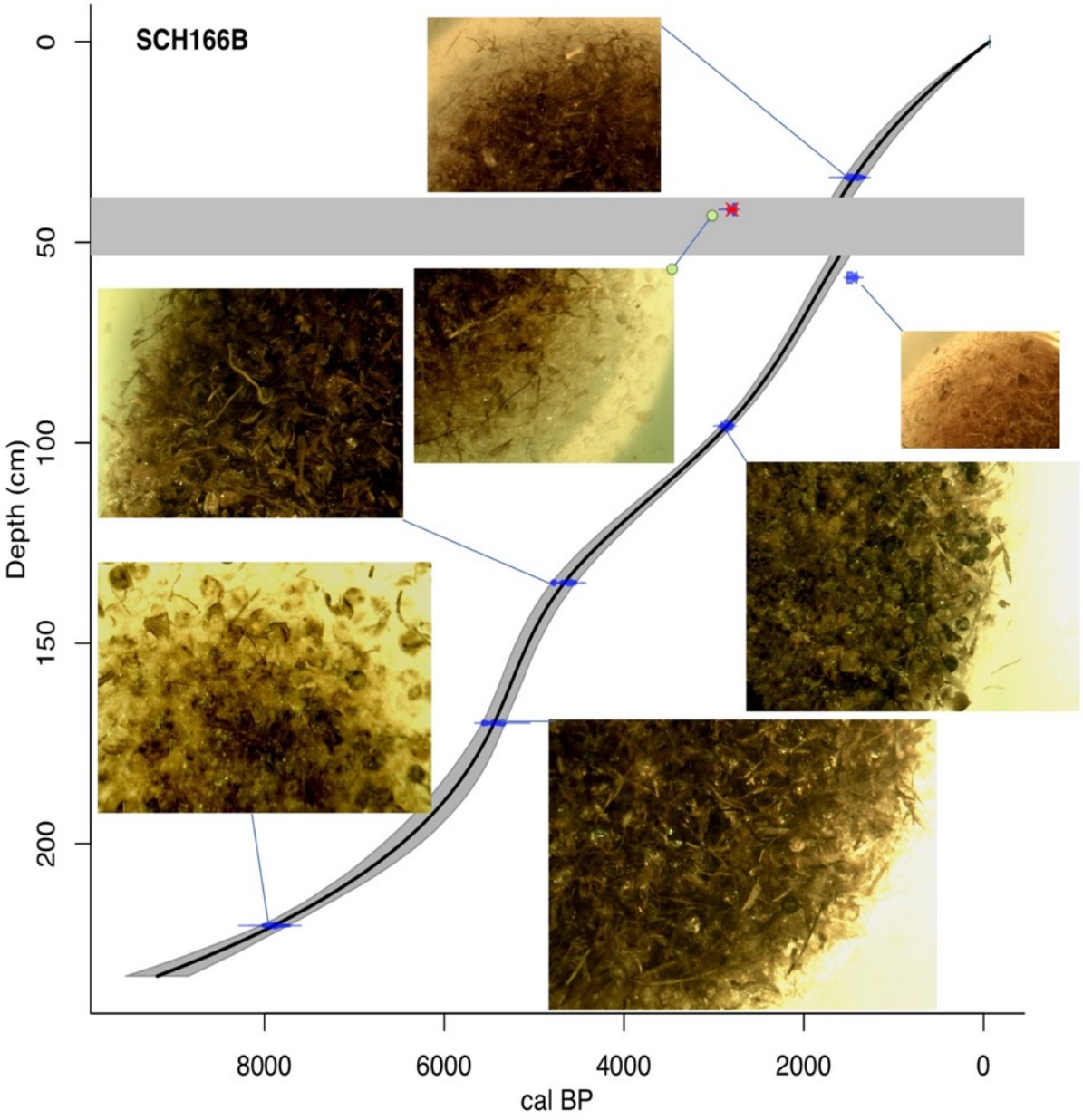


**Figure A-4.** Age model for SCH6B and photos of $^{14}C$ samples. Red star denotes sample not used in age model. Grey bar = slump deposit.

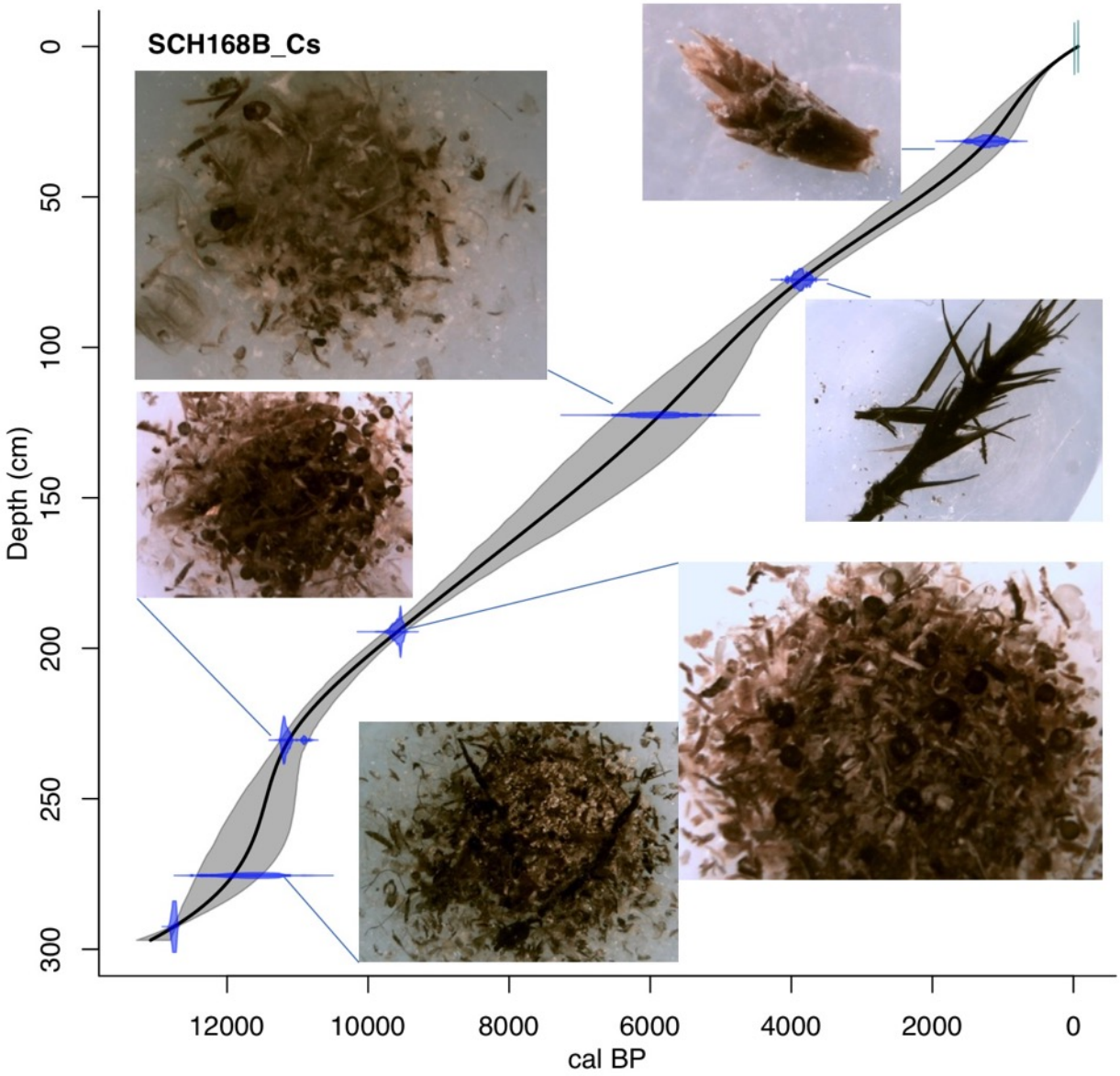


**Figure A-5.** Age model for SCH8B and photos of $^{14}C$ samples.

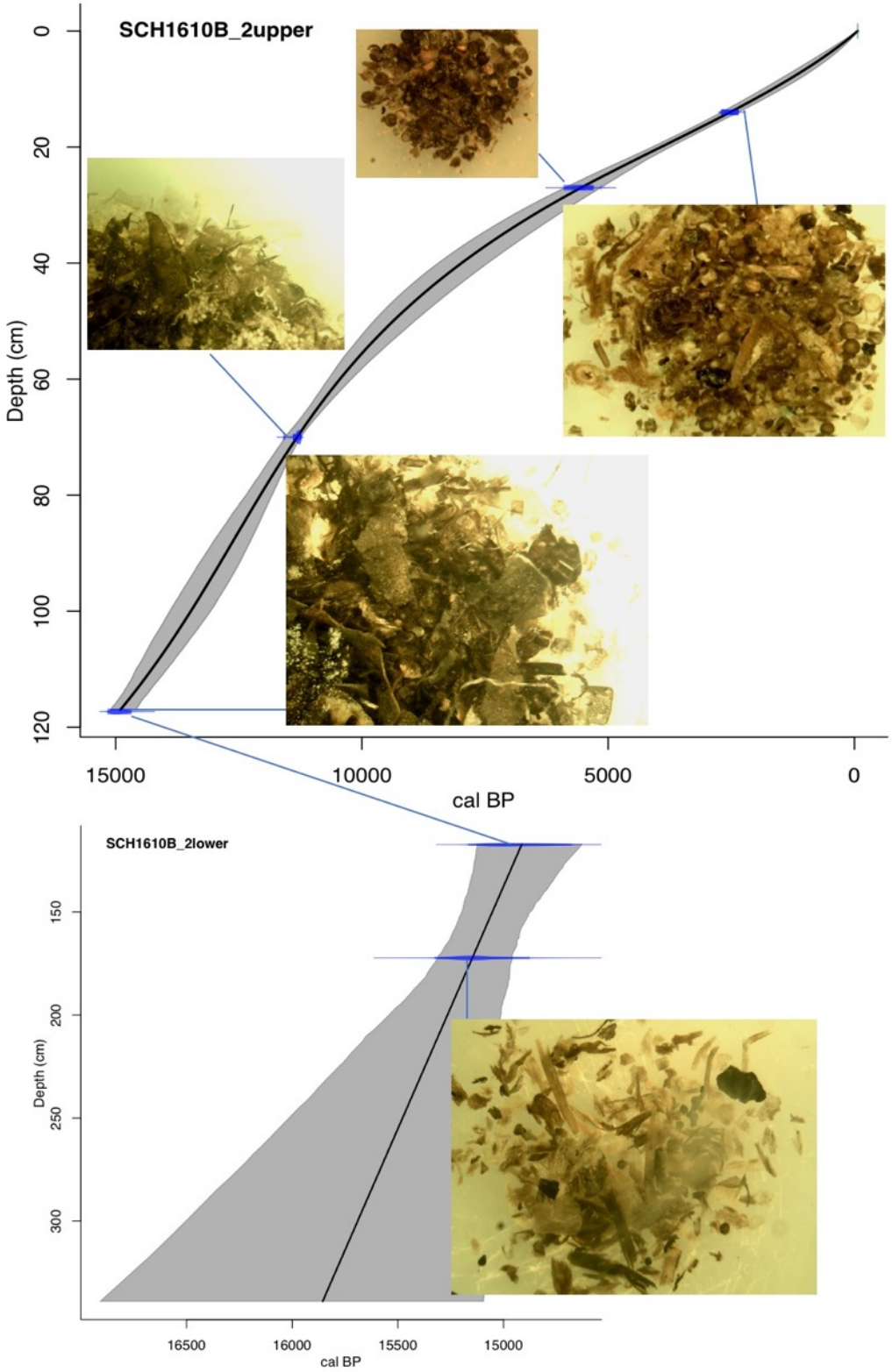


**Figure A-6.** Age model for SCH10B, upper and lower sections and photos of $^{14}C$ samples.

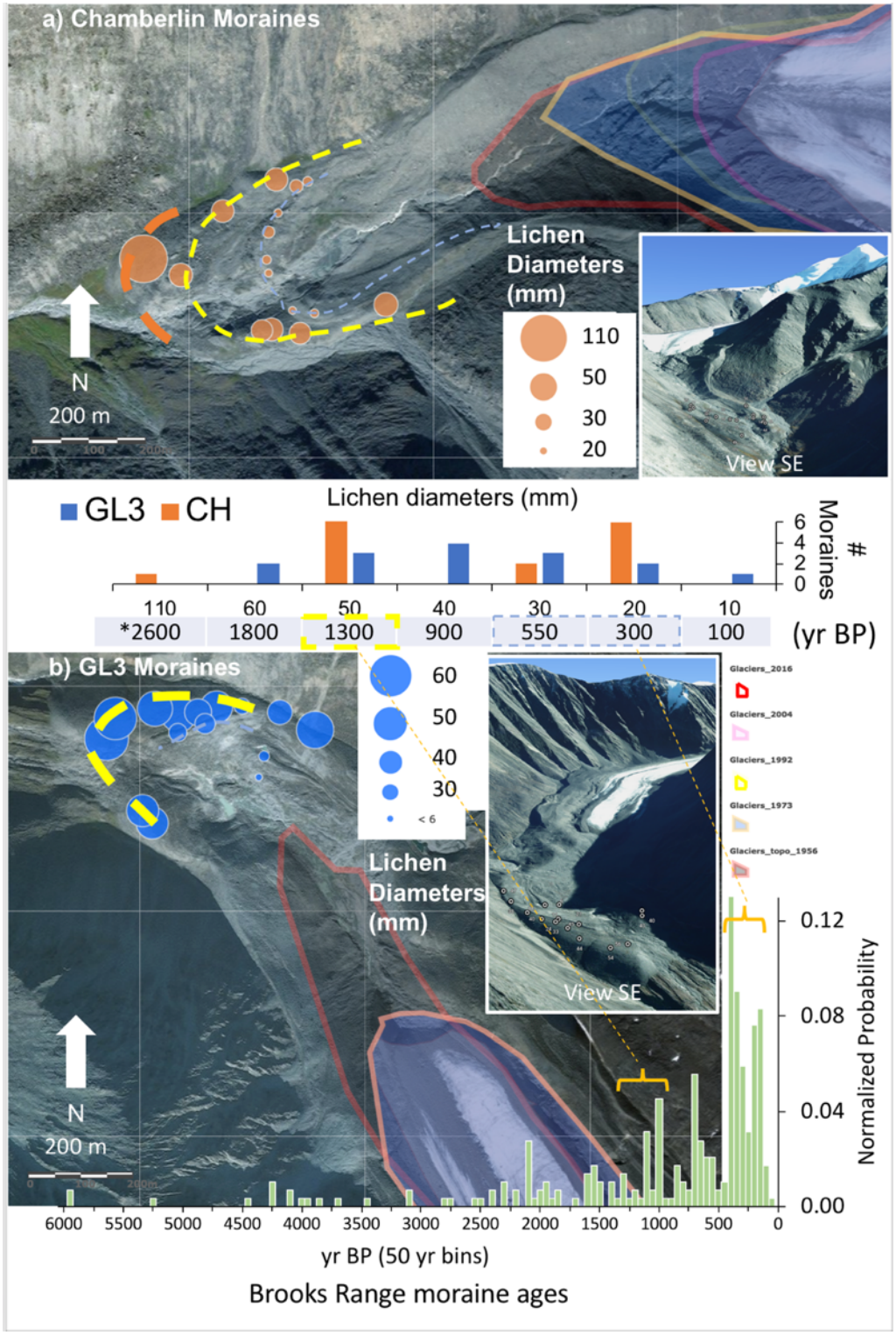


**Figure B-1.** (a) Location of average of the five largest lichens for the Chamberlin forefield moraines and (b) GL3 moraines. Inset photos oblique google earth images. (middle) Histogram of lichen sizes in 10 mm bins. (bottom) Brooks Range moraine frequency diagram (Pendleton et al., 2017).

**Figure B-2.** View east towards Chamberlin Glacier forefield. Note people for scale. Orange and yellow lines highlight moraine ridges with 105 mm lichen and 40-50 mm lichens respectively. Blue line denotes LIA moraine with infrequent and <10 mm lichens.

**Figure B-3.** View southwest at GL3. Note people for scale. Yellow and blue lines highlight moraine ridges with 40-50 mm and 20–30 mm lichens respectively.